THE INFLUENCE OF NONLINEAR ADVECTION AND TIDAL ASYMMETRIES ON ESTUARINE EXCHANGE FLOW

By

NUVIT BERKAY BASDURAK

A DISSERTATION PRESENTED TO THE GRADUATE SCHOOL
OF THE UNIVERSITY OF FLORIDA IN PARTIAL FULFILLMENT
OF THE REQUIREMENTS FOR THE DEGREE OF
DOCTOR OF PHILOSOPHY

UNIVERSITY OF FLORIDA

2010

To my mom, dad and uncle

ACKNOWLEDGMENTS

I want to thank my advisor Dr. Arnoldo Valle-Levinson, for his constant support throughout my study. I want to thank him for giving me the courage whenever I needed, for believing in me. It is an honor to be your student. I also want to thank my committee members Dr. Kirk Hatfield, Dr. Robert J. Thieke and Dr. Jonathan B. Martin for their constant support. Dr. Kirk Hatfield and Dr. Robert J. Thieke I could not thank you enough for helping me through the way when I could not see the light. I want to thank Peng Cheng for sharing his knowledge, giving his support and encouraging me in my study. My gratitude is extensive to all the students in the coastal group. All of them helped me in some way along my doctorate. Thanks go out to my mother and my father who have been thinking about me in these years. Their love and support has helped me focus and learn what is truly important.

TABLE OF CONTENTS

page

LIST OF FIGURES

Abstract of Dissertation Presented to the Graduate School
of the University of Florida in Partial Fulfillment of the
Requirements for the Degree of Doctor of Philosophy

THE INFLUENCE OF NONLINEAR ADVECTION AND TIDAL ASYMMETRIES ON ESTUARINE EXCHANGE FLOW

By

Nuvit Berkay Basdurak

August 2010

Chair: Arnoldo Valle-Levinson
Major: Civil Engineering

In an effort to better understand the dynamics of estuarine circulation, this work primarily discusses the influence of nonlinear advective accelerations on exchange flow at both tidal and subtidal scales. In most observations the subtidal flow is horizontally sheared, with saline water inflow and freshwater outflow appearing on the side of the cross-section expected from Earth's rotation. The observations show that nonlinear advective terms contribute to the along-channel momentum balance at leading order. Nonlinear advection (longitudinal and lateral advection) has higher values at spring than neap tides due to weaker stratification. Lateral advection induces both vertically and laterally sheared patterns depending on tidal forcing. At springs it mainly acts against Coriolis forcing, by hindering lateral shear in along-channel flow. At neaps it reinforces the vertically sheared along-channel flow. Longitudinal advection increases the lateral shear in the along-channel flow (i.e., seaward over shoals and landward in the channel). Residual flows induced by tidal asymmetries in mixing also affect along-channel exchange flow. Stratified flood and well mixed ebb tides produce reversed residual flow (i.e., landward near surface, and seaward near bottom).

CHAPTER 1
INTRODUCTION

In partially mixed estuaries, the along-channel, tidally averaged, momentum balance is traditionally considered to be between pressure gradient and friction. Pritchard (1956) was the pioneer in defining such balance after his observations in the James River estuary. This linear momentum balance approach set the foundation for estuarine dynamics and was used in studies by Hansen and Rattray (1965), Chatwin (1976), and Officer (1976) just to name a few. This approximation leads to a vertically sheared residual circulation with landward flow near bottom and seaward flow near surface over a flat bathymetry.

Transverse variations in bathymetry can cause exchange flow to be laterally sheared with landward flow in channels and with seaward flow over shoals (Wong, 1994). Kasai et al. (2000) showed the influence of Earth's rotation on exchange flow structure in terms of the vertical Ekman number (Ek), friction dominates over rotation (Ek>1) transverse variations in exchange flow get larger (i.e., laterally sheared exchange flow), and as rotation dominates over friction (Ek<1) vertical variations in exchange flow get larger (i.e., vertically sheared exchange flow). Valle-Levinson (2008) included the channel width influence by characterizing the exchange flow patterns as a function of both the Kelvin (i.e., the ratio of basin's width to the internal radius of deformation, Ke) and Ekman numbers. Under large frictional influences (Ek>1) regardless of the basin's width, the exchange flow shows a laterally sheared structure. When friction is weak, the exchange flow shifts from laterally sheared to vertically sheared structure as the basin gets narrower.

Recent studies have pointed out to the importance of nonlinear advective terms in the along-channel momentum balance. Lerczak and Geyer (2004) applied a three-dimensional numerical model illustrating an idealized, straight estuary with a small tidal amplitude/depth ratio. They showed that in the tidally averaged, along-channel momentum equation, nonlinear advective terms ($vu_y + wu_z$, lateral and vertical advection) act as a driving term for the estuarine exchange flow and can be larger than the along-channel pressure gradient. They concluded that particularly for weakly stratified estuaries, nonlinear advective terms enhance the two-layered estuarine circulation.

Huijts et al. (2009) presented an analytical model to decompose along-channel residual flows into components induced by individual mechanisms including horizontal density gradients, tidal rectification processes (i.e., nonlinear advective terms, $vu_y + wu_z$), river discharge, wind, channel curvature, and Earth's rotation. They used scaling and perturbation techniques to obtain the analytical expressions. They found that the along-channel residual flow shows the same patterns as the ones resulting from tidal rectification processes meaning that advective terms enhance the along-channel residual flow. They also distinguished the contribution of each term concluding that vu_y shows similar flow patterns as wu_z near surface, and opposite flow patterns near bottom. Scully et al. (2009) used a validated numerical model of the Hudson River to examine the forces driving the residual exchange and found that nonlinear advective terms contribute to the tidally averaged along-channel momentum balance at leading order, driving a landward flow near bed. They pointed out to a correlation between interfacial stress and advective momentum flux, and their opposite influence on along-

channel flow. Cheng and Valle-Levinson (2009) examined the influence of nonlinear advective terms ($vu_y + wu_z$) on exchange flow with a scaling analysis, and idealized numerical experiments. They found that these terms are important in narrow and deep estuaries, particularly under relatively weak vertical mixing. They analyzed the change in lateral exchange flow patterns with respect to Rossby (Ro) and Ekman (Ek) numbers by using linear and nonlinear numerical models. They concluded that the nonlinear advective terms, which are more effective at large Ro and small Ek, generate vertically sheared, two layer exchange flow structure, and tend to reduce the lateral variability of estuarine exchange flow.

The studies that have pointed out the importance of advective terms mainly focused on their contribution at subtidal scale. On a tidal scale the studies mentioned above made the following contributions. Lerczak and Geyer (2004) showed the trend of cross-sectional averages of the nonlinear advective terms, and found them to be strongest near peak flood. Huijts et al. (2009) illustrated the flow patterns of vu_y and wu_z during flood and ebb based on their analytical model results. Scully et al. (2009) pointed out asymmetries of advective flux over a tidal cycle, and how they might contribute to along-channel subtidal flow.

Research objectives. The objectives of this study are: (1) to show the importance of the lateral advection term, vu_y along with uu_x to the tidally averaged along-channel momentum budget; (2) to analyze the influence of vu_y on exchange flow patterns and validate with the results of recent numerical and analytical models; (3) to explore the fortnightly variability of vu_y and to determine the effects of wind forcing and river discharge on subtidal along-channel flow and vu_y; (4) to examine the tidal variability of

vu_y and residuals driven by asymmetries in nonlinear terms; (5) to investigate the influence of temporal and spatial asymmetries in vertical mixing on estuarine exchange flow. This is done by using the information from observations carried out at Hampton Roads, Virginia, at the transition between the James River and Chesapeake Bay.

CHAPTER 2
STUDY AREA

Hampton Roads is located at the entrance to the James River estuary, which is the southernmost tributary of the Chesapeake Bay. A map showing the location and the bathymetry of the study area is presented in Figure 2-1. The bathymetry consists of a main channel located on the north of the estuary and a shallower shoal. The depth ranges from 0.5 m to 20 m at the entrance.

The James River estuary is a micro-tidal, partially mixed estuary with a well-developed gravitational circulation. Direct freshwater discharge and tides are the main forcing mechanisms. The annual mean freshwater discharge gauged at Richmond, Virginia, is approximately $200 m^3 s^{-1}$. The highest and the lowest monthly discharges occur between February and April (~335 m^3/s), and July and September (~95 m^3/s), respectively (U.S. Geological Survey, Hydrologic Unit Code 02080205, Site ID 02037500 http://waterdata.usgs.gov/va/nwis/monthly) (Figure 2-2a). Tides are predominantly semidiurnal with M_2, N_2, and S_2, in order of importance, being the most energetic constituents. The interaction between M_2 and S_2 causes fortnightly variability generating differences in the baroclinic pressure gradients, advective accelerations and friction between neap and spring tides (Valle-Levinson et al., 2000). The tidal amplitudes of spring and neap tides are 0.45 m and 0.20 m, respectively. Seasonal wind forcing consists of northeasterly winds in fall/winter and southwesterly in summer. Due to the orientation of the entrance, northeasterly winds cause the mean sea level to rise, and southwesterly winds cause it to fall (Figure 2-3).

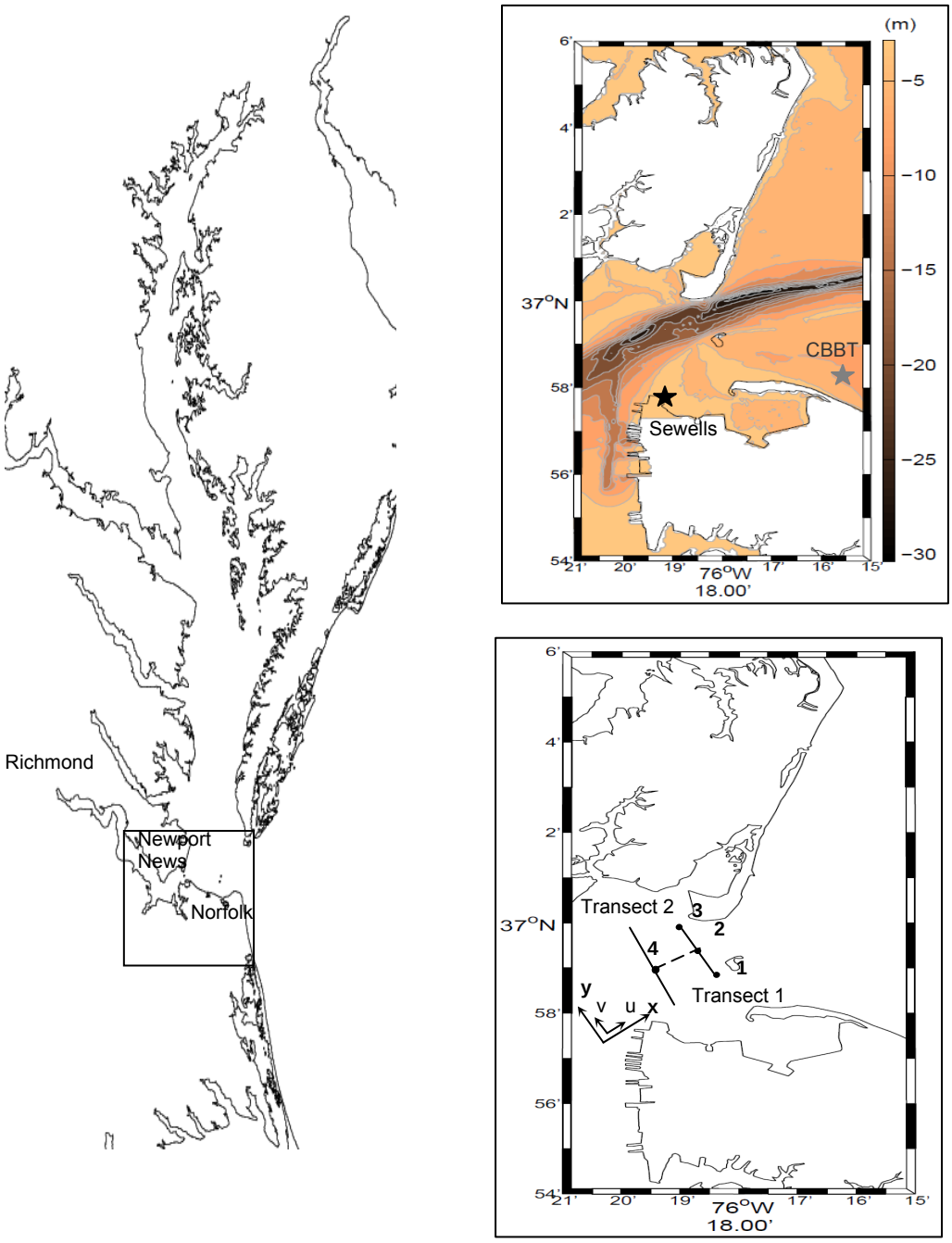

Figure 2-1. Map of the study area. It is located in the lower James River estuary (one of the tributary of the Chesapeake Bay, Virgina). Bathymetry, the transects sampled, and 4 stations where the CTD casts were taken, are presented. The locations of Sewells Point, CBBT, NOAA's stations are marked as stars.

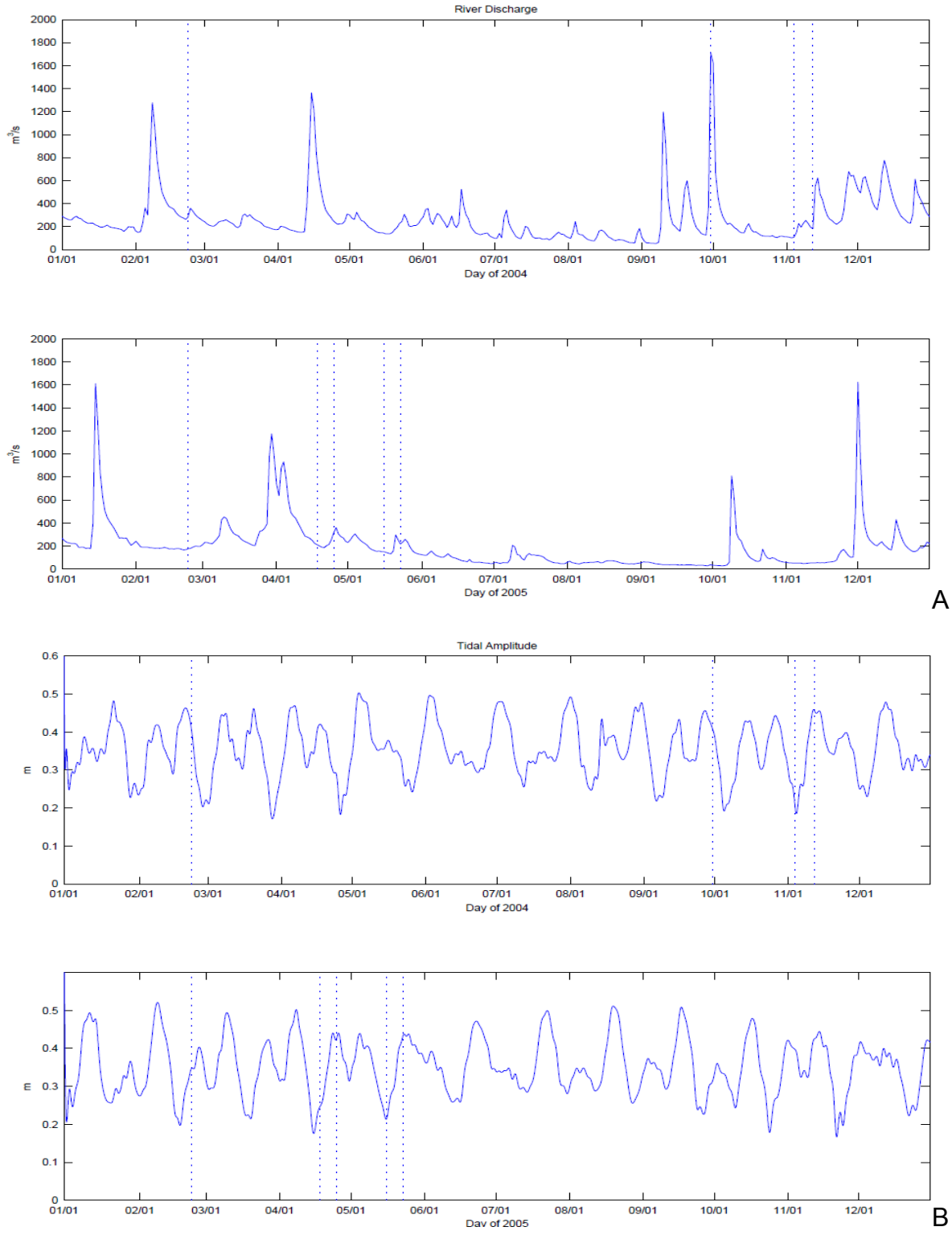

Figure 2-2. Annual river flow rates and tidal elevations. A) For the year 2004. B) For the year 2005. Measurements were taken for discharge and elevations at a station near Richmond, VA, and at Sewells Point, Norfolk, VA, respectively.

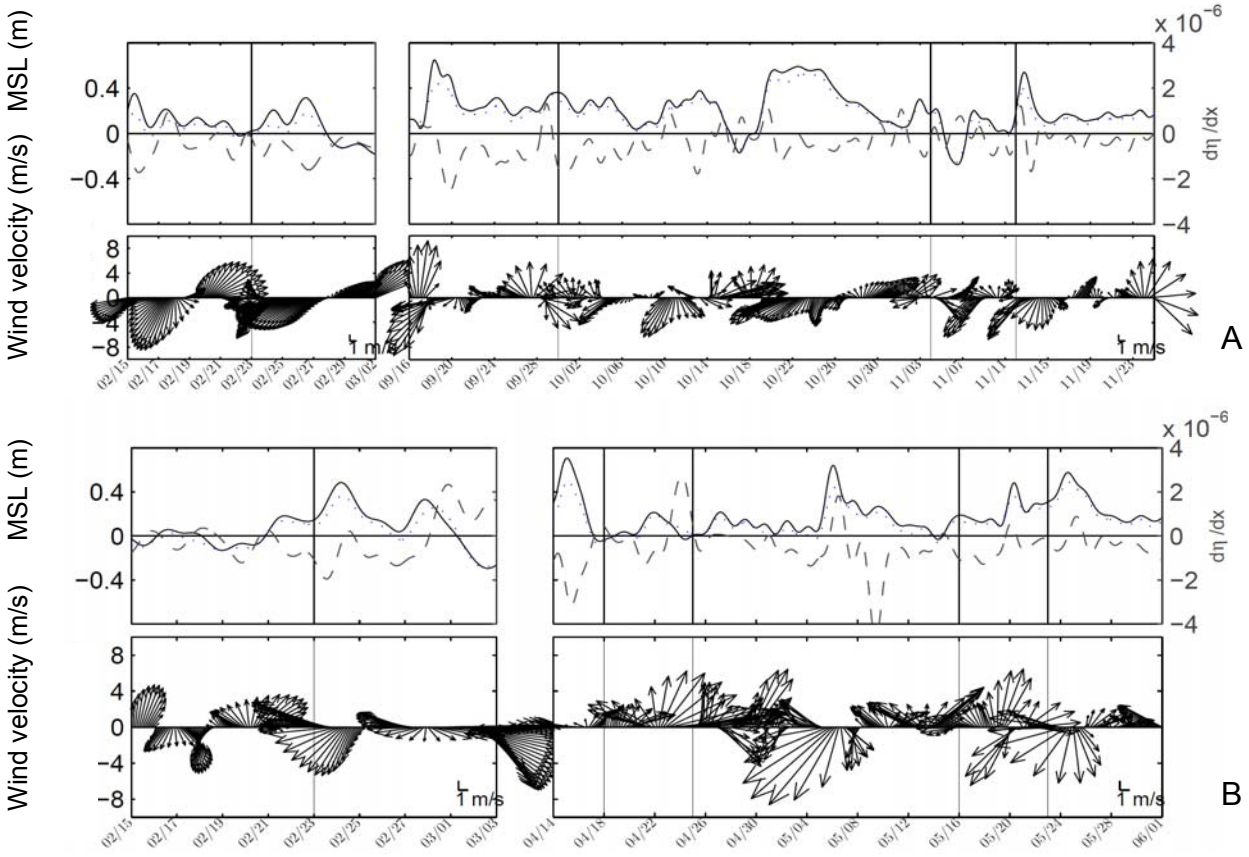

Figure 2-3. Mean surface elevations and wind directions at the Sewells Point. A) For the year 2004. B) For the year 2005. The gradients (dashed gray lines) were calculated based on the measurements at Sewells and CBBT.

CHAPTER 3
DATA COLLECTION AND PROCESSING

Data were collected from a 2 km long, cross estuary transect at Hampton Roads, Virginia under different tidal forcing, wind forcing and river discharge conditions in 2004 and 2005. In order to observe fortnightly variations, the transect was sampled during three successive neap - spring tidal cycles (November 4 – 12, 2004, April 18 – 25, and May 16 – 23, 2005). Four surveys took place during spring tides (February 23, September 30, 2004, January 26, and February 23, 2005) and were also included to illustrate seasonal variability. Anchored station data (January 26, 2005) were obtained from a location that was ~1.4 km upstream of the center of transect (Figure 2-1), and used to evaluate the vertical advection term, wu_z.

Continuous velocity measurements and station density profiles were obtained over a period of approximately 12-13 hours, with RD instruments acoustic Doppler current profiler (ADCP) and a Sea Bird (SBE-25) conductivity-temperature-depth (CTD) recorder, respectively. The towed ADCP collected 1 s pings, which were averaged over 20 ensembles, along transect. This gave a horizontal resolution of ~50 m, cruising at ~2.5 m/s. The vertical bin size was 0.5 m for the data set collected in 2004 and the anchored ADCP, and 1 m for the rest of the data. Data were compass-calibrated and corrected by the method of Joyce (1989) using Global Positioning System data. For each data set trajectory repetitions on average 15 were carried out. The CTD profiles were recorded at 4 different stations, three of which were along transect (Figure 2-1). The CTD profiles taken from Station 4 were used to calculate the horizontal baroclinic pressure gradient. This station was occupied during the surveys in 2005.

Hourly time series of mean sea level, wind speed and direction were obtained from Sewells Point (station # 8638610), which is at the entrance to the James River in Norfolk, Virginia (Figure 2-1) and maintained by NOAA's National Ocean Service. Historical and present data are available on their website (http://tidesandcurrents.noaa.gov). All records of sea level and wind velocity were low-passed with a 34-hr Lanczos filter to eliminate tidal variability. Tidal elevations for Sewells Point are shown in Figure 2-2a.

Subtidal for low-passed sea level data were used to calculate the barotropic pressure gradient. Since the two stations (i.e., Sewells and CBBT) are not on the same axis, a method that depends on the celerity is used. The celerity was calculated by least square fitting the mean sea levels to M_2, N_2 and S_2 harmonics, and finding the phase difference between two stations. The coordinate system used in this study was illustrated in Figure1. The x-axis coincides with the along-estuary direction and is positive toward the mouth of the estuary. Looking into the estuary, the y-axis is positive toward the right (Figure 2-1). The z-axis is positive upward. The along estuary direction was identified as that of maximum tidal current variance for the cross section. Time series of current velocities at each depth were rotated (~25°T) to match the coordinate system. The principal component of flow, u represents inflows and outflows and the lateral component, v represents the flow aligned with the transect. For each transect repetition, the flow components were interpolated onto a regular grid with a resolution of 100 m in the horizontal and 0.5 m in the vertical. The time series of flow components (u, v) at each grid point were fitted to semidiurnal (M_2 = 12.42 h), quarter-diurnal (M_4 = 6.21 h), and sixth-diurnal (M_6 = 4.14 h) harmonics using a least-squares method.

$$(u,v) = (u_0, v_0) + \sum_{j=1}^{m} (u_{Aj}, v_{Aj}) \sin(w_j t + u_{\theta j}, v_{\theta j}) \quad (3\text{-}1)$$

Here u_0 and v_0 are the residuals; m is the number of harmonics; u_{Aj} and v_{Aj} the amplitudes of the harmonic j of frequency w_j; $u_{\theta j}$ and $v_{\theta j}$ the phases for each harmonic; t is the time. The goodness of fit test was used to decide on how many harmonics to include. Mostly the best fit was obtained by including three constituents (M_2, M_4 and M_6) except for the data sets from Nov 12, 2004 and April 25, 2005 (M_2 and M_4).

By using the tidal parts of the velocity components (u and v), tidal variability of lateral advection was explored. Across channel patterns for lateral advective accelerations were extracted during peak ebb and peak flood. The times corresponding to peaks were chosen considering the tidal variation of cross-sectional averages of along-channel flow.

CHAPTER 4
RESULTS

4.1 Subtidal Flow

4.1.1 Volume Transport

The net transport through the cross-section, and some forcing agents (i.e., wind and tide) were summarized in Figure 4-1. At almost all surveys which lasted approximately 12 hours the net transport was into the estuary. Net outflow was observed at the 2nd survey due to the high river discharge.

4.1.2 River Discharge and Estuarine Adjustment

Since the river discharge data were taken from a station ~130-140 km away from the mouth of the estuary, it takes time for the peaks to reach to the mouth. To be able to estimate the river discharge effect on estuarine exchange, the age of water parcel should be known. Shen and Lin (2006) investigated the age of the water parcel distribution in the James River estuary using numerical model experiments. Their model results indicated that river flow is one of the dominant factors that influence mean age distribution. They found that it takes 95 and 35 days, respectively, for a water parcel to travel from the head to the mouth of the estuary under mean (200 m^3/s) and high river flow (700 m^3/s) conditions. In this study the lag was considered as ~20 to 30 days. The tidally averaged salinity profiles were also utilized to decide on the lag (Figure 4-2). We can consider that the 6th survey was affected by peak discharge rates prior to the survey date. The influence can be clearly seen from the salinity profile with stratification, showing a range between 10 to 25 psu acting in concert with weak tidal forcing. The 7th survey on April 25th 2005 showed a similar stratified characteristic with a smaller range due to higher tidal forcing.

The estuary may not re-adjust itself fast even after the peak discharge leaves the estuary. Re-adjustment time may take weeks depending on both the time scale of forcing variations and the sensitivity of estuary to changes in river discharge and tidal mixing. Studies showed that the sensitivity of an estuary is greater for high river discharge rates (Lerczak et al., 2008). Higher stratification observed on the 3rd, 5th and 8th surveys can be partly attributed to this adjustment time, together with weak tidal forcing. Discharge peaks (e.g., around 1600 m^3/s) prior to 3rd and 5th surveys, and longer lasting peaks prior to 8th survey affected the stratification.

4.1.3 Along-Channel Flow

In most observations the tidally averaged along-channel flow was laterally sheared, with saline water inflow and freshwater outflow, respectively, over the northern and the southern portion of the cross-section (Figure 4-3). However, each survey showed different exchange flow structure due to different forcing agents which lead to vertically sheared flow either to dominate or coexist with laterally sheared flow. Stronger flows were observed during spring tides due to higher tidal forcing (e.g., 1st, 2nd, 4th, 5th, 7th, and 9th surveys) (Figure 5). The salinity profiles also reflected this fortnightly variability, more stratified at neaps than at springs (i.e., 3rd, 6th and 8th surveys).

Comparing the river discharge rates to the salinity profiles for the 1st survey, the big pulse of 1200 m^3/s on February 10th didn't seem to reach to the mouth on the date of survey. Strong tidal forcing (0.4 m of amplitude) together with the low river discharge approximately 200 m^3/s, caused friction to dominate. In the 2nd survey the subtidal exchange flow was both laterally and vertically sheared. The peaks in river discharge

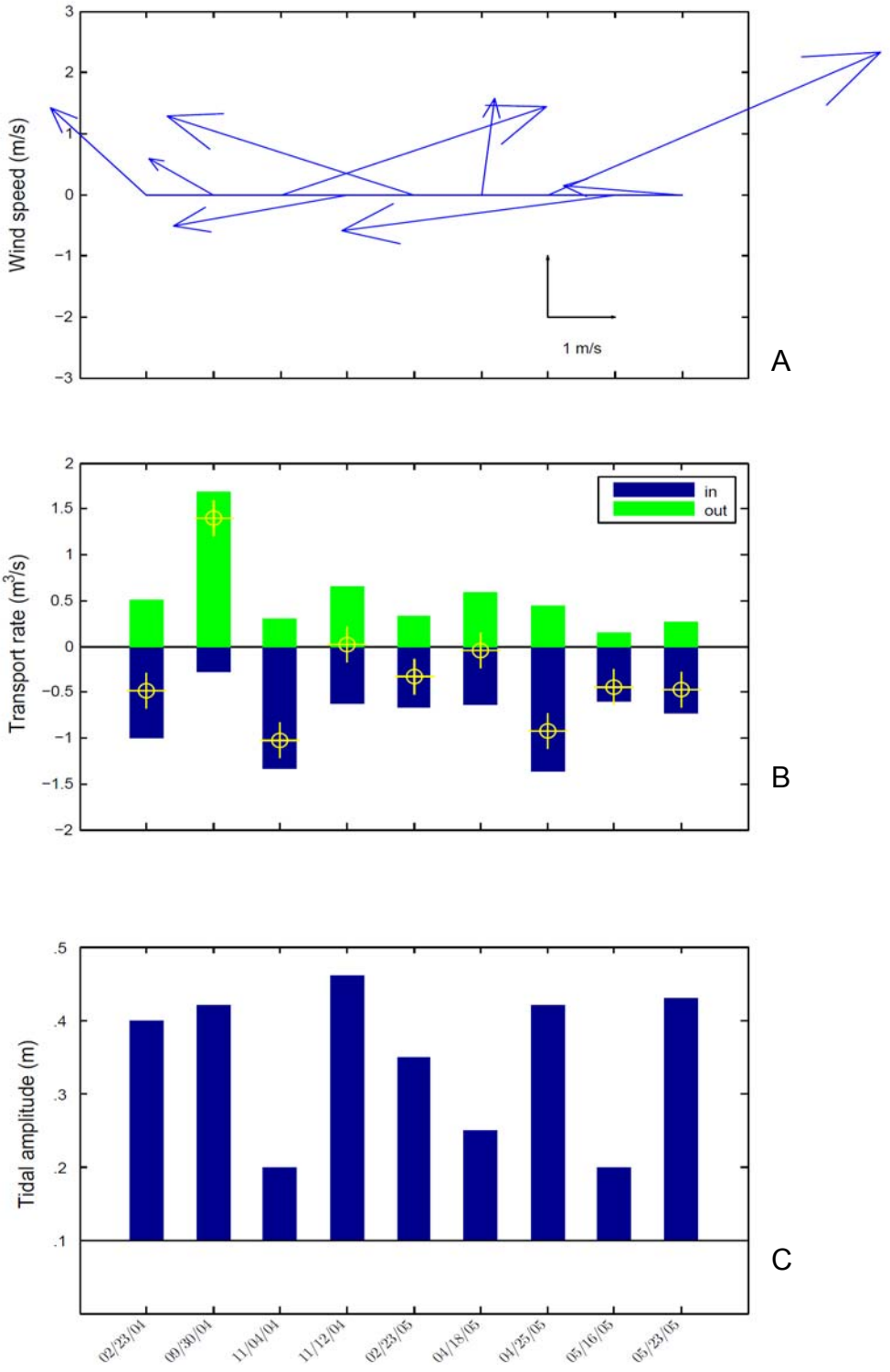

Figure 4-1. Hydraulic conditions. A) Daily wind speeds. B) Volume transport along the first cross-section. C) Tidal elevations at Sewells Point.

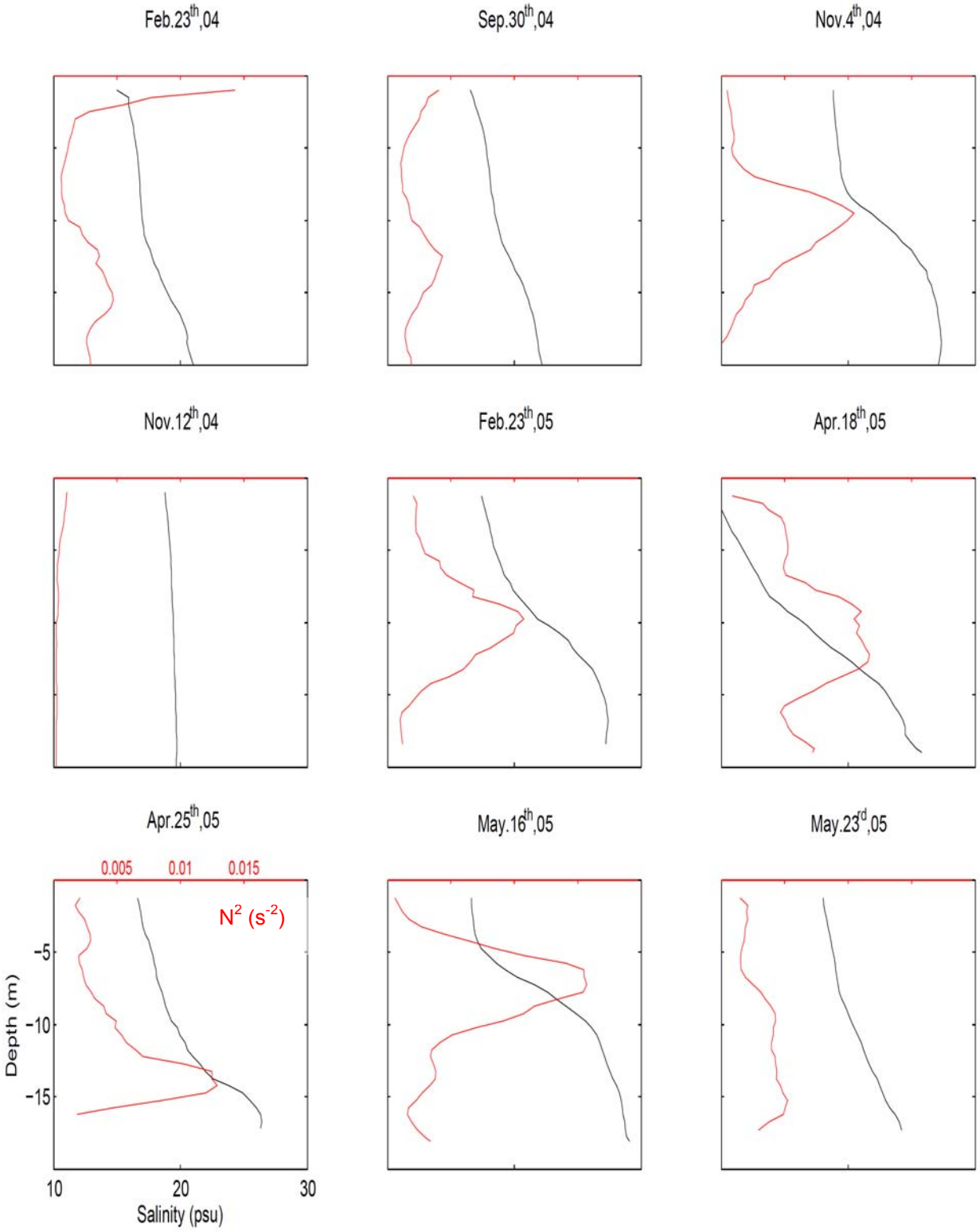

Figure 4-2. Subtidal salinity profiles and squared buoyancy frequencies. The plots presented are for the second station in the channel.

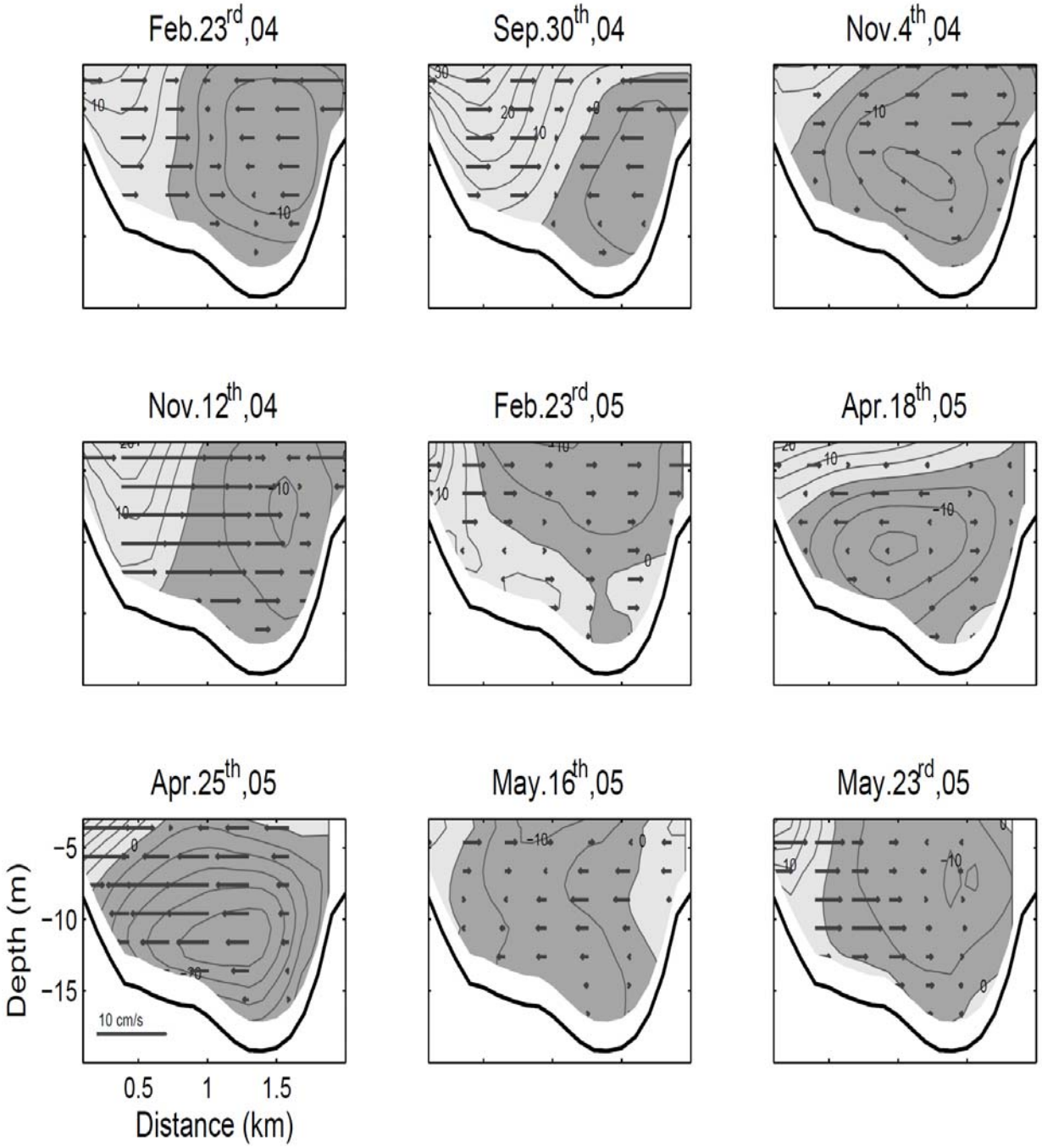

Figure 4-3. Subtidal along-channel and transverse flow for Transect 1. Darker and lighter shades represent landward and seaward flows, respectively and the units are in cm/s.

prior to the date of survey probably reached the estuary's mouth causing high outflow rates at the observed section. The net volume transport was out of the estuary, dominating the surface portion of the section and restraining the inflow closer to the bed, while keeping the lateral shear at depth. The 3rd survey (Nov 4th 2004) results showed inflow-dominated laterally sheared exchange flow. The strongest flows developed at a depth of ~11 m. Three peaks in river discharge prior to the survey caused a delay in the estuarine adjustment. Due to this delay and low tidal mixing rate (Neap tide with amplitude of 0.2 m), the isohalines were squeezed between 10 m and 15 m depth at Station 2. The last survey of 2004 (Nov 12th) was carried out a week later so as to observe the fortnightly variability. The exchange flow patterns showed a laterally sheared flow structure, which was similar to the first survey results. The spring tides had the highest amplitude (0.46 m) when compared to the rest of the observations. Higher tidal amplitude coupled with low discharge rates lead to a well mixed water column at all hydrographic stations.

The first survey from 2005 Feb 23rd, exhibited an exchange flow pattern that consisted of both vertically and laterally sheared structure. The denser water appeared to be flowing both at the thalweg and near surface. The tidal amplitude was 0.35 m, the weakest among all spring tide observations, leading to a stratified water column at Station 2. The delay in re-adjustment caused by a river discharge peak of 1600 m^3/s contributed to the stratification. Vertically sheared exchange flow was observed on April 18th, with saline water flowing landward near bed and fresher water flowing seaward near surface. The river discharge peak prior to the observation affected the circulation causing the salinity of the surface water to drop 10 psu. The successive spring tide on

April 25th showed a similar exchange flow pattern with lateral variation near the surface. The last two surveys showed laterally sheared exchange with landward flow in the channel and seaward flow over the shoals. The stronger landward fluxes appeared near the surface.

Buoyancy frequencies, N^2 were also calculated at the mid-transect to determine the stability of the water column (Figure 4-2). Strong stabilities were mostly observed at mid-depths. Instabilities occurred near bed and near surface, respectively due to bed stress and wind stress. The flow patterns shown in Figure 4-3 can be produced by baroclinic pressure gradients and by wind forcing, and modulated by tidal forcing and curvature effects. These processes will be explained next.

4.1.4 Wind Forcing

Both remote and local wind forcing can induce subtidal variability in estuaries. Remote forcing produced by winds on the adjacent continental shelf imposes sea level set-up or set-down at the mouth of the estuary and induces unidirectional flow throughout a cross-section (i.e., inflow or outflow, respectively) (Wong, 1994). Local forcing, on the other hand, induces bidirectional flow that is downwind near surface and upwind near bottom (Wong and Valle-Levinson, 2002). A lateral structure in bathymetry might cause the unidirectional remotely forced flow to be strongest over the deepest part of the cross-section (Wong, 1994), and the bidirectional locally forced flow to appear as laterally sheared, downwind over shallow and upwind at depth (Sanay and Valle-Levinson, 2005). The influence of lateral changes in bathymetry on local forcing also depends on stratification that shifts the laterally sheared pattern to vertically sheared pattern with downwind flow at the surface and upwind flow underneath (Guo and Valle-Levinson, 2008).

4.1.4.1 Local forcing

To examine the influence of local wind forcing on the exchange flow patterns, daily wind speeds and directions were analyzed. The highest wind speeds were observed during the on 3rd, 5th, 7th, and 8th surveys blowing at a range between 4.0 and 5.5 m/s. The rest of the observations showed weaker wind forcing ranging between 1.0 and 2.5 m/s. The exchange flows corresponding to southwesterly winds (i.e., 3rd and 7th survey) showed inflow domination at depth. The vertically sheared behavior can be partly attributed to local wind forcing, which drives upwind flow near bed and downwind flow near surface. The subtidal salinity profiles at 2nd station are also in agreement with such structure showing increased stratification from wind straining (Li et al., 2009).

Winds were northeasterly on the 4th and 8th surveys. Weak wind speed on the 4th survey yielded weak local forcing. When the subtidal patterns were considered, there was a strong lateral shear, reminiscent of local wind forcing for a well mixed water column. At the 8th survey, downwind flows near surface and near bottom in the channel, and upwind flows over shoals were observed. Southeasterly winds in 5th survey caused upwelling near the bed on the southern side of the transect. Along with the weak tidal amplitude (e.g., relative to the rest of the spring tides), southeasterly winds stratified the water column in the 5th survey.

The Wedderburn number was calculated in order to examine whether the reversal of flows observed on the 5th, 8th, and 9th surveys (i.e., surface inflows and bottom outflows) were due to wind forcing overpowering the baroclinic pressure gradient forcing, or not. The relative importance of the wind and buoyancy forcing can be represented by a Wedderburn number (Geyer, 1997 and Sanay, 2003):

$$W = \frac{\tau_S l}{g\Delta\rho H^2} \quad , \ \tau_s = \rho_a c_d w^2 \tag{4-1}$$

where τ_s is the wind stress, g is the acceleration of gravity, H is the mean water depth, $\Delta\rho/l$ is the horizontal density gradient, ρ_a is the density of air, and w is the wind speed. The drag coefficient, c_d was calculated as (Yelland and Taylor, 1996):

$$\text{For } 3< w <6 \text{ m/s;} \quad 1000c_d = .29 + 3.1/w + 7.7/w^2 \tag{4-2}$$

Values of W>1 indicates domination of wind forcing over baroclinicity. The calculations yielded Wedderburn numbers close to 1 (i.e., 0.86, 0.81, and 0.69 for 5_{th}, 7_{th} and 8_{th} surveys, respectively) indicating that wind forcing was as strong as the baroclinic influences for these surveys.

4.1.4.2 Remote forcing

Near-mouth locations are very sensitive to remote forcing which may have greater influence on exchange flow than local wind forcing. Observations at the Chesapeake Bay entrance showed that remote winds have greater influence on the barotropic exchange at the mouth of the estuary than local winds in most cases (Wong and Valle-Levinson, 2002). The reverse is true under strongly stratified conditions.

In order to quantify remote forcing, the variation of mean sea levels and surface elevation gradients with respect to wind speed and direction were analyzed (Figure 2-3). The water level gradient was calculated by using the de-meaned and filtered sea level data from Sewells Point and CBBT (Chesapeake Bay Bridge Tunnel). Strong northeasterly and southeasterly winds caused the mean sea level to rise at Sewells Point, piling the water into the estuary. This resulted in negative gradients, and set down at the adjacent shelf. Southwesterly winds led to positive gradients due to set up. The trend of Sewells' surface elevations and surface gradients were mostly opposite to each

other. The remote forcing was prominent during 2005 surveys when the winds blowing prior to the survey date were strong. Southeasterly winds prior to the 5th and 8th surveys caused set-down, which yielded an increase in seaward flows whereas southwesterly winds blowing prior to the 6th and 7th surveys caused set-up, leading to increase in landward flow during the survey dates.

4.1.5 Curvature Effects and Lateral Flow

Lateral flows are driven by channel curvature, interactions between bathymetry and barotropic tidal currents, and differential advection of along-channel density gradient (Lerczak and Geyer, 2004). Model results for an idealized, tidally dominated estuary with a parabolic bathymetry showed that subtidal lateral circulation produced by Coriolis and lateral density gradients differ from each other. Counter-clockwise circulation was induced by Coriolis, whereas either clockwise or two-cell circulation (i.e., lateral flows converging near surface, and diverging near bottom) appeared depending on the lateral density gradient (i.e., constant or linearly increasing, respectively) (Huijts et al., 2006). Two-cell circulation was also shown by Peng and Valle-Levinson (2009) in their numerical results (i.e., without tidal forcing). They pointed out to the asymmetry in such circulation occurring under weak friction when Coriolis effects tilt the halocline upward from left to right (looking up-estuary). This tilt yields a stronger circulation on the right side of the channel.

Lateral flow patterns get more complex when the lateral variability of bathymetry and morphology of the estuary are taken into account. With the inclusion of lateral density gradients the complexity is further increased. Under well-mixed conditions around a curvature, helical flow (i.e., directed towards the bend near bed and out of the bend near surface) occurs due to centrifugal forcing if the along channel flow has a

logarithmic profile. For stratified cases, lateral density gradients may oppose curvature-induced lateral flow (Chant, 97). Buijsman and Ridderinkof (2008) analyzed the mechanisms that govern the lateral circulation around a bend with low curvature. They concluded that under stratified conditions lateral density gradients dominates over centrifugal and Coriolis accelerations whereas centrifugal accelerations dominate over Coriolis under well-mixed conditions. A field experiment showed that the development of baroclinic pressure gradient produces a three layered profile (Nidzieko et al., 2009) around curvature and causes reversed helical flow at the downstream of the bend.

To better represent the lateral flow patterns, depth averaged values were subtracted (Figure 4-3). At most of the surveys 3-layered lateral flows were observed except in the 1st and the 4th surveys, when one-cell counter-clockwise circulation persisted. Spring tides caused tilted 2-cell circulations. As the tidal amplitude decreased, and stratification increased, lateral flow patterns became more vertically sheared causing counter-clockwise circulation near bottom and clockwise circulation near surface (e.g., 3rd, 5th, 6th and 8th surveys). Due to bed friction and lateral variability of the bathymetry, the magnitude of the flows decreased with depth.

Two bends; one near Norfolk, and the other at Newports News with a larger radius (i.e., on the southern end of transect, and upstream from the northern end of transect, respectively) influenced the lateral flow. Curvature induced helical flow near the southern side of the cross-section can be seen on the 2nd, 3rd, 5th, 7th and 8th surveys. The tilted two-cell circulations due to Coriolis forcing were observed at spring tides. One-cell circulations on the 1st and 4th surveys can be attributed to the minimal influence of lateral density gradients. Strong northward lateral flows seen on some surveys might

be related to the discharge of the Elizabeth River draining near the mouth. During neap tides three-layered lateral flows accompanied by clockwise circulation near surface and counter-clockwise circulation near bed, became prominent.

The influence of morphology on lateral flow can be clearly seen from a 3rd transect which was located between the 1st and the 2nd transects (Figure 4-4). Moving along the transect, either the velocity profiles shifted from 3-layered to 2-layered, or changed their sign. This might be due to the reduced influence of curvature near Norfolk, and increased influence two rivers draining into James River close to the mouth. Also as stated above, exit of the curvatures may carry the reversed helical flow patterns. The 5th and 9th surveys showed this lateral flow distribution, due to the curvature near Newport News.

Lateral density gradients are relevant in driving lateral flows. Huijts at.al. (2006) showed that for Ekman numbers greater than ~0.03 lateral transport mostly driven by lateral density gradients rather than Coriolis as lateral density gradients dominates over horizontal density gradients. For the James River their calculation yielded $\rho_y \cong 1.75\ \rho_x$. Subtidal lateral density gradients were demonstrated in Figure 4-5 along the first transect by using the density profiles from 2004 CTD casts. Modulation in lateral density gradients can be seen in Figure 4-5, showing laterally or vertically sheared structure depending on the tidal forcing and river discharge. For the high river discharge rates (i.e., 2nd survey) the gradients became more vertically sheared. The tidal variation of lateral density gradients is also important for they may introduce asymmetries in lateral flow.

The complex flow patterns observed may also be related to the asymmetries in tidal straining which causes tidal residuals and affect lateral transport. Due to the asymmetric vertical mixing, flood and ebb flows can present different lateral flow structures. Tidal residuals can carry either one of the structures depending on the strength and duration (i.e., flood dominant or ebb dominant).

.

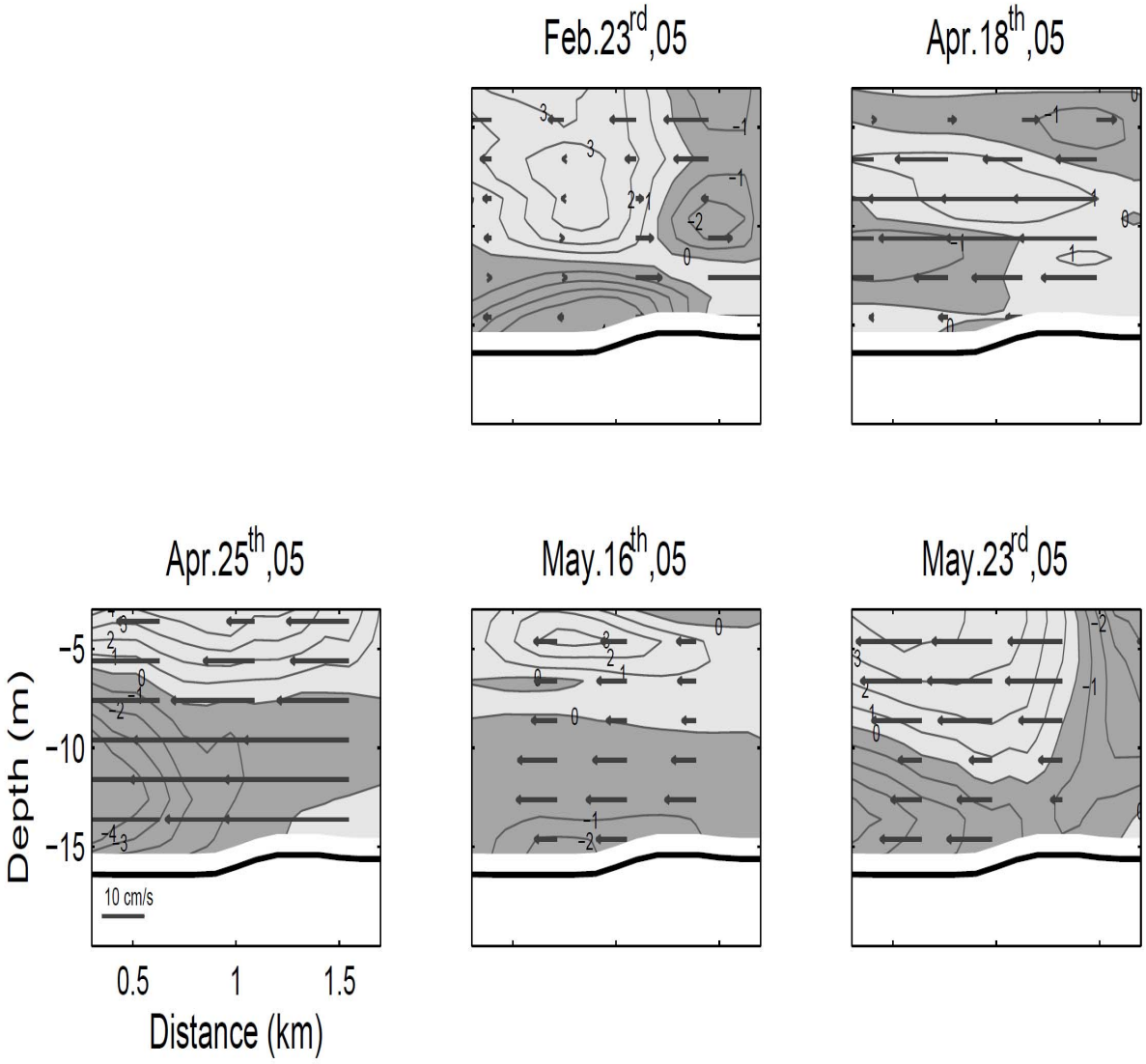

Figure 4-4. Subtidal transverse flow for Transect 3. Contours represent the transverse flow; positive values denote northward flow and negative values denote southward flow. Along-channel flow is shown as vectors.

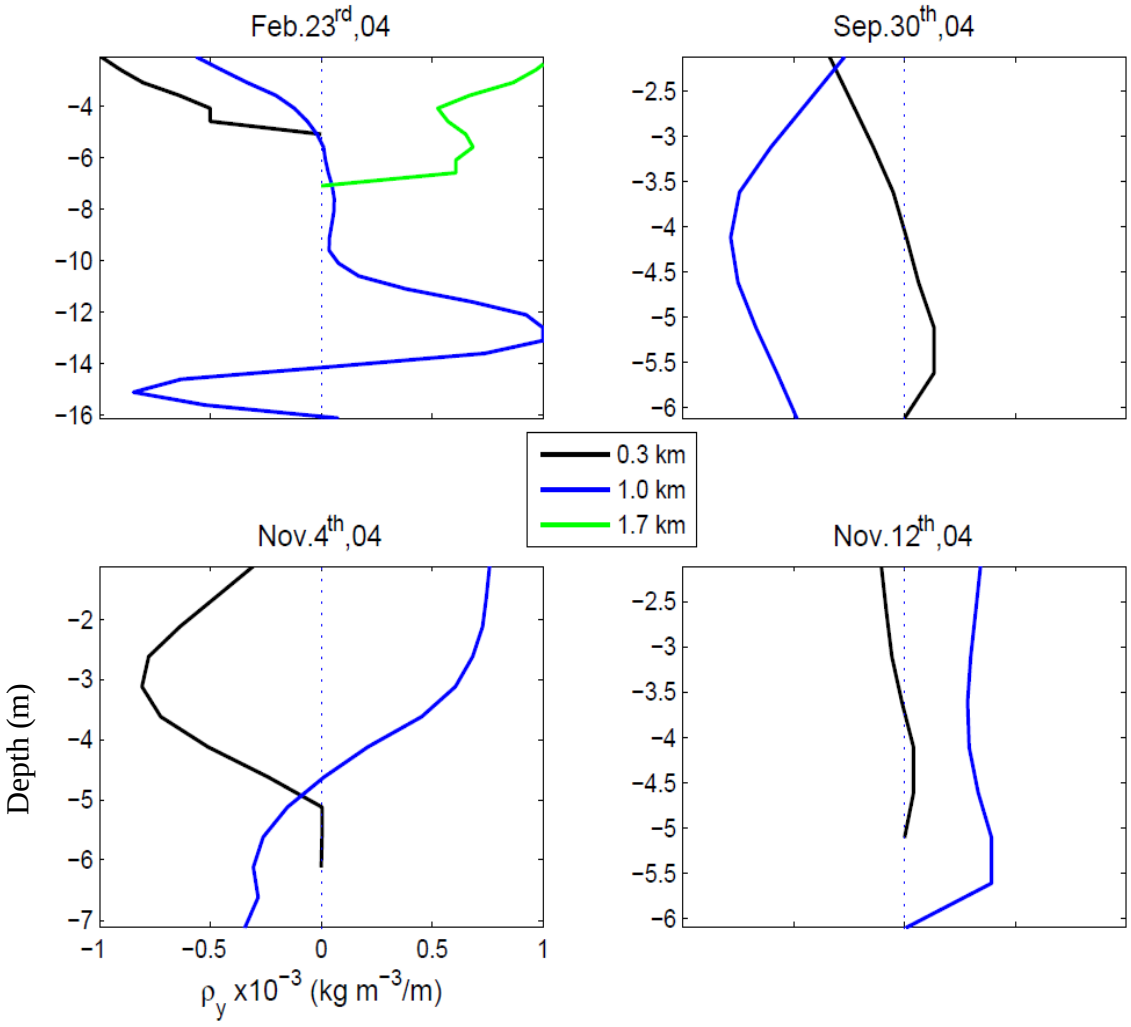

Figure 4-5. Lateral density gradient profiles along Transect 1. Distances to southern end are shown in the legend.

4.1.6 Along-Channel Momentum Balance

The relative importance of lateral advection was investigated by quantifying the terms contributing to the momentum balance. Along -channel momentum equation can be written as:

$$\frac{\partial u}{\partial t}+u\frac{\partial u}{\partial x}+v\frac{\partial u}{\partial y}+w\frac{\partial u}{\partial z}-fv=-g\frac{\partial \eta}{\partial x}-\frac{g}{\rho}\int_z^{\eta}\frac{\partial \rho}{\partial x}dz+\frac{\partial}{\partial x}\left[A_x\frac{\partial u}{\partial x}\right]+\frac{\partial}{\partial y}\left[A_y\frac{\partial u}{\partial y}\right]+\frac{\partial}{\partial z}\left[A_z\frac{\partial u}{\partial z}\right] \qquad (4\text{-}3)$$

where u, v, and w are velocity components in along-estuary, cross-estuary and vertical directions, f is the Coriolis parameter, η is the surface elevation, ρ is the water density, A_i (i=x,y,z) is the eddy viscosity. The first term on the LHS stands for the temporal variation of along-channel flow, the next three terms represent the nonlinear advective terms (horizontal, lateral and vertical advection), and the last term represents the effects of Earth's rotation. The first two terms on the RHS stand for pressure gradient (barotropic and baroclinic) and the rest of the terms stand for mixing/friction in three directions. It can be simplified to the form below by keeping the vertical mixing term as rest of the mixing terms are insignificant when compare to vertical mixing.

$$\frac{\partial u}{\partial t} + u\frac{\partial u}{\partial x} + v\frac{\partial u}{\partial y} + w\frac{\partial u}{\partial z} - fv = -g\frac{\partial \eta}{\partial x} - \frac{g}{\rho}\int_z^\eta \frac{\partial \rho}{\partial x}dz + \frac{\partial}{\partial z}\left[A_z\frac{\partial u}{\partial z}\right] \quad (4\text{-}4)$$

In this study, using available information from observations, the lateral and longitudinal advection, Coriolis, baroclinic and barotropic pressure gradient and vertical mixing terms were calculated. The Coriolis parameter, f was calculated as $8.8\text{x}10^{-5}$ s^{-1}. The density data from CTD casts at station 2 and 4 was used to get the baroclinic pressure gradient.

In order to calculate the barotropic pressure gradient more precisely, celerities for each date were utilized (Lacy and Monismith, 2001). This was achieved by finding the phase differences between the least squared fitted mean sea levels of Sewells Point and CBBT, getting the tidal variation of this term with the relation given below. M_2, N_2 and S_2 harmonics were included to the fit, and the phase difference of the biggest contributor M_2 was utilized. Celerity was found out to be in the range of 5-8 m/s.

$$g\frac{\partial \eta}{\partial x} = \frac{g}{c}\frac{\partial \eta_{Sewells}}{\partial t} \quad (4\text{-}5)$$

A Richardson number dependent turbulent closure (Pacanowski and Philander, 1981) was used to determine the vertical eddy viscosity coefficient, A_z. This closure performs best among the low order schemes (Nunes Vaz and Simpson, 1994).

$$A_z = 0.01(1 + 5R_i)^{-2} + 10^{-4} \tag{4-6}$$

$$R_i = \frac{\frac{g}{\rho_0}\frac{\partial \rho}{\partial z}}{(\frac{\partial u}{\partial z})^2 + (\frac{\partial v}{\partial z})^2} \tag{4-7}$$

Here R_i stands for gradient Richardson number, a dimensionless ratio of buoyant production of turbulence to shear production of turbulence. The density data from CTD casts along the transect (e.g., 3 casts from 2004 surveys and 1 cast from 2005 surveys) was used in calculating R_i. Calculations for R_i, and A_z are shown in Figure 4-6. As can be seen from the figure the Richardson number for the first 4 cruises is close to the critical (R_i =0.25), which means high turbulence, and eventually mixing. The R_i values less than critical, denote dynamical instability. The vertical eddy viscosity coefficients were in the range of 10^{-4} to 10^{-2} m^2/s, increasing near bed (due to bed friction), and near surface (due to wind forcing). In some plots it was greater in the mid-depth, due to internal friction. Squeezed isopycnals increased Ri. In turn the frictional term can be expressed as in equation 4-8. This decomposition represents mean and oscillating part.

$$\overline{(A_z u_z)}_z = (\overline{A_z}\,\overline{u}_z)_z + \overline{(A'_z u'_z)_z} \tag{4-8}$$

Geyer et al. (2000) found that the oscillating part of the friction term contributes more to the dynamics in Hudson River, whereas observations from James River showed that oscillating and mean parts make similar contributions (Valle-Levinson et al., 2000). The oscillating part of the friction term was calculated separately here and

compared to the total friction term to see whether the oscillating part was dominant or not. The oscillating part gave results very close to the total, meaning that at the estuary entrance this part became more pronounced (Figure 4-7).

The absolute value of each term in equation 4-4 was cross-sectionally and tidally averaged (Figure 4-8). On the first four surveys the friction term was dominant. The influence of barotropic forcing was the strongest on 2005 surveys except for the 6th survey, which showed higher baroclinicity. Friction and lateral advection had similar contribution to the balance dominating over baroclinic pressure gradient. The lateral advection term was of the same order of magnitude as the rest of terms in the balance. On all the surveys carried out, the Coriolis term had the least contribution to the balance

4.1.7 Lateral Advection

The lateral advection term was calculated by using the observations. As stated previously the tidal and sub-tidal parts of the velocity components (u and v), were obtained by applying least square fit to the observations for each grid point over the entire cross-section. After that, the tidal lateral advection term vu_y was calculated for each grid, as follows.

$$\overline{vu}_y = \overline{v}\,\overline{u}_y + \overline{v'u'_y} \tag{4-9}$$

$$\overline{v'u'_y} = \frac{1}{n}\sum_{t=t_1}^{t=t_n} v'_t \frac{\Delta u'_t}{\Delta y} \tag{4-10}$$

The tidally averaged lateral advection term was obtained by taking the mean over a tidal cycle (Eq. 4-10). Tidal averages of the oscillating part $\overline{v'u'_y}$ were compared to the mean part, $\overline{v}.\overline{u}_y$ (Figure 4-9). Except for the second survey when the outward flux was dominant, the absolute values of cross-sectional averages of $\overline{v'u'_y}$ were greater

than $\bar{v}.\bar{u}_y$. The fortnightly variability can also be seen clearly from the sectional averages, spring surveys having the stronger advective fluxes with respect to neaps. The magnitude of tidally averaged lateral advection term was found out to be in the order of 10^{-5} m/s^2.

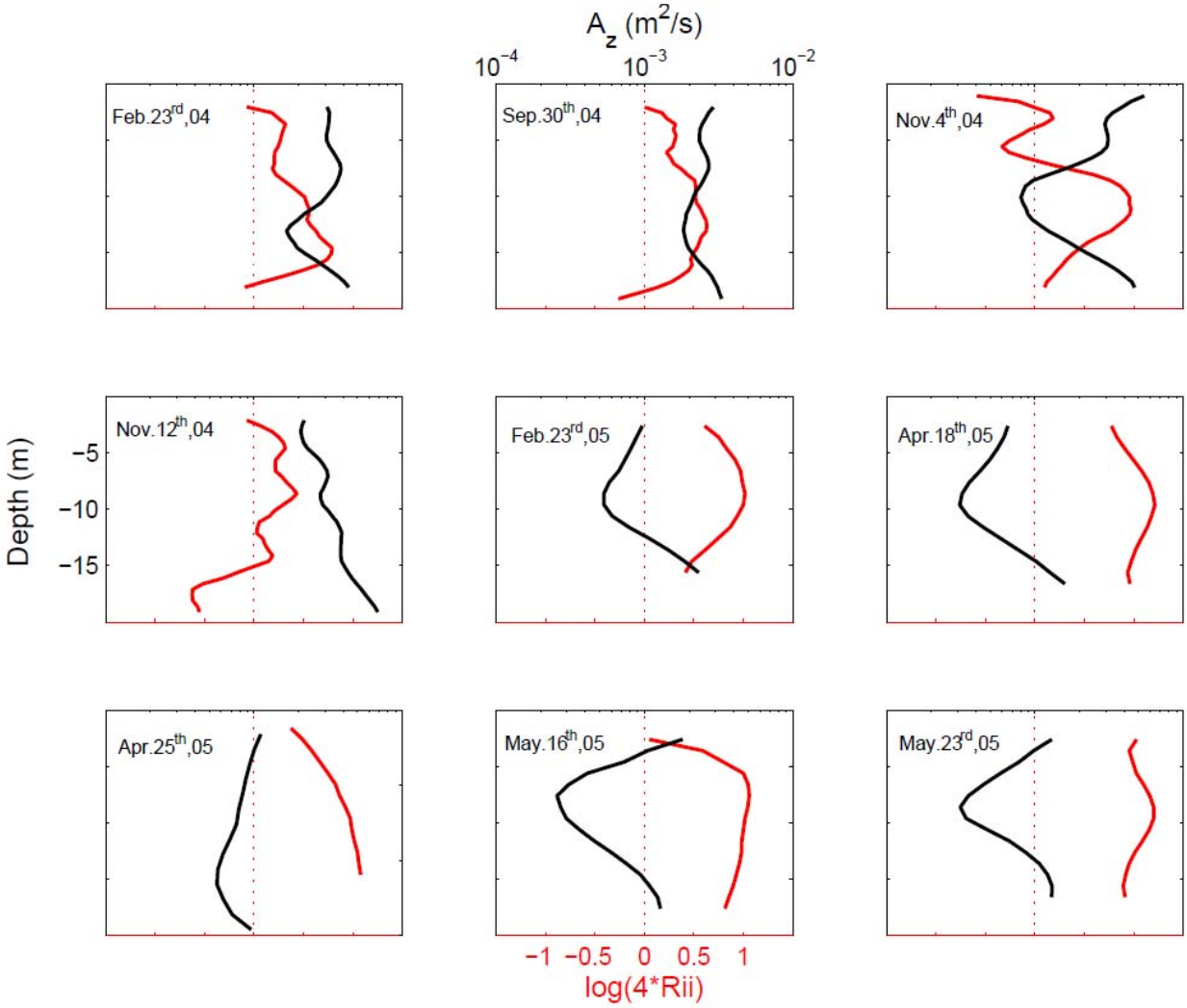

Figure 4-6. Vertical mixing coefficient and Richardson number profiles. The profiles are obtained for Station 2 in the channel. Critical R_i (= 0.25) number marked as a dotted line.

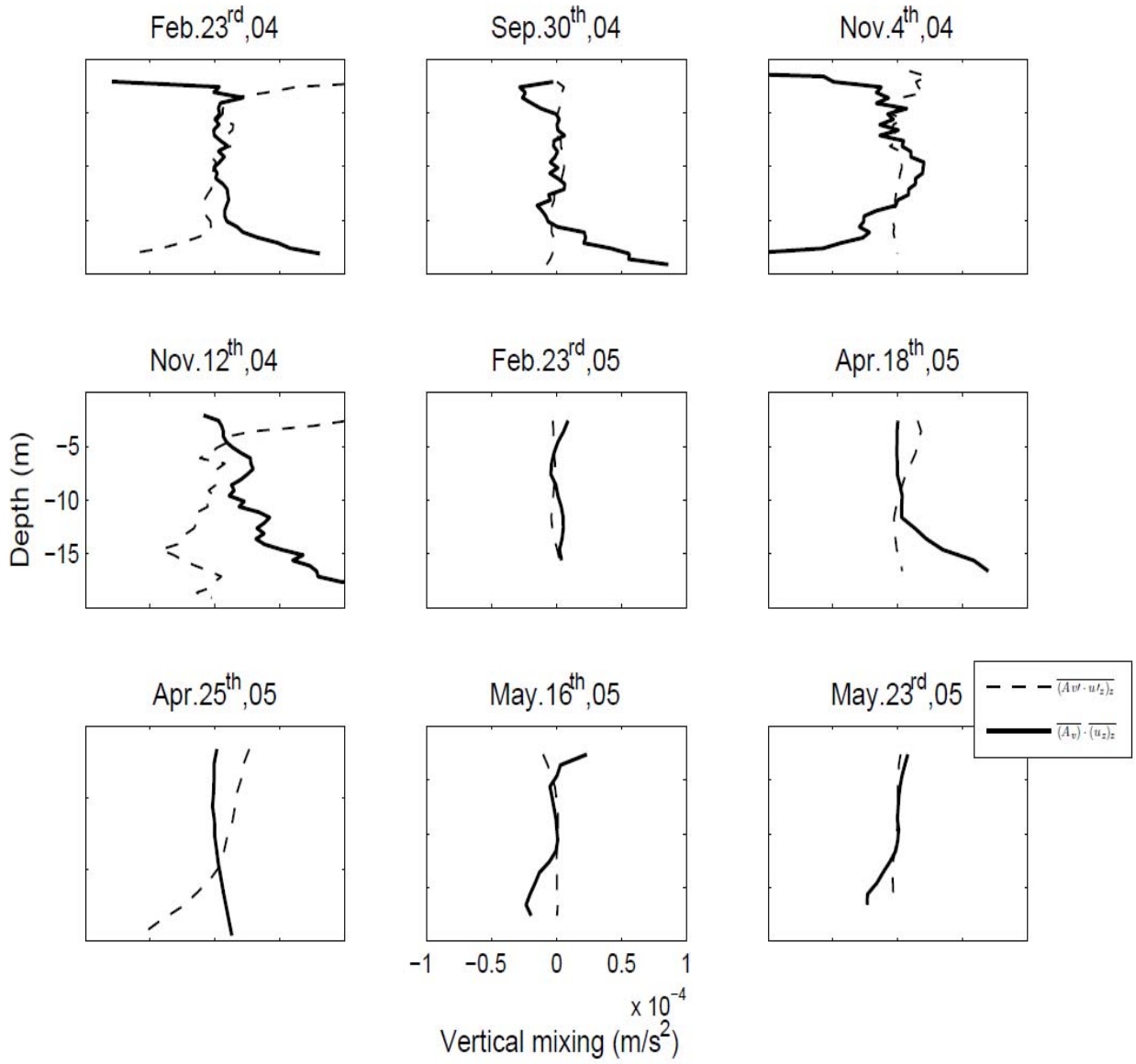

Figure 4-7. Subtidal vertical mixing. The profiles are obtained for Station 2.

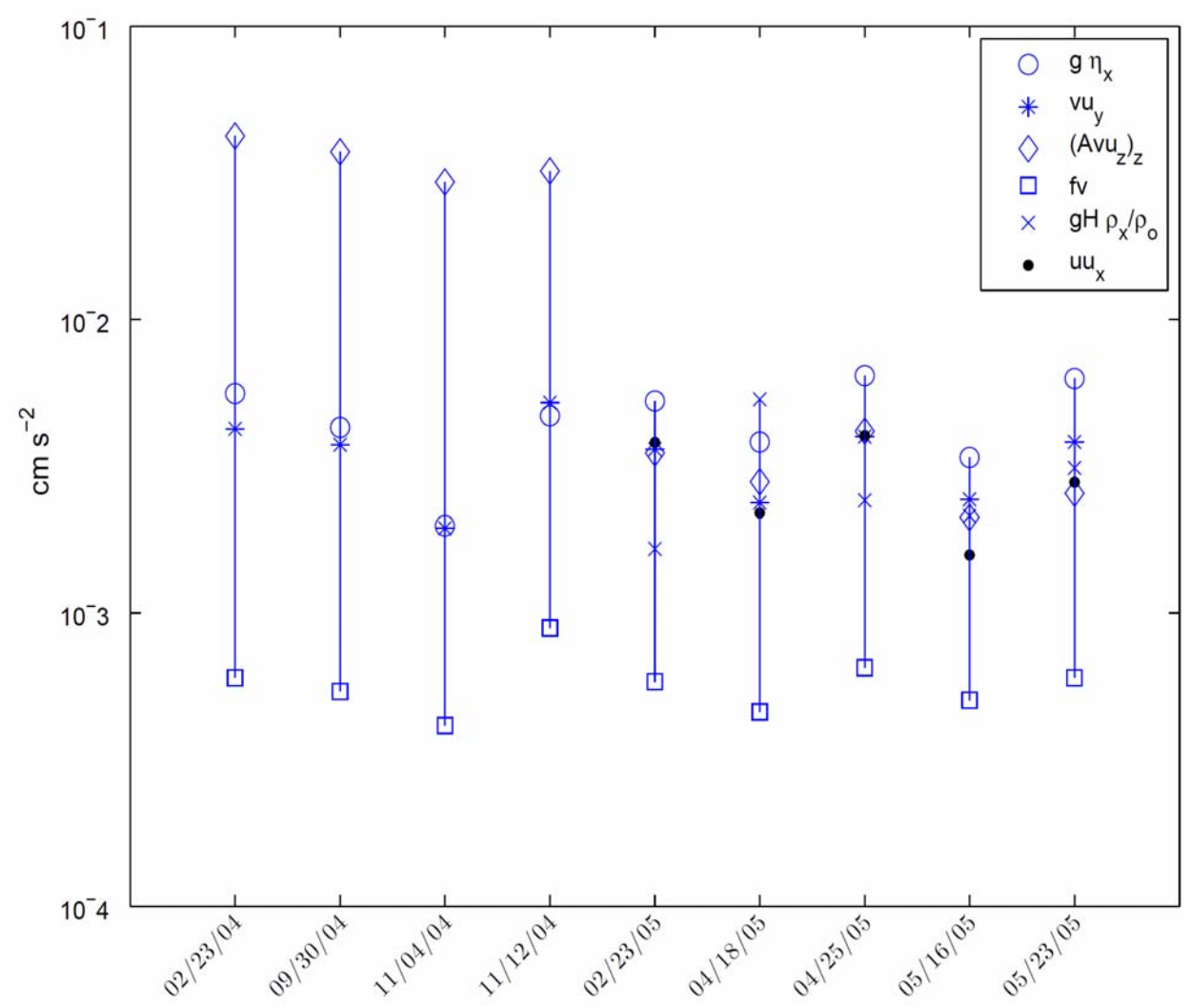

Figure 4-8. Cross-sectional averages of absolute values of terms in along-channel momentum balance.

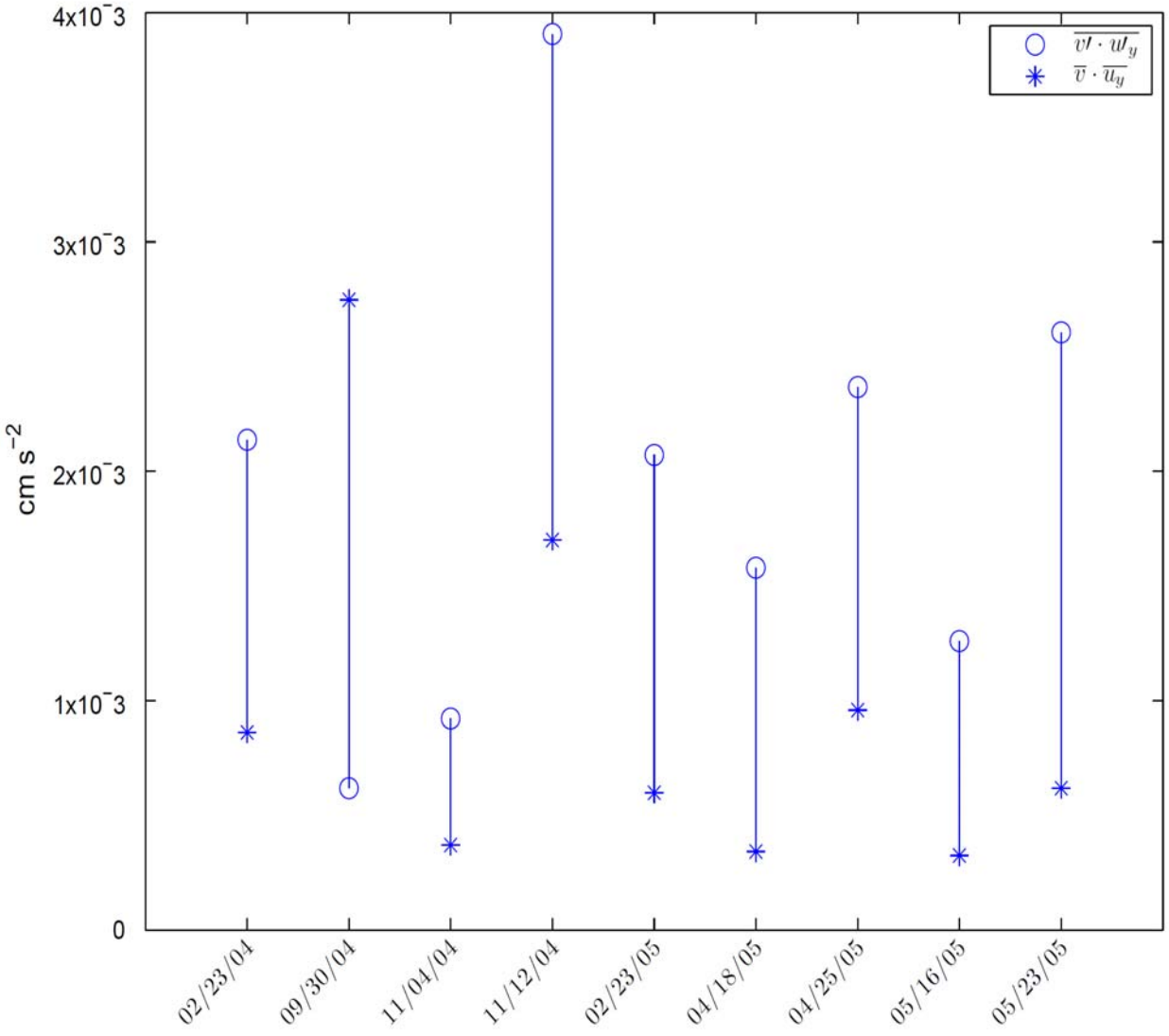

Figure 4-9. Cross-sectional averages of lateral advection.

4.1.8 Lateral Advective Flux Patterns

All surveys showed landward lateral advective fluxes near bed, over abrupt bathymetry changes and steep slopes (Figure 4-10). The landward fluxes were prominent with respect to seaward fluxes. The seaward advective fluxes were mostly stronger near surface or mid-depths of the water column. The mid channel seaward fluxes developed at the depth where the stability was maximum, in other words where

the stratification was greatest. The modulation caused by fortnightly variability was clear yielding stronger fluxes at spring tides than neap. As tidal forcing decreased so did the magnitude of accelerations. Not only did fortnightly variability alter the strength of fluxes, but patterns as well. At spring tides, when the tidal mixing was higher, the seaward accelerations had a tendency to appear on the northern side of the transect whereas at neap the seaward accelerations were strongest over the shallow southern side.

Landward accelerations were dominant at spring tides and seaward accelerations occupied mostly the northern side of the transect. Depending on contributions of the forcing mechanisms, the seaward fluxes shifted from surface to near bed. As friction increased the seaward flux concentrated at the center of the cross-section. This can clearly be seen on both friction (e.g., 1st and 2nd) and barotropic (e.g., 5th and 7th) terms that dominated spring tide surveys. As the contribution of lateral advection to the momentum balance increased, the seaward flux occupied the whole water column over channel (e.g., 4th and 9th surveys). The up-estuary southeasterly winds caused the landward accelerations increase over the shoals.

Seaward accelerations were dominant at neap tide surveys appearing on the southern end of transect, mostly strongest near the surface. When the friction was high on Nov 4th the seaward accelerations were dominant near the surface. In the 6th survey, as the friction contribution decreased, the seaward flux dominated over the southern side of the cross-section. The 8th survey showed the highest influence of advective accelerations to the momentum balance. The up-estuary northeasterly winds created landward flux near surface.

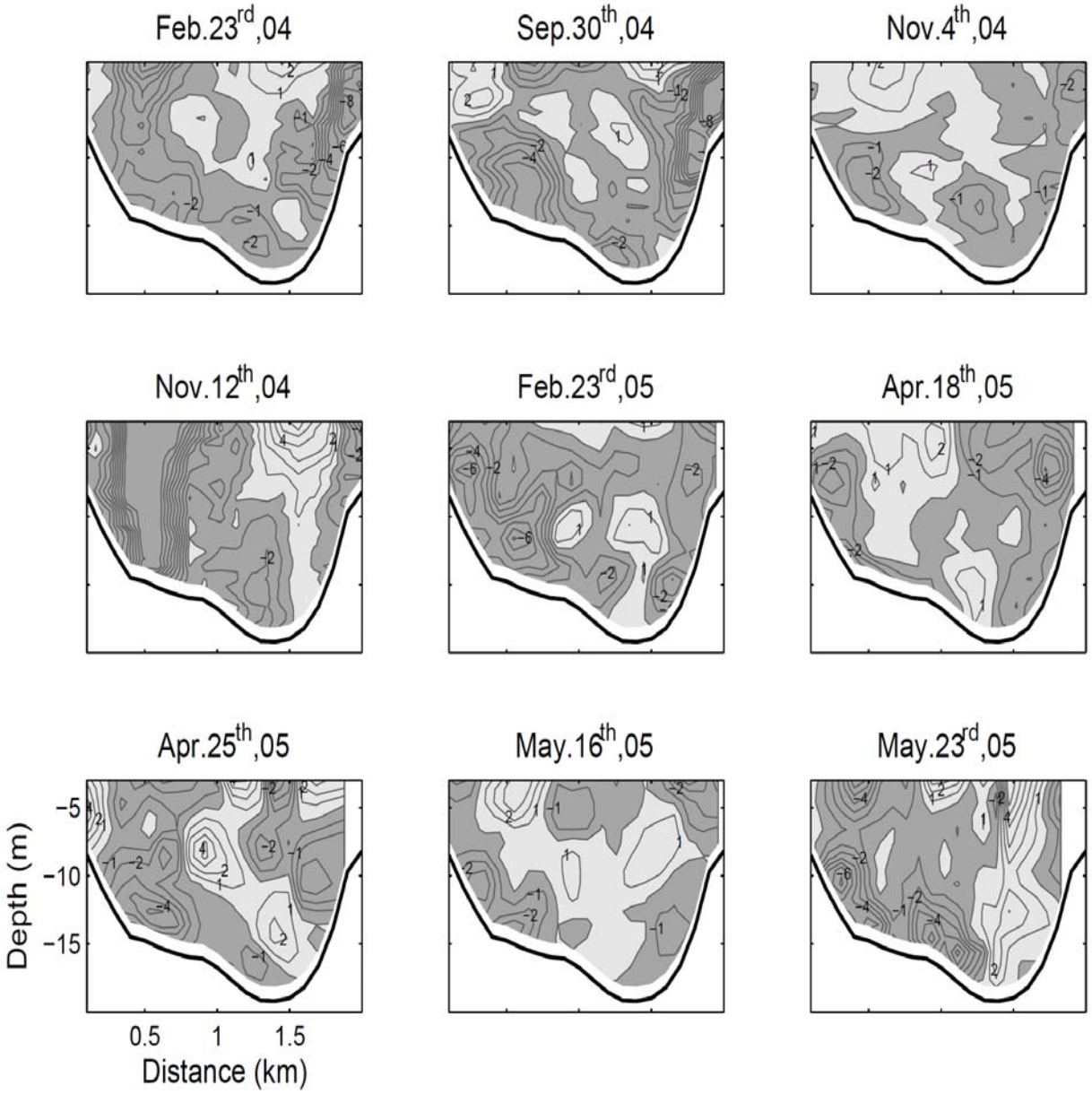

Figure 4-10. Subtidal lateral advection. Darker shades represent landward accelerations. The scale is 10^{-5} and the units are in m/s^2.

At spring tides, the lateral advective term showed a horizontally sheared structure (i.e., seaward over channel and landward over the shoal), acting against the Coriolis forcing and hindering the laterally sheared flow pattern. At neaps, it also served as a driving mechanism of vertically sheared exchange by either strengthening the two

layered exchange (i.e., 3th and 6th surveys) or hindering the lateral shear (i.e., 8th survey). Most of the times the seaward influence covered the southern portion of the channel concentrated at the surface, and northern portion at depth. The steep slopes and abrupt changes in bathymetry caused landward influence shifting the positive accelerations into the middle of the channel. The lateral advection was greater at spring tides than at neaps. Spring tides (Nov.12th, Apr.25th, and May.23rd) showed different patterns; seaward accelerations dominating the whole water column on the right side of the cross-section (i.e., opposite of Coriolis forcing).

4.1.9 Along-Channel Advection

Previous numerical studies (Lerczak and Geyer, 2004; Cheng and Valle-Levinson, 2009) showed that along-channel advection term, uu_x is an order of magnitude smaller than the rest of the nonlinear advective terms (vu_y and wu_z). For this reason the influence of this term on along-channel flow was ignored. However this may not be the case for channels with significant morphologic variability along the estuary. Lateral variability in along-channel flow due to the variations in bathymetry (e.g., phase lags due to friction between shoal and channel causing flood dominant channels and ebb dominant shoals) may be different from one transect to another.

Curvature induced variability in lateral flow can also influence the along-channel variability both laterally and vertically, as stated earlier. This influence can also be different from one transect to the other depending on the locations of curvatures. These cause along-channel gradients to be stronger. Since our study area also includes variations in bathymetry and curvature influences along the estuary, longitudinal nonlinear term uu_x was calculated for 2005 surveys. The gradients were obtained by

using the data from the first and second transect. The second transect was 2 km upstream of the first transect.

$$\overline{u'u'_x} = \frac{1}{n}\sum_{t=t_1}^{t=t_n} u'_t \frac{\Delta u'_t}{\Delta x} \tag{4-11}$$

The magnitude of tidally averaged longitudinal advection term was found to be in the order of 10^{-5} m/s^2, similar to the rest of the terms, showing its equally important contribution to the momentum balance.

4.1.10 Longitudinal Advective Flux Patterns

As can be seen from Figures 4-3 and 4-11, there was a significant change in along-channel flow patterns from transect 1 to 2 which represent strong along-channel gradients. Landward flows dominated the channel, whereas seaward flows occupied the sides of the channel (Figure 4-12). The stronger flows occurred at spring (5th, 7th and 9th surveys) than neap due to increased tidal forcing. Over the sides of the channel, seaward flows were prominent near surface at neaps.

The effect of uu_x can also be clearly examined by comparing along-channel flows observed at Transect 2 to the ones at Transect 1. Second transect demonstrates stronger lateral flows, and patterns more influenced by Coriolis, less affected by barotropic forcing when compared to the first transect. With the addition of longitudinal advective fluxes to such patterns, the flow became more laterally sheared due to the increased seaward flows over the shoals (e.g., 5th, 8th and 9th surveys).

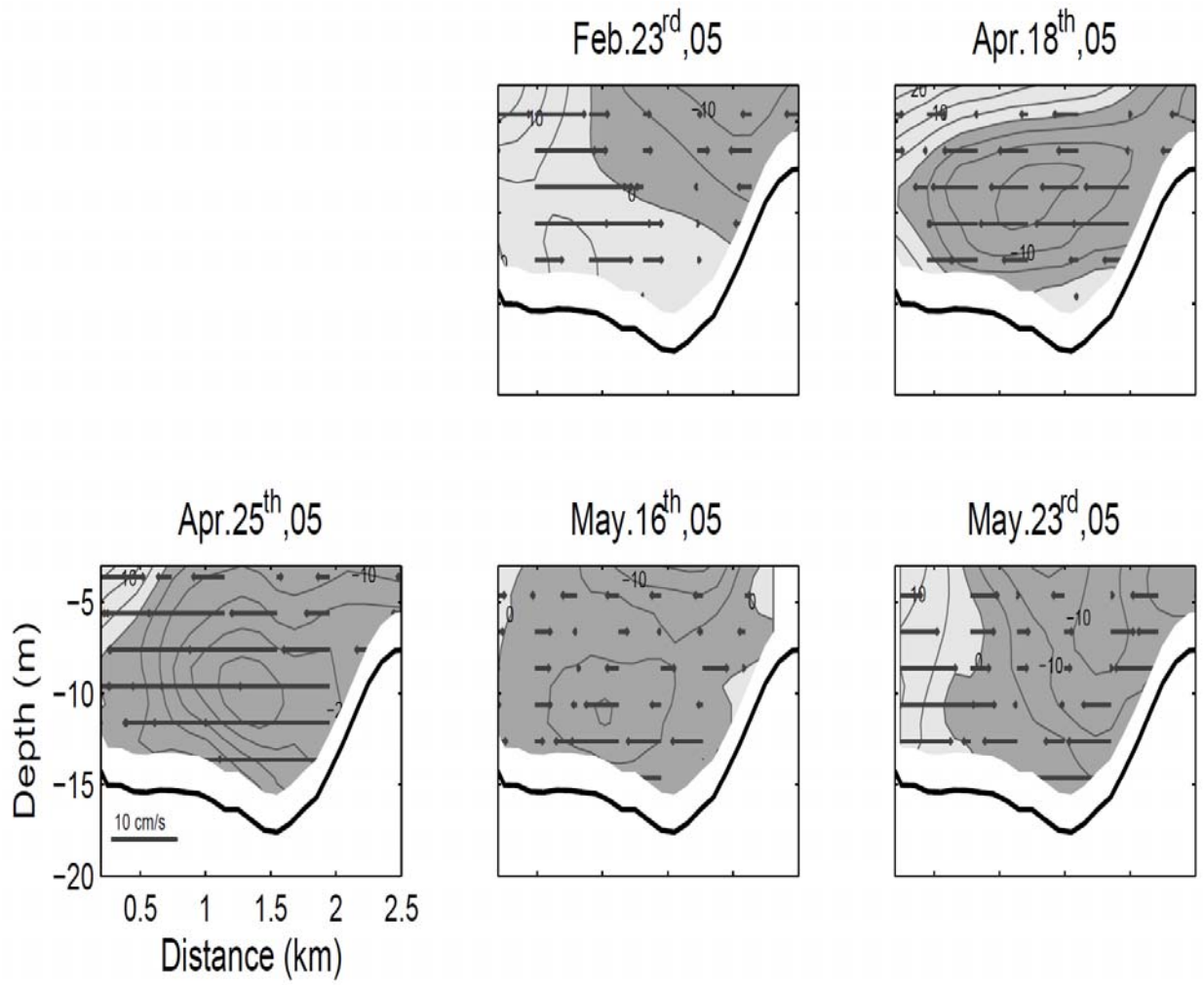

Figure 4-11. Subtidal along-channel and transverse flow at Transect 2. Darker shades represent landward accelerations. The scale is 10^{-5} and the units are in m/s^2.

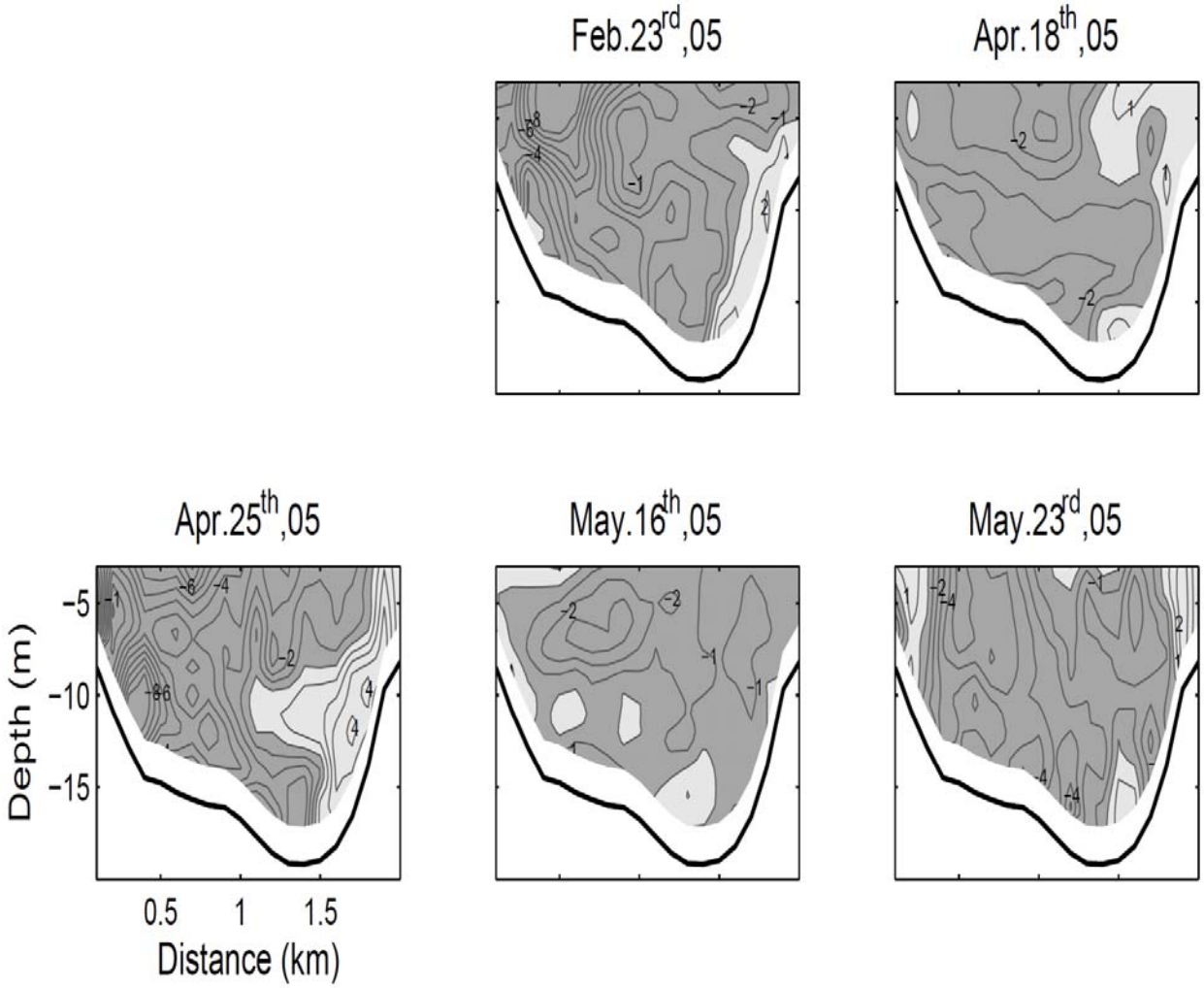

Figure 4-12. Subtidal longitudinal advection. Darker shades represent landward accelerations. The scale is 10^{-5} and the units are in m/s^2.

4.1.11 EOF Analysis

To be able to extract the principal circulation features and reduce the data set to a more manageable size, empirical orthogonal function (EOF) analysis was conducted. An EOF analysis decomposes the data into orthogonal eigen functions, or modes, the first several of which generally account for a large part of the data variance and can generally be related to physical phenomena. The structure of the modes (and their time-

varying amplitudes) can be used to explore spatial and temporal coherence, to reveal higher-order structures, and to provide smoothed versions of the flow field. While EOFs offer the most efficient statistical compression of the field data, a single physical process may be spread over more than one EOF.

4.1.11.1 EOF for subtidal along-channel flow

Data from all surveys used to analyze the spatial structure of the modes for the first transect. The temporal variation of EOF modes, which represents the intensity of each mode through time, was also shown (Figure 4-13). The first three modes accounted for a total of 92.1% (60.4%, 22.5%, and 9.2%, respectively) of the variance. The first mode showed almost unidirectional landward flow throughout the cross-section except for the northern side of the channel which carried seaward flow. This flow structure can be attributed to tidally induced residuals. The temporal variation shows higher intensity of this mode during 2005 surveys. Higher barotropic pressure gradient contribution to the momentum balance during 2005 was also summarized in Figure 4-8. The residuals created by tidal asymmetries in mixing might also be contributing to such spatial structure. The second mode can be an indicative of baroclinic pressure gradient, depicting a two-layered flow; landward near bed, seaward near surface. The third mode might be considered as sum of lateral and vertical advective terms (vu_y+wu_z) as shown in analytical model results (Huijts et al., 2009).

4.1.11.2 EOF for subtidal lateral advection

49.4% of the variance was denoted by a laterally sheared structure, seaward over the northern side and landward over the southern side of the cross-section, opposite of Coriolis forcing expected for the Northern hemisphere (looking up-estuary) (Figure 4-14). This pattern mostly coincides with the accelerations observed at spring tides.

18.2% of the variance was represented by the second mode, which corresponds to the patterns mostly seen at neaps. The third term may be accounted for the asymmetry induced flows in lateral advection.

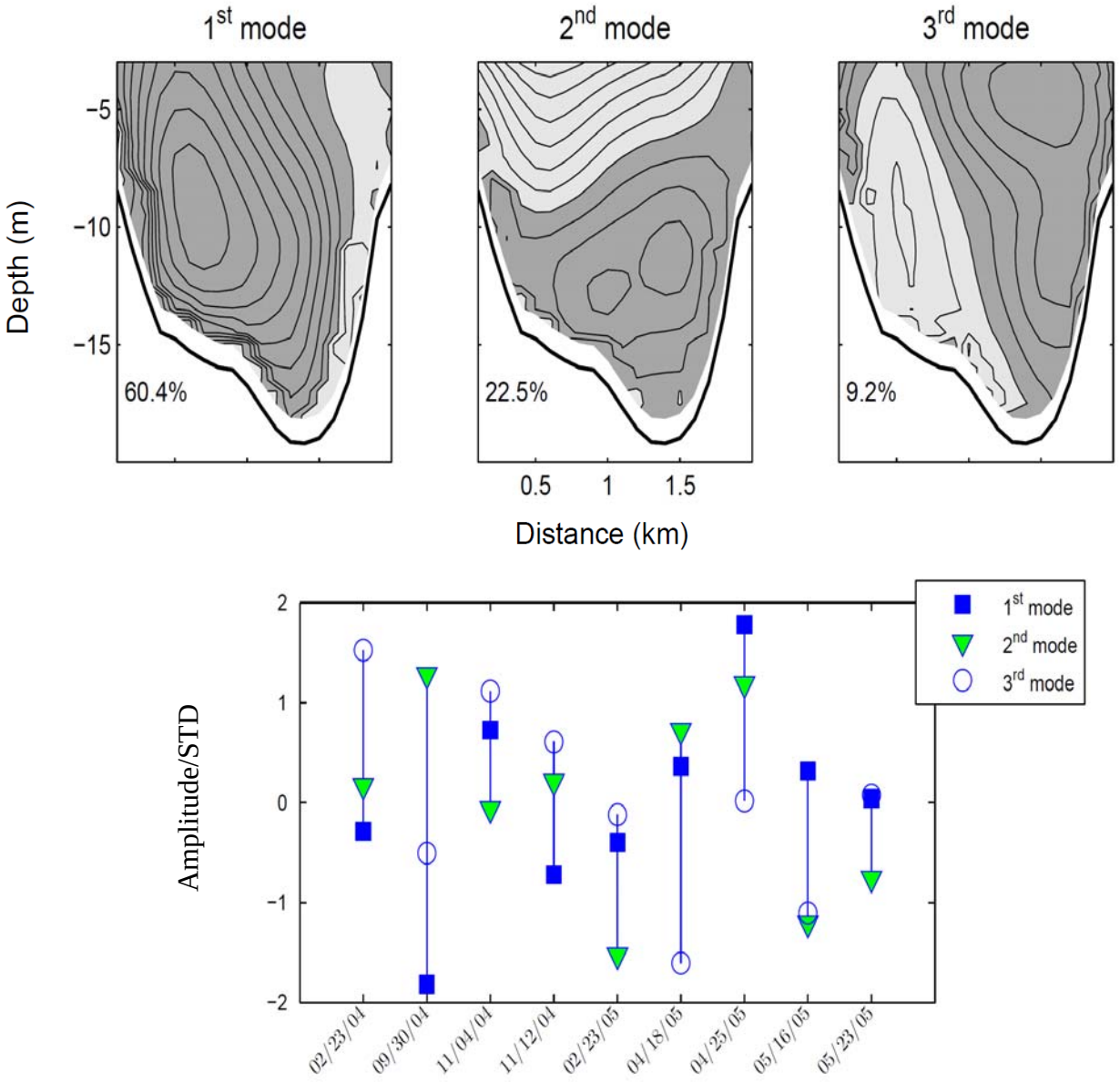

Figure 4-13. Spatial and temporal variation of EOF modes for subtidal along-channel flow. Amplitudes were normalized by standard deviation.

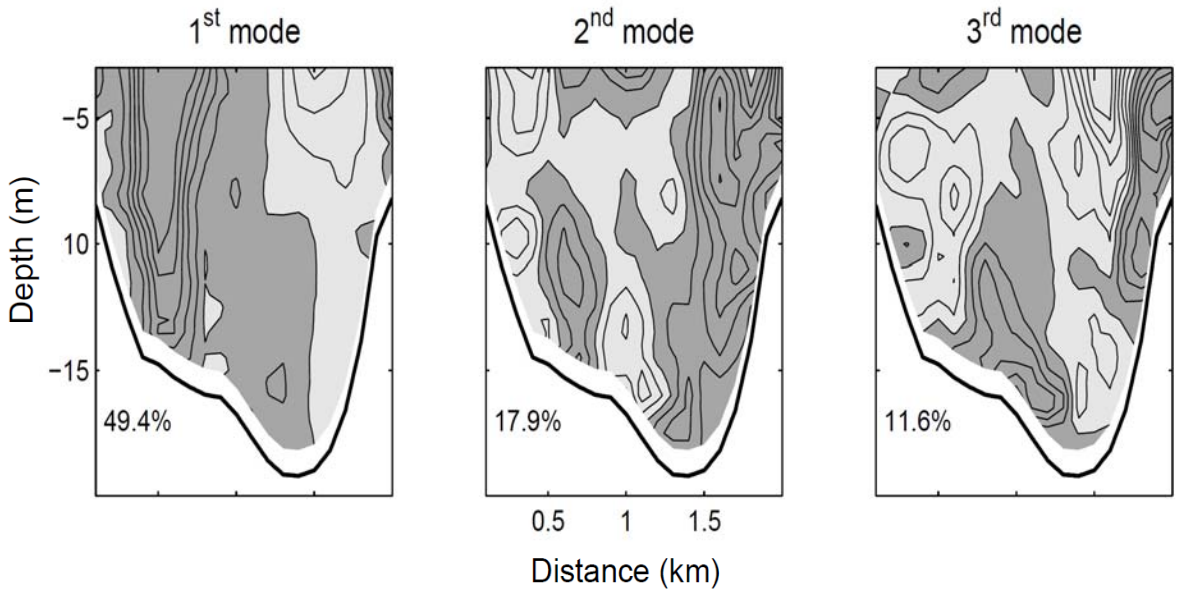

Figure 4-14. Spatial variation of EOF modes for lateral advection.

4.2 Tidal Flow

4.2.1 Along-Channel Flow

In most of the surveys the strongest along channel flow appeared in the channel over the right side of the cross-section during flood and over the left side during ebb, decreasing with depth due to bottom friction (Figure 4-15a, and b). However, there was a marked spring-neap modulation in along channel flow during both flood and ebb tides. The most energetic flows occurred at different locations of the cross-section. During neap floods, maximum along channel flows tended to occur at mid-depth over shallow regions; while at spring tides they appeared at the surface in the channel. During ebb, the strongest flows occurred over shallower regions mostly near the surface at both spring and neap tides.

In some of the surveys, particularly during ebb tides the maximum along channel flow occurred at the locations where the lateral flow converged. In each layer throughout the water column the same behavior observed which might be due to lateral variation in bathymetry. Valle-Levinson et al. (2000) observed such behavior in transects across the James River (upstream of Hampton Roads) where there was a phase lag up to an hour between shoals and channel. The phase lag triggered by the lateral variation of bathymetry caused lateral flow convergences.

4.2.2 Lateral Flow

During flood mostly two or three layered lateral flows were observed (Figure 4-15a, and b). Three layered pattern consisted of southward flows near the surface and bed and northward flows at mid-water. High river discharges and low tidal forcing distorted this flow pattern. As can be seen from November surveys when the estuary had not adjusted to prior river peaks, the lateral flows became either vertically or laterally sheared. Divergences occurred at the mid channel at neap or when the tidal amplitude is small. The effect of lateral bathymetry variation on lateral flow patterns was more prominent during ebb phase than flood. The lateral flow mostly converged over the shallower regions.

The lateral flows observed in this study showed a marked flood-ebb asymmetry in terms of both cross sectional flow patterns and magnitude. The feedback between tidal asymmetry in the strength of lateral flow and nonlinear advective terms was also identified by Scully et al. (2009). Their numerical simulations and estuarine observations showed a stronger lateral flow during flood, which contributes to the importance of advective momentum flux. They described the mechanism causing this asymmetry for an idealized channel of uniform depth. The interaction between lateral shear and

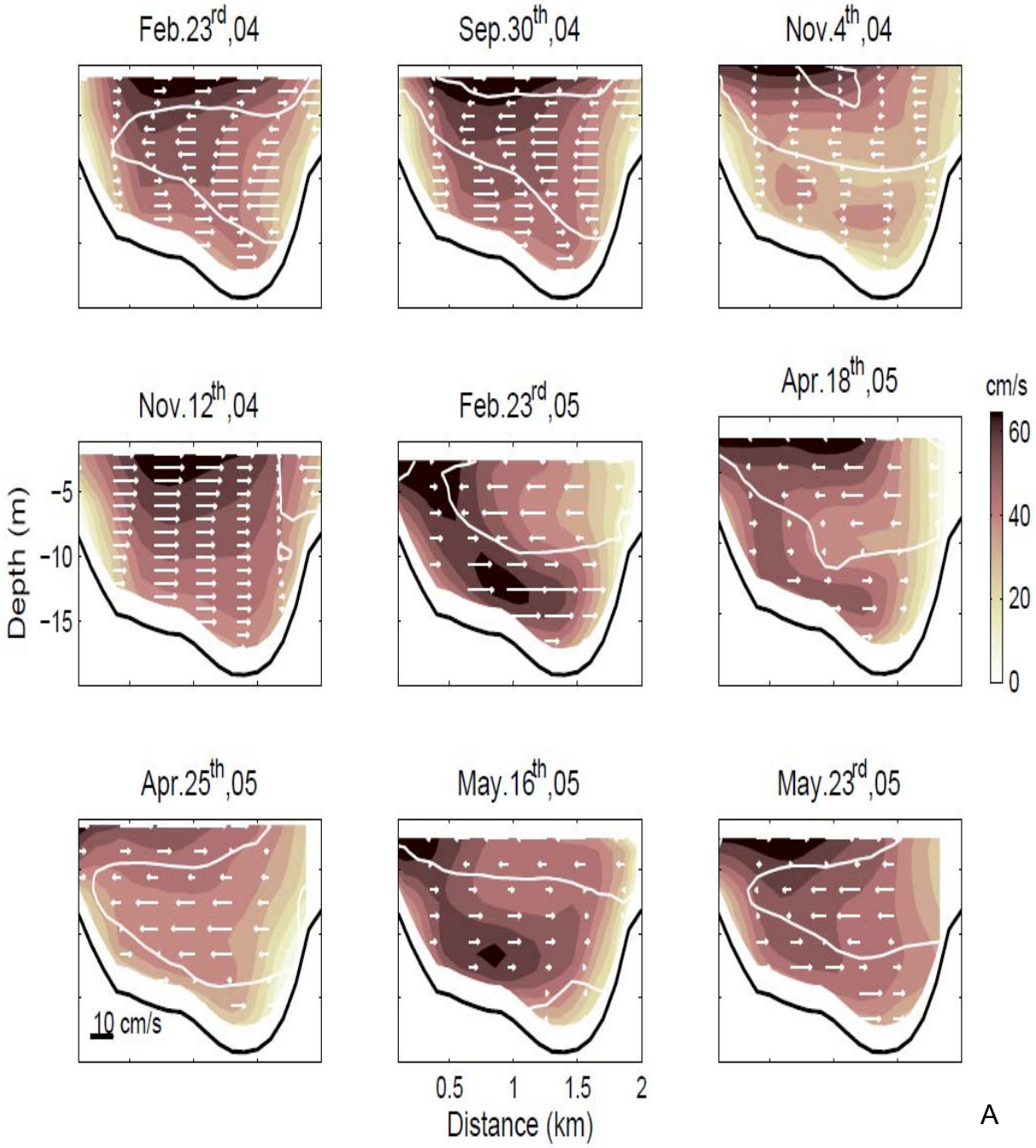

Figure 4-15. Tidal variability of along and across channel flows. A) At maximum ebb. B) At maximum flood. White contours represent zero transverse flow.

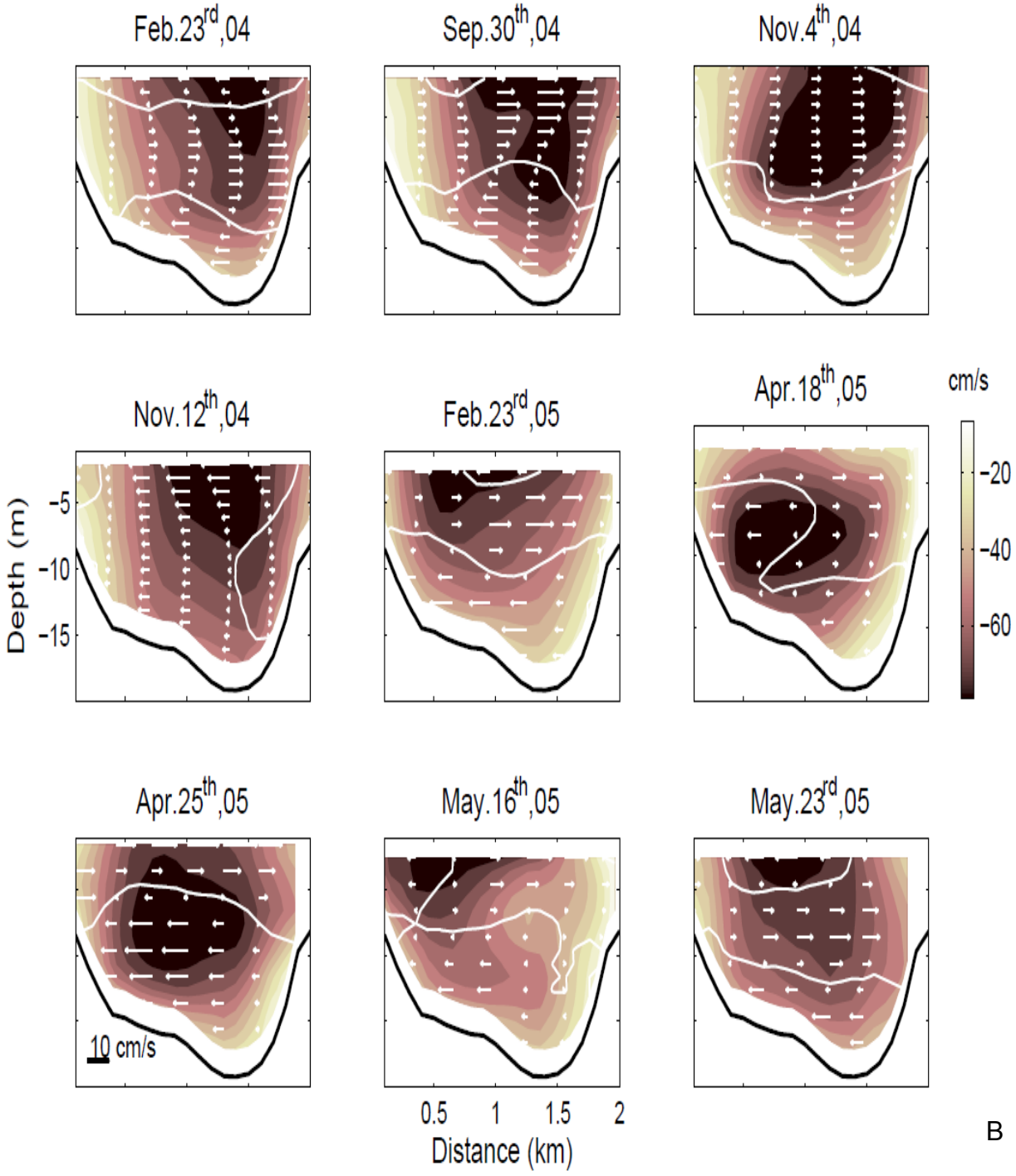

Figure 4-15. Continued

longitudinal density gradient (i.e., $u_y\rho_x$) which induces a lateral baroclinic pressure gradient, enhances lateral baroclinicity caused by Ekman transport (i.e., $w_y\rho_z$) during ebb, and opposes it during flood. The reduced lateral baroclinicity yields stronger lateral flows during flood.

4.2.3 Density

The density profiles showed a range between 10 and 30 kg/m^3, reaching the lowest value on April 18th (Figure 4-16). Tidal variation of density profiles showed higher stratification at neap than at spring tides (i.e., mixing caused by weaker tidal energy was not sufficient enough to disturb the stratification created by longitudinal advection). The lateral bathymetry variation also played an important role in stratification. Due to bottom friction, shallower regions exhibited weaker stratification with respect to deeper parts.

Another process that affects stratification is tidal straining. Tidal straining refers to a vertically stratified water column during ebb resulting from faster moving fresh surface water with denser water underneath, and a well mixed water column during flood due to instabilities caused by accelerated heavier water at the surface (Simpson et al, 1990). In most of the observations at Hampton Roads the mid-channel water column showed opposite pattern to typical tidal straining, exhibiting well mixed ebbs and stratified floods or slacks. This is probably caused by lateral density gradients.

Lateral density gradients contributed to the dynamics at leading order. A study by Huijts et al. (2006) pointed out the importance of this term. They calculated the ratio of lateral density gradient to along-estuary density gradient as a function of Ekman number. For the James River, having an Ekman number of ~0.11, their calculation showed that $\rho_y \cong 1.75\ \rho_x$. Valle et al. (2000) pointed out a mechanism where strong

lateral density gradients were balanced by lateral barotropic gradients, and horizontal density gradients balanced by fortnightly modulation of vertical mixing after their observations in James River. This term was proven to be important in modulating exchange flow. In a curved and narrow channel the lateral density gradients are produced by differential advection of salt due to lateral variations in bathymetry and may dominate over lateral flow.

4.2.4 Buoyancy Frequency

In order to examine the stability of the water column throughout the tidal cycle, buoyancy frequencies were calculated for all stations (Figure 4-16). Positive values indicated stability, whereas negative values indicated instability in the water column. The southern side of the channel was highly unstable over the tidal cycle, because of high mixing rates. The northern side showed higher stabilities when compared to the southern side.

Higher stabilities were observed in the mid-channel at the locations where the stratification was high. As stability of the water column is correlated with stratification, neap tides with weak mixing rates caused higher stability. The stability persisted between depths 10-15 meters for the 3rd survey, and 5-10 meters for the 8th survey through the whole tidal cycle. Flood-ebb influence can be seen in 5th and 6th surveys more clearly. The 4th survey showed instability all the time because of the higher mixing rates which persisted through out the day.

4.2.5 Curvature Effect

Curvatures together with the differential advection of density gradients have great impact on modifying the lateral flows, thus lateral advection. The interaction between curvature induced lateral flows and tidal variation of stratification can produce different

flow patterns over a tidal cycle. Well mixed conditions allow the development of two-layer helical flow (i.e., toward the inside of the bend at the bottom and toward the outside of the bend in the upper water column) around a bend (Nidzieko et al., 2009). The development of lateral density gradients opposes this circulation yielding to three layered lateral flows.

There are two bends which have influences on lateral flow. One is located near Norfolk (i.e., on the southern end of transect) and the other is located at Newport News (i.e., at the upstream on the northern side of transect). The bend on the southern side has a greater effect overall considering its bigger radius. This can also be observed from the bathymetry near the James River entrance. Flood tides favor the distortions caused by southern bend, while ebb tides favor the distortions caused by both bends.

As mentioned earlier tidal variation of stratification has a great impact on curvature induced helical flow. The opposing flow due to augmented lateral baroclinic pressure gradient arising from stratified flood tide caused three layered lateral flows which were observed near the southern bend on 1st, 2nd and 9th surveys. When compared to these surveys, the 3rd survey which had weaker stratification at peak flood showed similar patterns except the southward near surface flow seemed to be weak due to the reduction in lateral density gradient. Curvature, Coriolis and lateral density gradients might be responsible for driving this kind of flow pattern on the southern end. When the flood was well mixed, the regular helical flow emerged. During the well mixed peak ebb tides, strong helical flows were observed at the northern side of transect (e.g., 3rd and 5th surveys).

When considering the curvature-induced lateral flow the structure of along-channel profiles should also be kept in mind. Decoupling of water column due to bottom friction causes non-logarithmic along channel profiles (Monismith, 2001). If the along-channel flow is not logarithmic, the centrifugal forcing shifts from being helical.

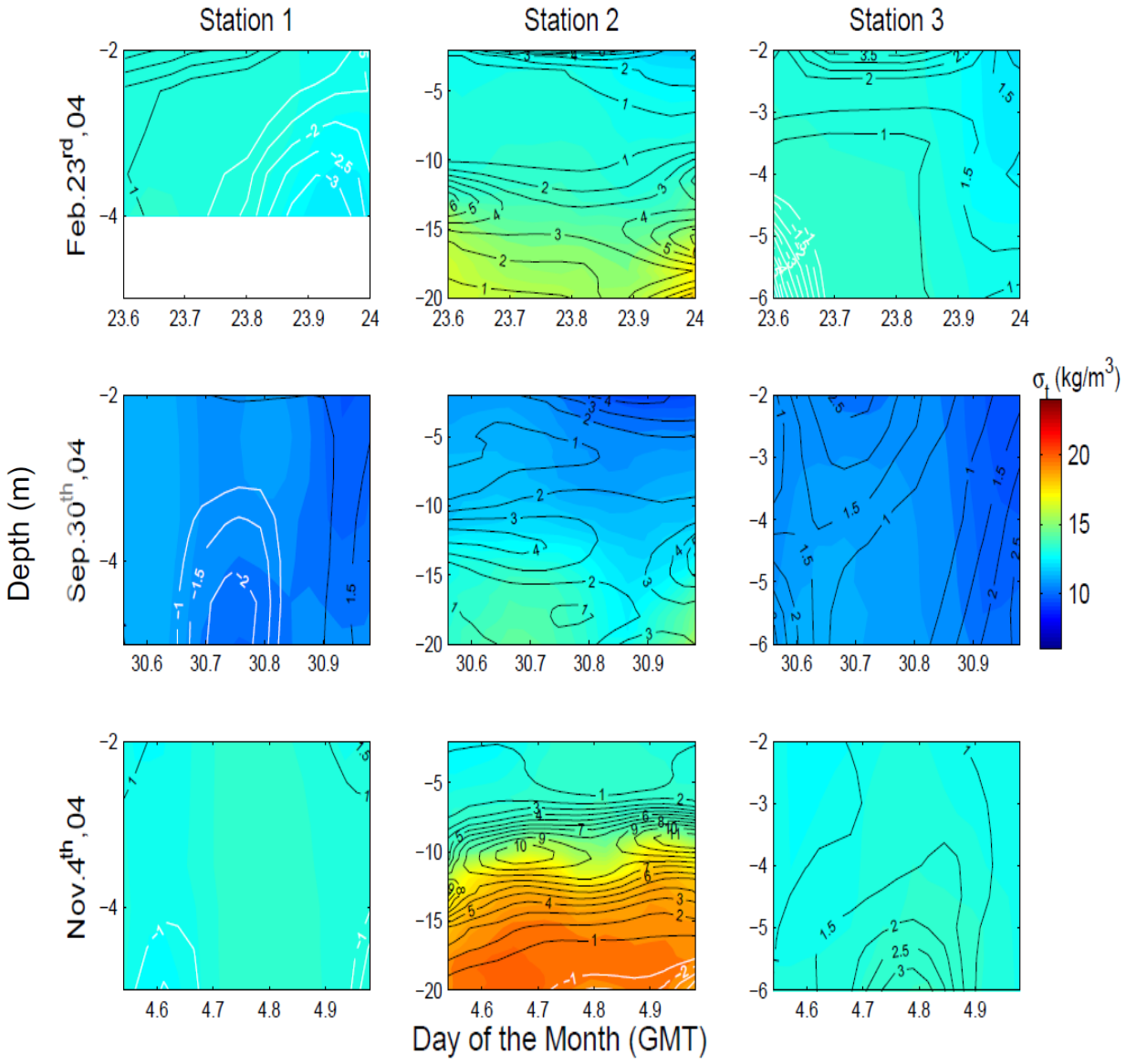

Figure 4-16. Tidal variation of density profiles and squared buoyancy frequency. Scaled as 10^{-3} s^{-2}, black and white contours represent positive and negative buoyancy frequency, respectively.

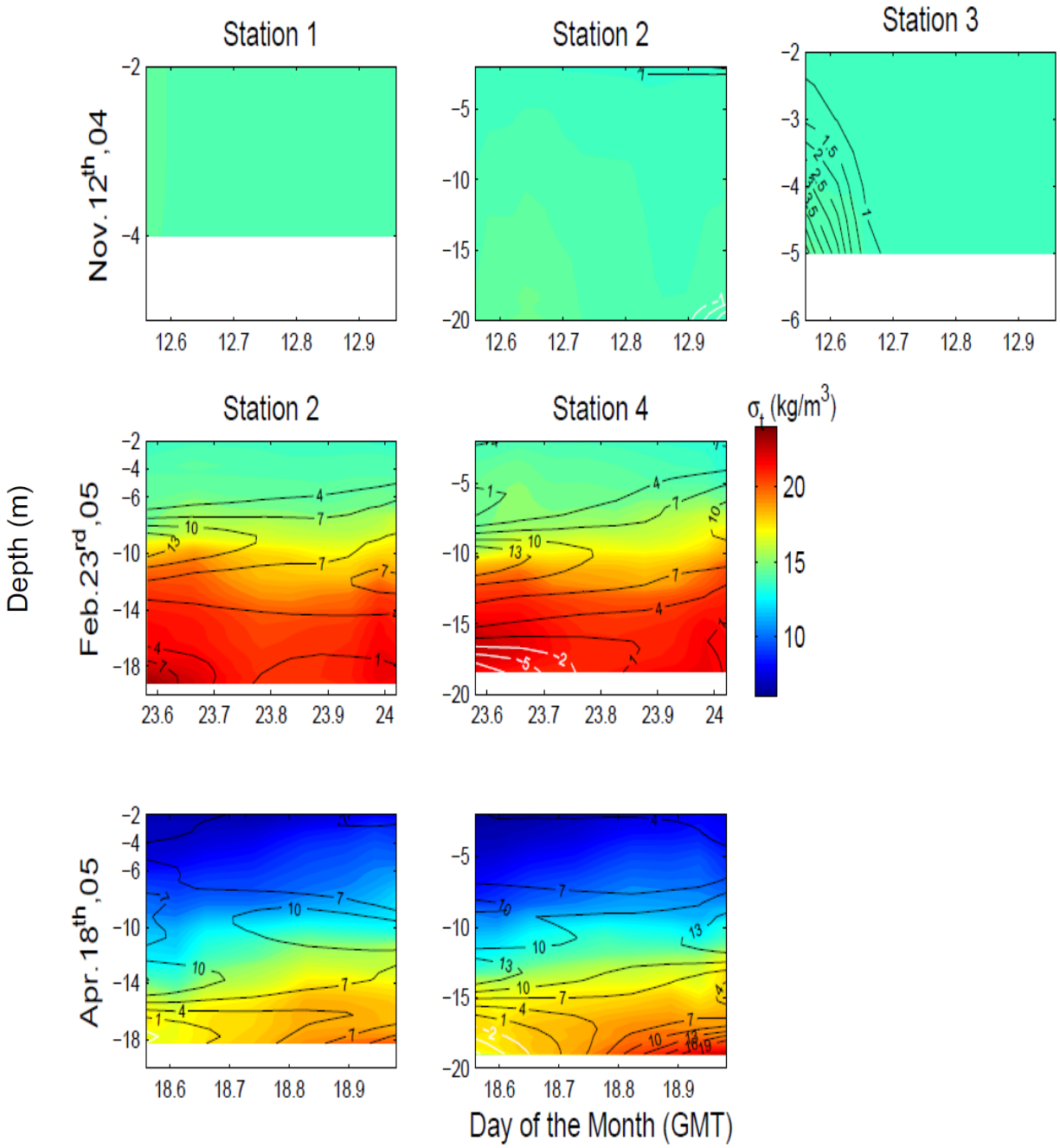

Figure 4-16. Continued

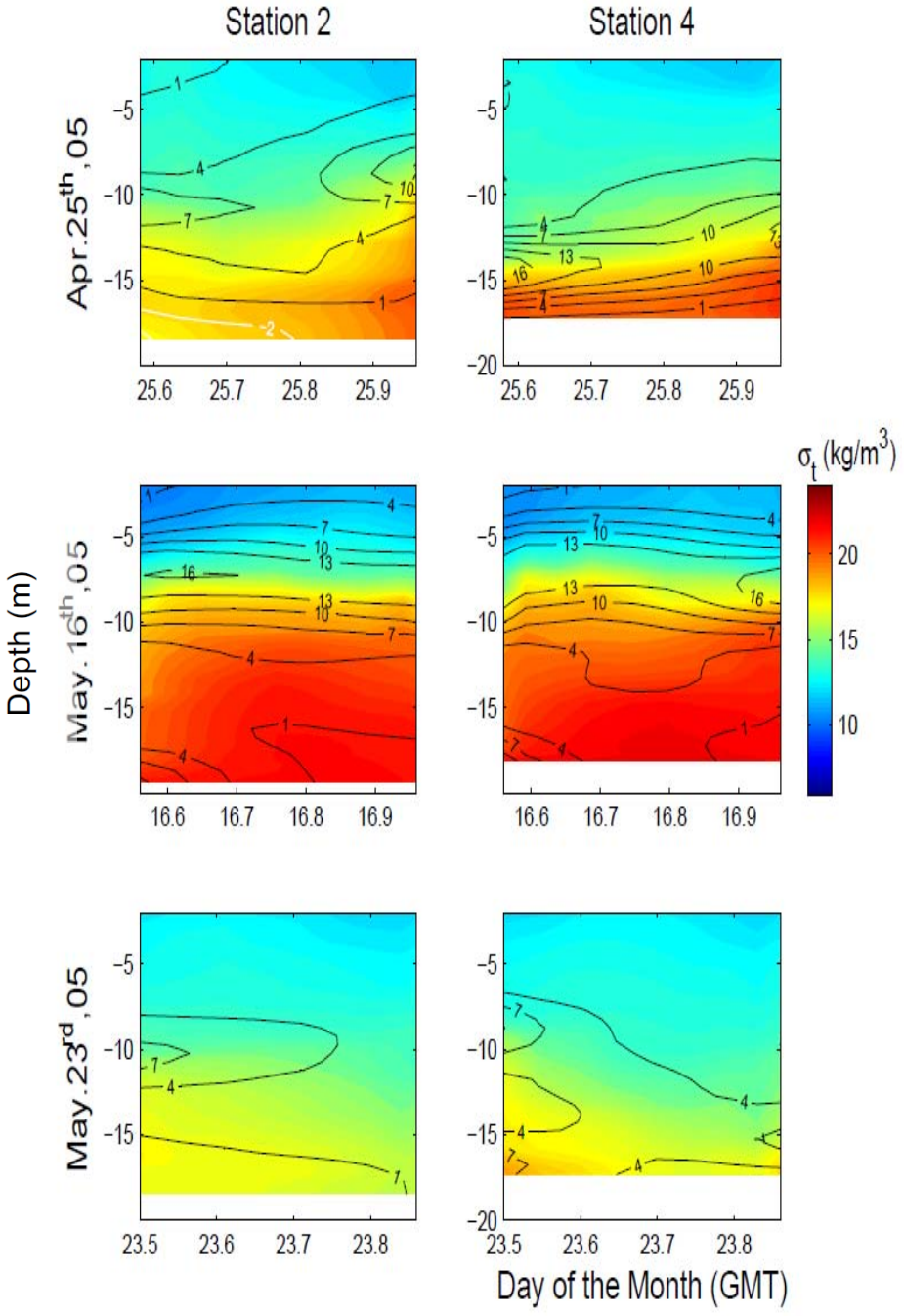

Figure 4-16. Continued

4.2.6 Momentum Budget

Absolute values of the main terms in the momentum budget were averaged over the cross-section in order to compare the tidal variations in their magnitudes over a tidal cycle (Figure 4-17).

4.2.6.1 Baroclinic pressure gradient

Since there was only one station along the channel during 2004 surveys, the baroclinic pressure gradient term is missing in the plots for that year. During neap flooding tides, a general trend of decreasing gradient with a slight increase near peak was observed whereas it increased at spring tides. During ebb, surveys exhibited different trends (e.g., increasing at 5^{th} & 9^{th}, decreasing at 6^{th} & 7^{th}) regardless of spring-neap modulation. In all surveys carried out in 2005 an increase in baroclinic pressure gradient can be seen near slacks.

4.2.6.2 Barotropic pressure gradient

The trends in both accelerating and decelerating phases of the flood and ebb were analyzed. At most springs the barotropic pressure gradient increased in the first phase of flood reaching its maximum potential at peak flood and decreased in the second phase. At neaps strongest gradients were observed after the peak flood. During ebb there was no spring-neap modulation to the trend which showed gradients reaching to a peak in the decelerating phase.

4.2.6.3 Vertical mixing

Observations made in 2004 showed higher mixing rates. Spring-neap modulation to the trend was clear, indicating higher mixing at spring than neap. However there was a flood-ebb asymmetry as mentioned before causing increases at either ebb (e.g., 2^{nd} and 4^{th} survey) or flood (e.g., 1^{st}, 5^{th}, 6^{th}, and 9^{th} surveys).

4.2.6.4 Coriolis

This term has the weakest impact on the along-estuary momentum balance most of the time. Its tidal trend was very close to the trend of lateral advection. At neap tide due to the weak tidal forcing, the magnitude of Coriolis term decreased.

4.2.6.5 Lateral advection

A clear fortnightly modulation yielding to weaker lateral advection terms (i.e., 5 $\times 10^{-5}$ m/s^2) at neap were observed. Higher tidal forcing resulted with stronger advection up to 2 $\times 10^{-4}$ m/s^2 at spring. The tidal variation at neap spread over a wider range than at spring tides. Mostly the highest magnitudes were reached at peak floods or near peak floods with some exceptions being the 2nd and 4th surveys which showed near ebb peaks. The minimum values were observed at slack tides.

4.2.7 Lateral Advective Acceleration Patterns

Huijts et al. (2009) described the flow patterns resulting from tidal rectification due to vuy+wuz and distinguished the separate contribution from vu_y and wu_z term. They found a general flow pattern for various bathymetric steepness parameters and Stokes numbers. Lateral variations in bathymetry and friction at the bed cause differentiations in tidal velocity. Coriolis deflection of along channel flow together with the mass conversation yield a clockwise circulation during flood and counter-clockwise circulation during ebb (looking up-estuary in the northern hemisphere).

Both the circulation and along-channel tidal flows with different strengths result in tidal momentum transfers across the cross-section. During both flood and ebb, the relative excess of tidal momentum appears near surface at the right side, and near bed at the left side, whereas the relative shortage of tidal momentum appears near surface at the left side, and near bed at the right side of the channel. However this description of

flow patterns does not take into account the influence of lateral and horizontal density gradients since their model supporting such circulation uses constant horizontal density gradient and constant vertical mixing.

The flow patterns driven by lateral advection during maximum flood and ebb for nine surveys were presented in Figure 4-18. Mostly north side of the channel carried up-estuary accelerations near surface, and down-estuary accelerations near bed. The opposite behavior was observed in the south side of the channel. Abrupt changes in bathymetry at the southern side influenced up-estuary accelerations to dominate the whole water column. When the tidal energy decreased down-estuary accelerations started to dominate. Tidal amplitude influence can be clearly seen on 3rd, 5th, 6th, and 8th surveys. Especially during peak floods, the separation between up-estuary and down-estuary accelerations occurred at depths where the stability is highest throughout the water column. The observations exhibited a clear flood-ebb asymmetry in terms of both magnitude and flow patterns except 4th, 8th and 9th surveys.

4.3 Tidal and Lateral Asymmetry in Stratification

The dynamics of the estuarine circulation have been considered to involve a balance between the pressure gradient induced by the surface slope, the baroclinic pressure gradient due to along-channel density gradient, and the stress divergence (Pritchard, 1956; Hansen and Rattray, 1966; Chatwin 1976). The contribution of tidal processes into such balance is through the stress divergence which is parameterized in terms of vertically and tidally averaged eddy viscosity. However, the spatial and temporal asymmetries in turbulent mixing may influence the estuarine exchange by introducing residual currents. Recent studies showed that tidal asymmetries can lead to

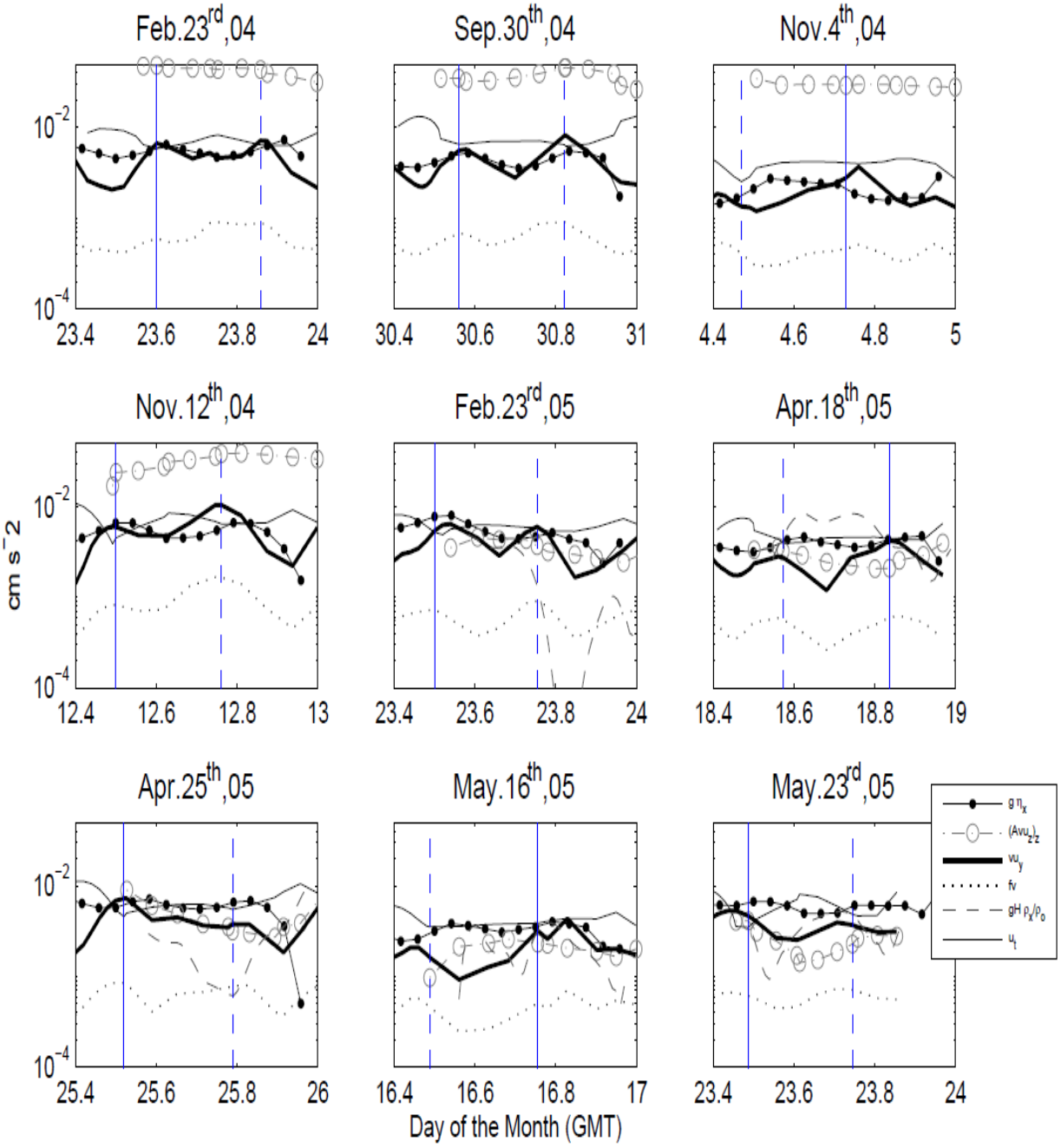

Figure 4-17. Cross-sectional averages of the absolute value of the terms in along-channel momentum equation over a tidal cycle. Blue straight and dashed lines represent maximum flood and maximum ebb, respectively.

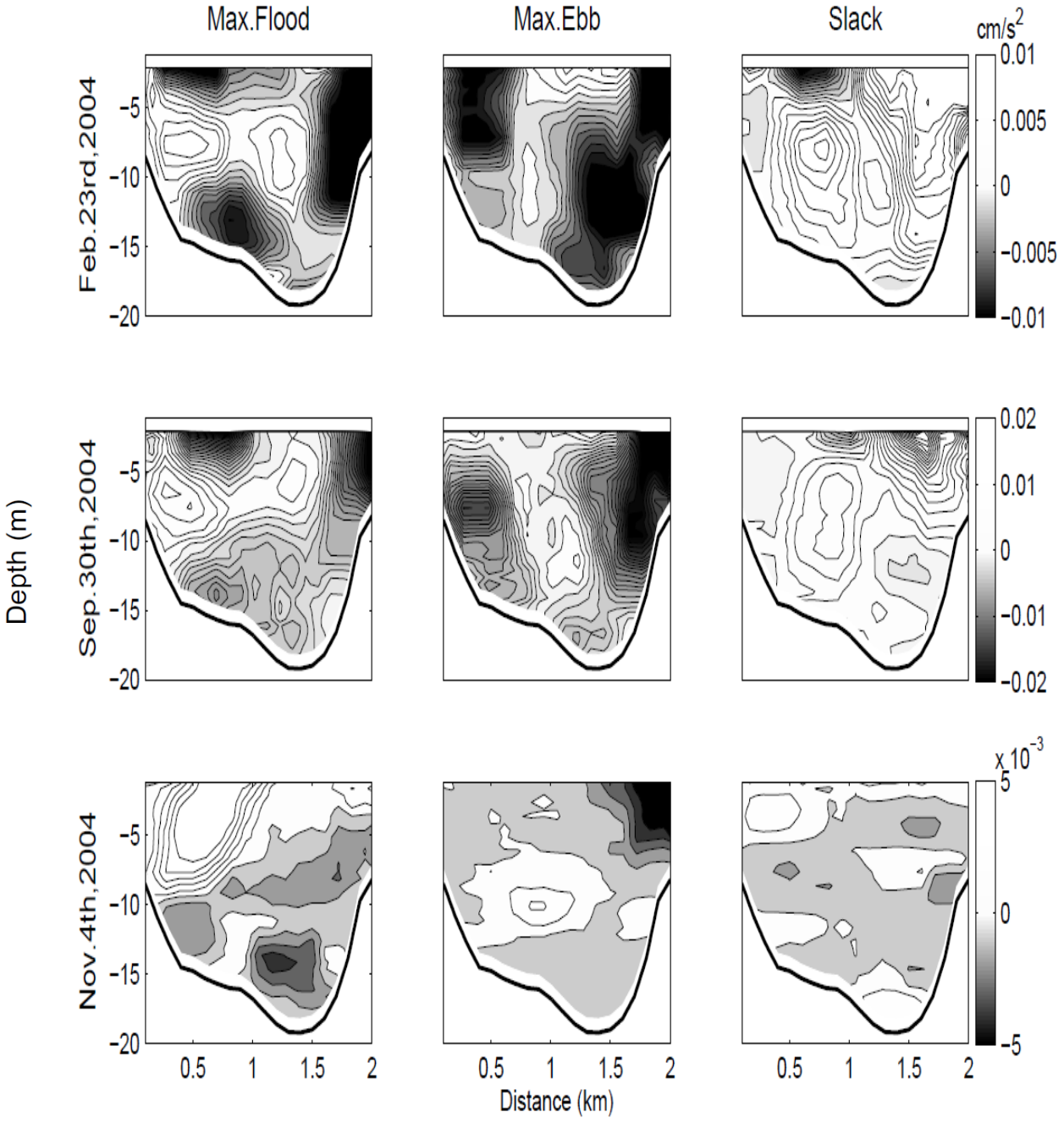

Figure 4-18. Tidal variation of lateral advection.

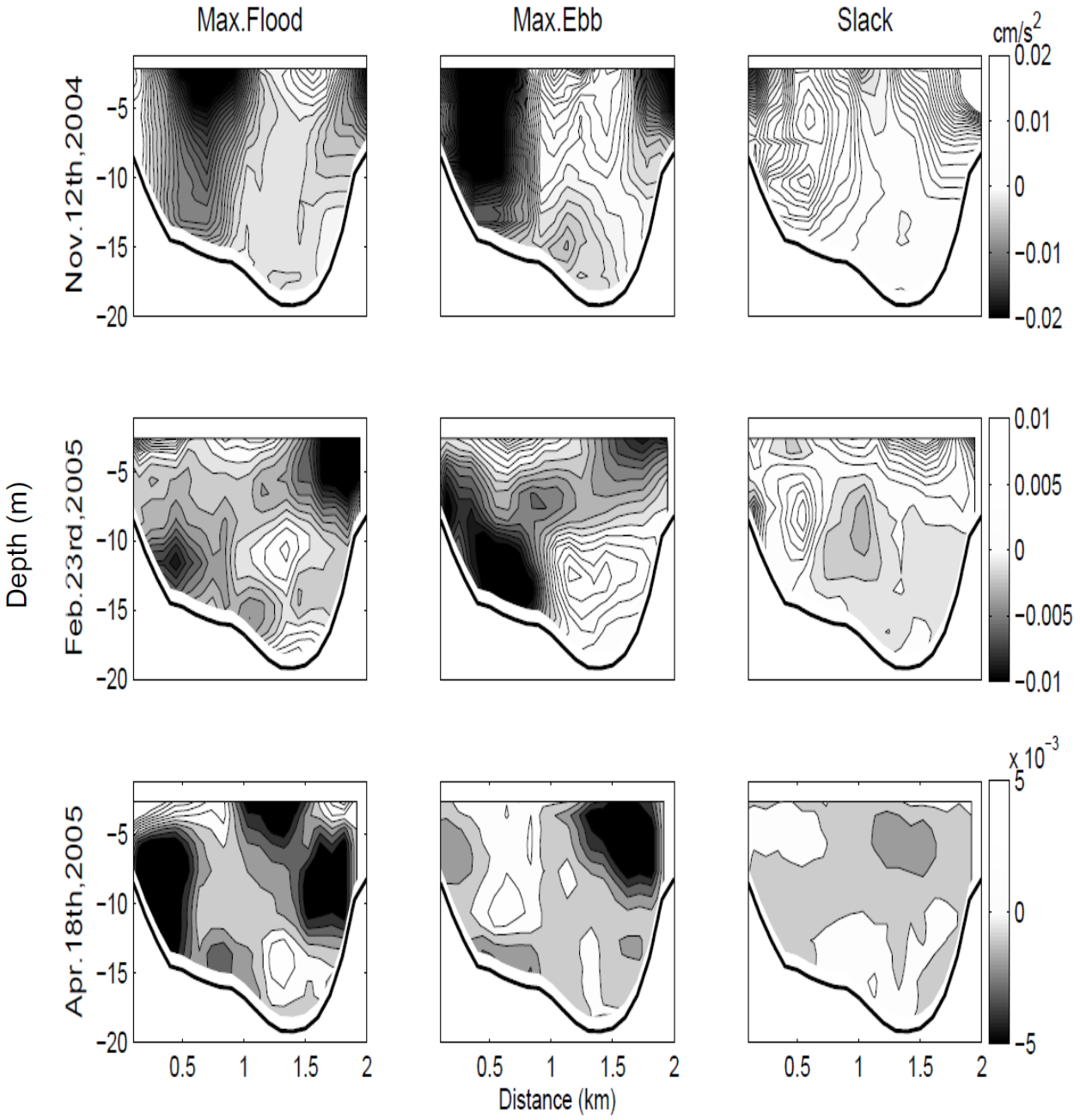

Figure 4-18. Continued

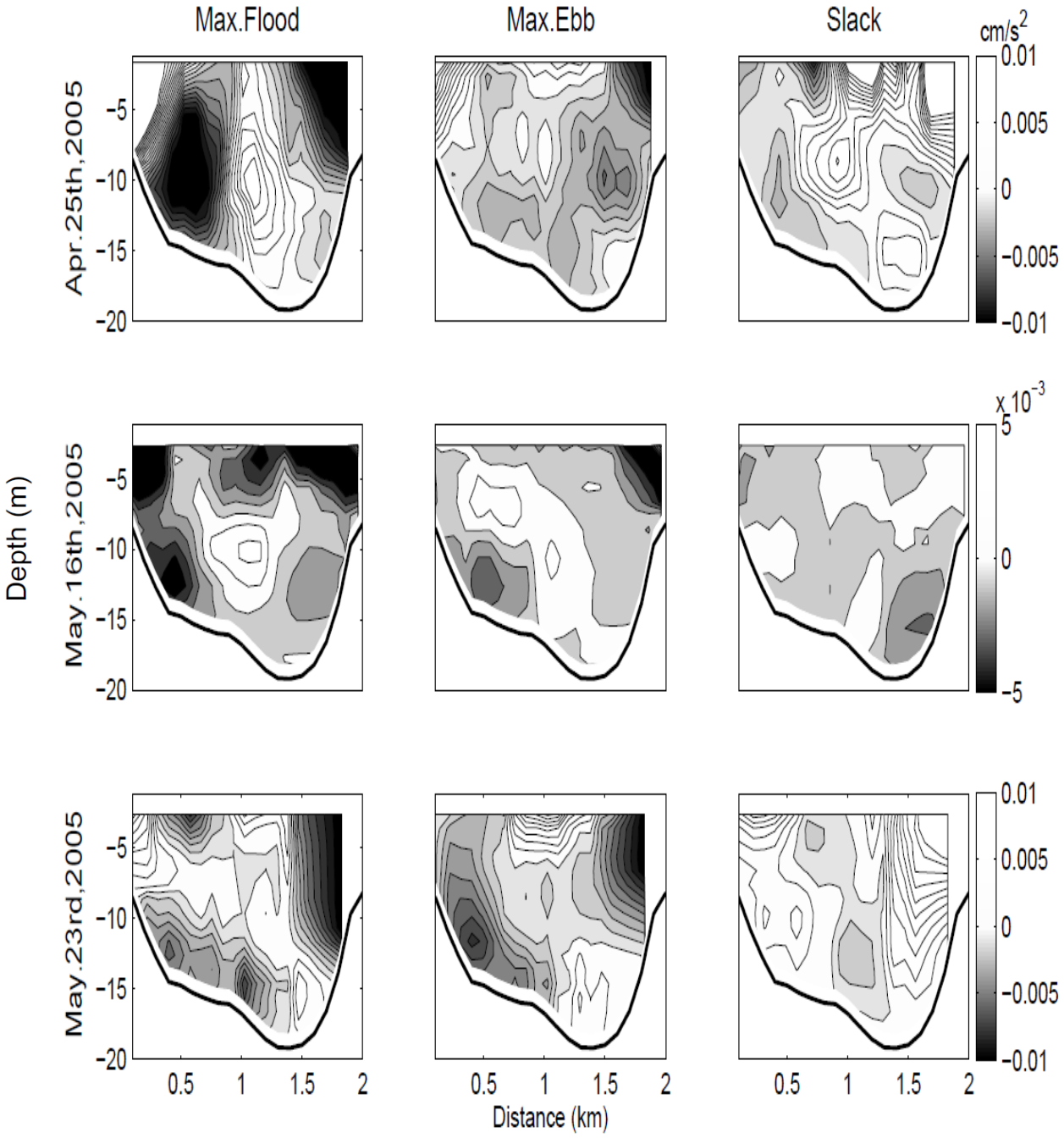

Figure 4-18. Continued

asymmetric mean velocity profiles resulting in an Eulerian subtidal flow (Jay and Musiak, 1996; Stacey et al., 2001). The interaction between along-channel density gradients and vertical shear in tidal currents (i.e., tidal straining) may produce stratified ebb tides and well-mixed flood tides, causing tidal asymmetries in vertical mixing (Simpson et al., 1990). Jay and Musiak (1996), and Stacey et al. (2001) stated that this mechanism accelerates near-surface currents during ebb creating vertically sheared velocity profile, and near-bottom currents during flood, which may lead to two-layered subtidal patterns, same as the density driven circulation (i.e., up-estuary near bottom, down-estuary near surface).

Although the previous studies are in agreement with the influence of tidal asymmetries on near-surface subtidal currents, there are conflicting views on near-bottom influence. Geyer et al. (2000) stated that near bed subtidal circulation is slightly affected by asymmetries in vertical mixing. Trowbridge et al. (1999), and Scully and Friedrichs (2003) showed the increase in vertical shear during ebb but did not observe an intensification in near-bottom currents during flood due to convective mixing.

Stacey et al. (2008) pointed out to the importance of timing of stratification and its strong impact on subtidal flow. Their numerical model results showed that for the flood tide being well-mixed and ebb tide being stratified, the subtidal circulation generated by this asymmetry was the same as the gravitational circulation. However for the case of reversed asymmetry (i.e., stratified flood, well-mixed ebb), they obtained reversed subtidal circulation (i.e., up-estuary near surface, down-estuary near bottom).

Cheng et al. (2010) examined the residual currents induced by asymmetric tidal mixing in a weakly stratified narrow estuary. They found that the strength of residual

currents and tidal asymmetry is directly proportional to each other. Consistent with Stacey et al.'s results, they suggested the impact of stratification phase on residual currents (Figure 4-29). The asymmetries in vertical mixing not only exist on a temporal scale but on a spatial scale as well. Therefore their impact on estuarine exchange should also be considered. Previous studies showed the lateral bathymetry variability impact by using spatially and temporally constant eddy viscosity (Wong 1994; Kasai et al. 2000; Valle-Levinson et al. 2003). Scully and Friedrichs (2006) showed that lateral asymmetries in turbulent mixing may induce laterally sheared residual circulation with up-estuary flow over the shoal, and down-estuary in the channel.

4.3.1 Asymmetry in Velocity Field

4.3.1.1 Along-channel currents

The tidal variation of current profiles over the thalweg showed distinct patterns (Figure 4-19). Mostly the strongest flood tides were observed at the surface diminishing near the bottom due to bed friction (i.e., logarithmic velocity profile). September and April surveys showed different structures with maximum floods occurring at mid-depth of the water column. Strongest ebb tides were observed near-bed (e.g., Feb. 23rd 05, May. 16th 05), or co-existing both at surface and near bed except for Nov 12th survey which showed a logarithmic velocity profile. At neaps when the tidal forcing decreased slack tides showed more of a two-layered exchange, similar to gravitational circulation after maximum ebb and reversed circulation after maximum flood. Not only the location but the magnitudes of strong currents showed asymmetry as well. In all surveys maximum flood tides are stronger than maximum ebb tides over the thalweg. In order to analyze the overall asymmetry the currents were averaged over ebb and flood separately representing the entire flood and ebb. The flood-ebb asymmetry increased either near

surface or at mid-depth of the water column. Figure 4-20 shows the flood and ebb dominance across the section.

4.3.1.2 Lateral variation of along-channel currents

Tidal variations over shoals showed different current profiles than in the channel. Over shoals the ebb tides became more dominant with stronger currents occurring at surface. The flood tides mostly got stronger near the bed which is the opposite of what was observed in the channel. Flood-ebb asymmetry increased near mid-depth in 2005 surveys when the barotropic pressure gradient is higher. Surveys in 2004 showed increased near-surface asymmetry with ebb dominance.

4.3.1.3 Secondary currents

Lateral flows are important in advecting the salt laterally and distorting the salinity gradients created by differential advection of along-channel currents. They contribute to the asymmetries in stratification in terms of lateral straining. The strength of lateral flow over a tidal cycle was calculated to show the variation with respect to phase later to be compared with stratification.

In order to account for the depth variation while considering the stratification, absolute values of secondary currents above and below the isopycnals were averaged to represent respectively, near-surface and near-bottom variability (Figure 4-21, 4-22). At springs the lateral flow was stronger during maximum flood than maximum ebb whereas at neaps they were almost equivalent. November surveys showed similar strength of lateral flow throughout the water column. However the rest of the surveys showed different tidal variability of lateral flow (i.e., weaker near-bed and greater near-surface) especially during slack tides.

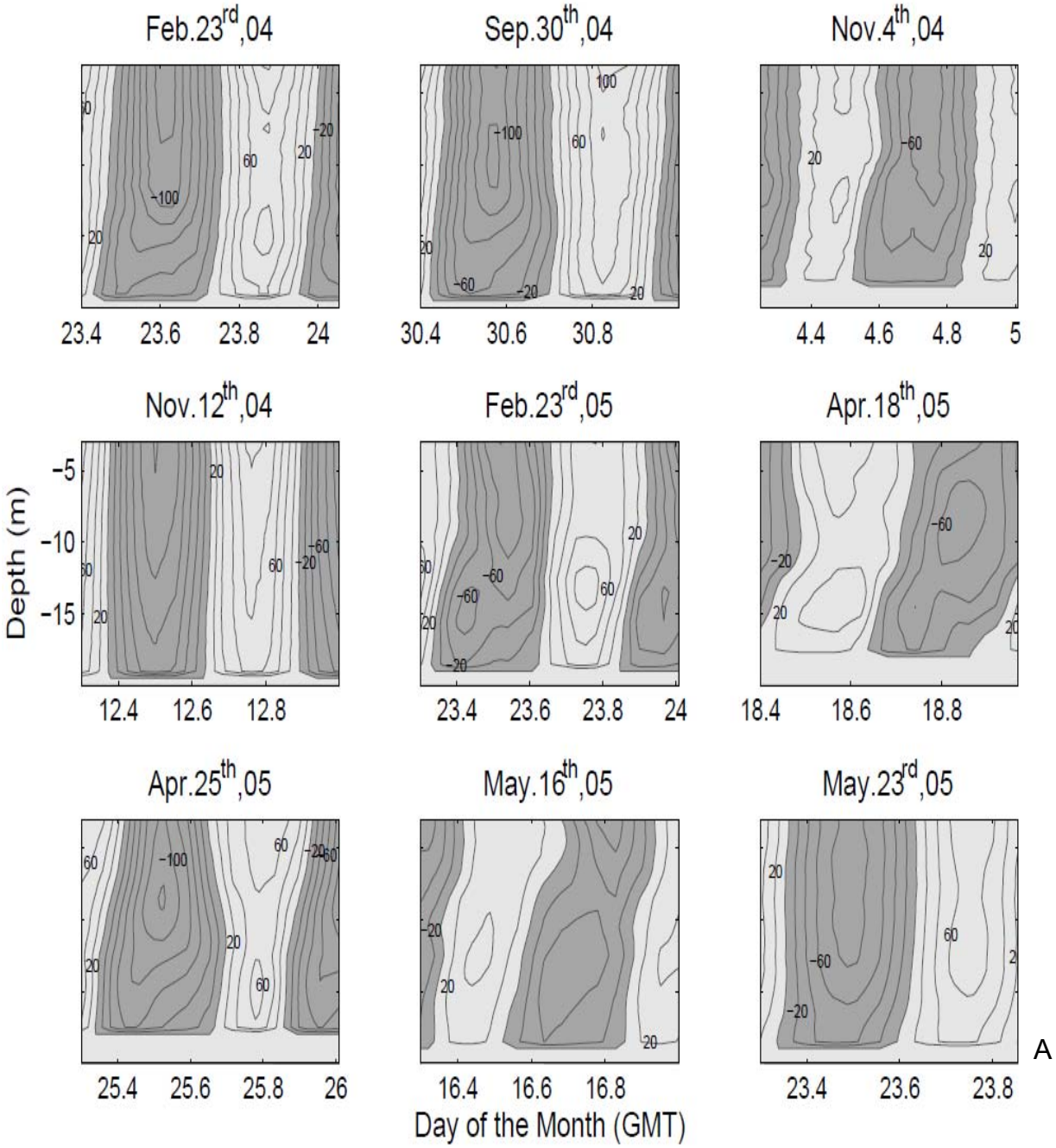

A

Figure 4-19. Tidal variation of current profiles. A) Over thalweg. B) Over shoal.

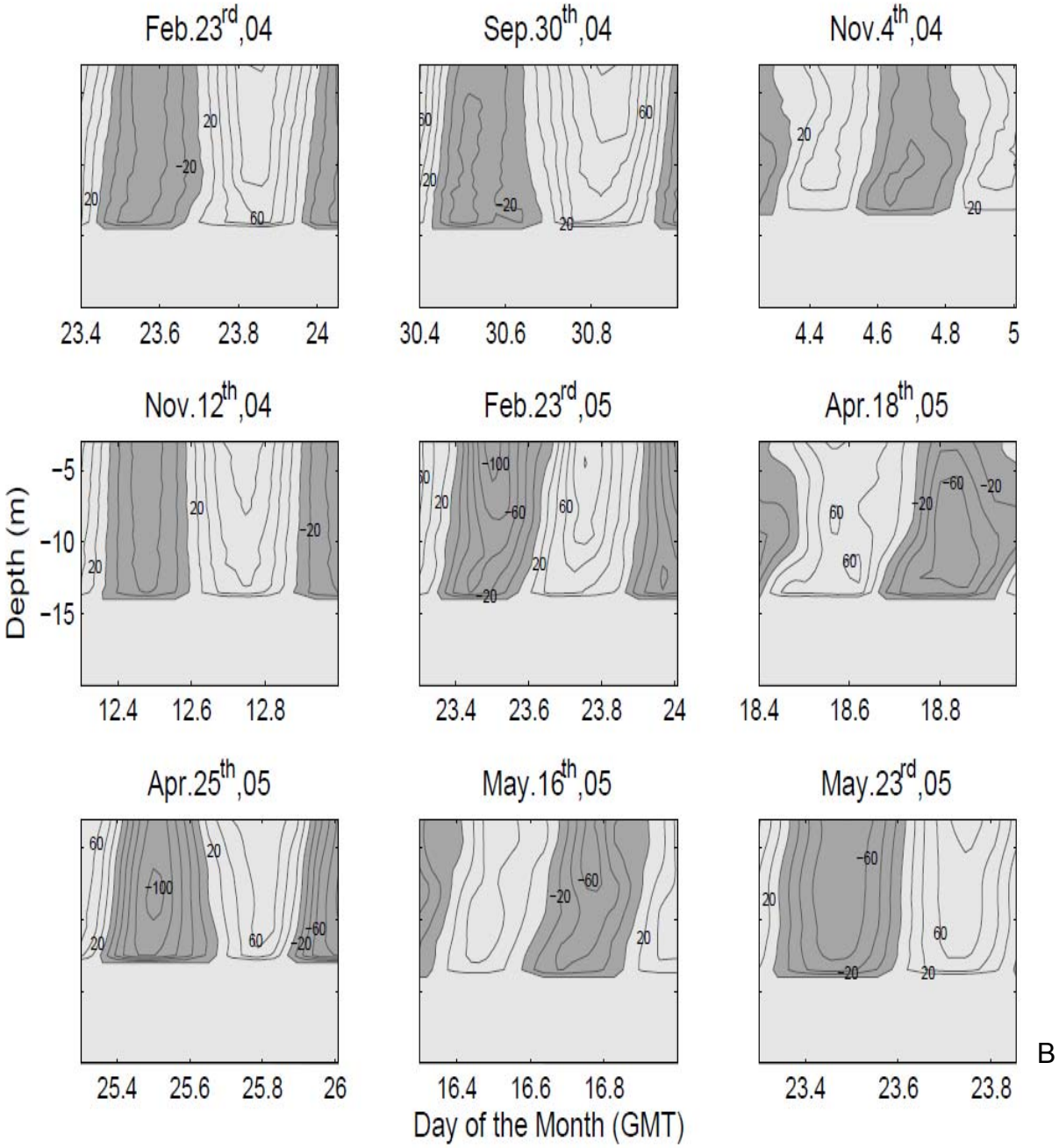

B

Figure 4-19. Continued

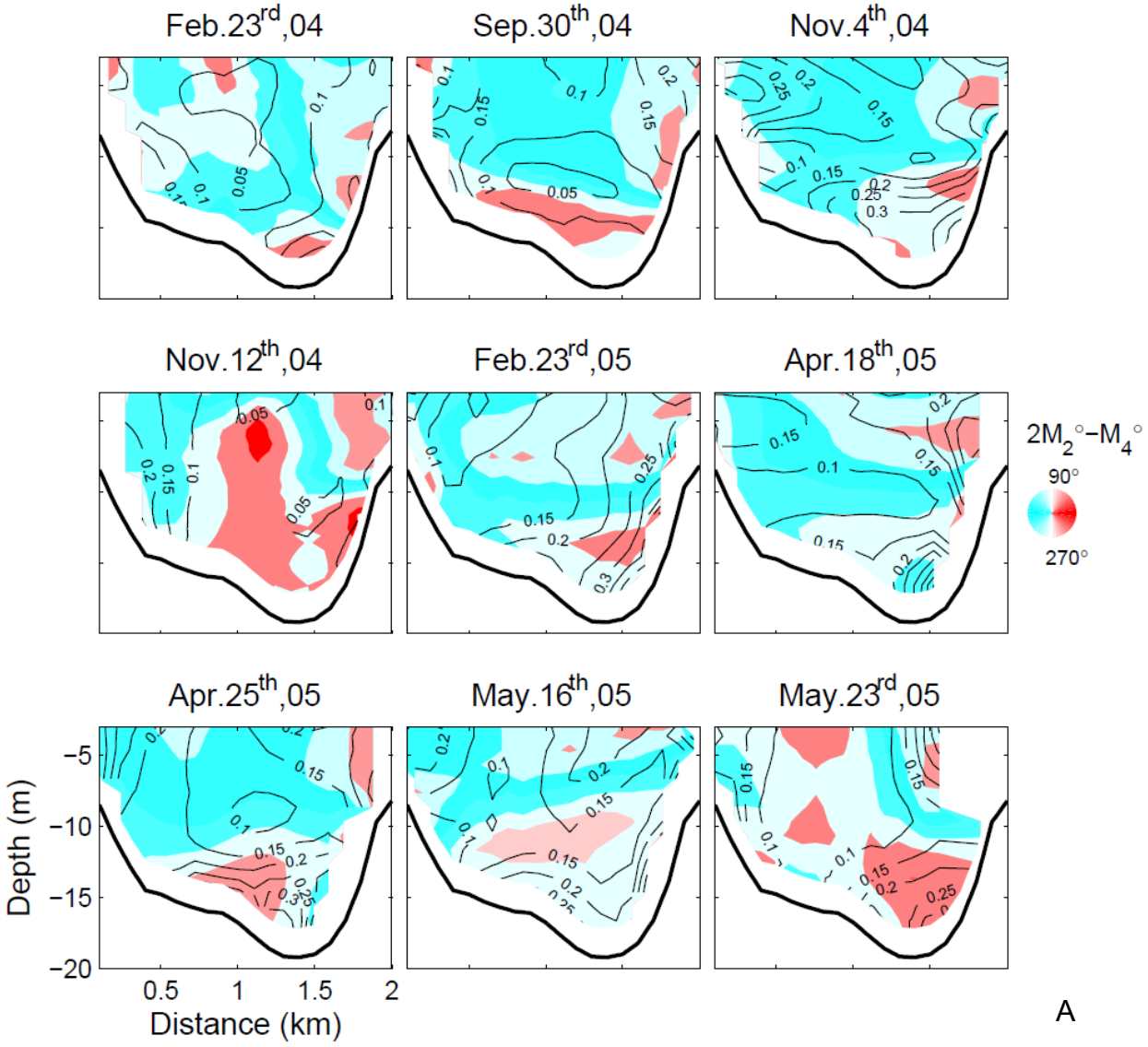

Figure 4-20. Tidal current asymmetries in terms of phase differences in overtides. A) $2M_2$-M_4. B) $3M_2$-M_6. Contours stand for amplitude ratios M_2/M_4 and M_2/M_6.

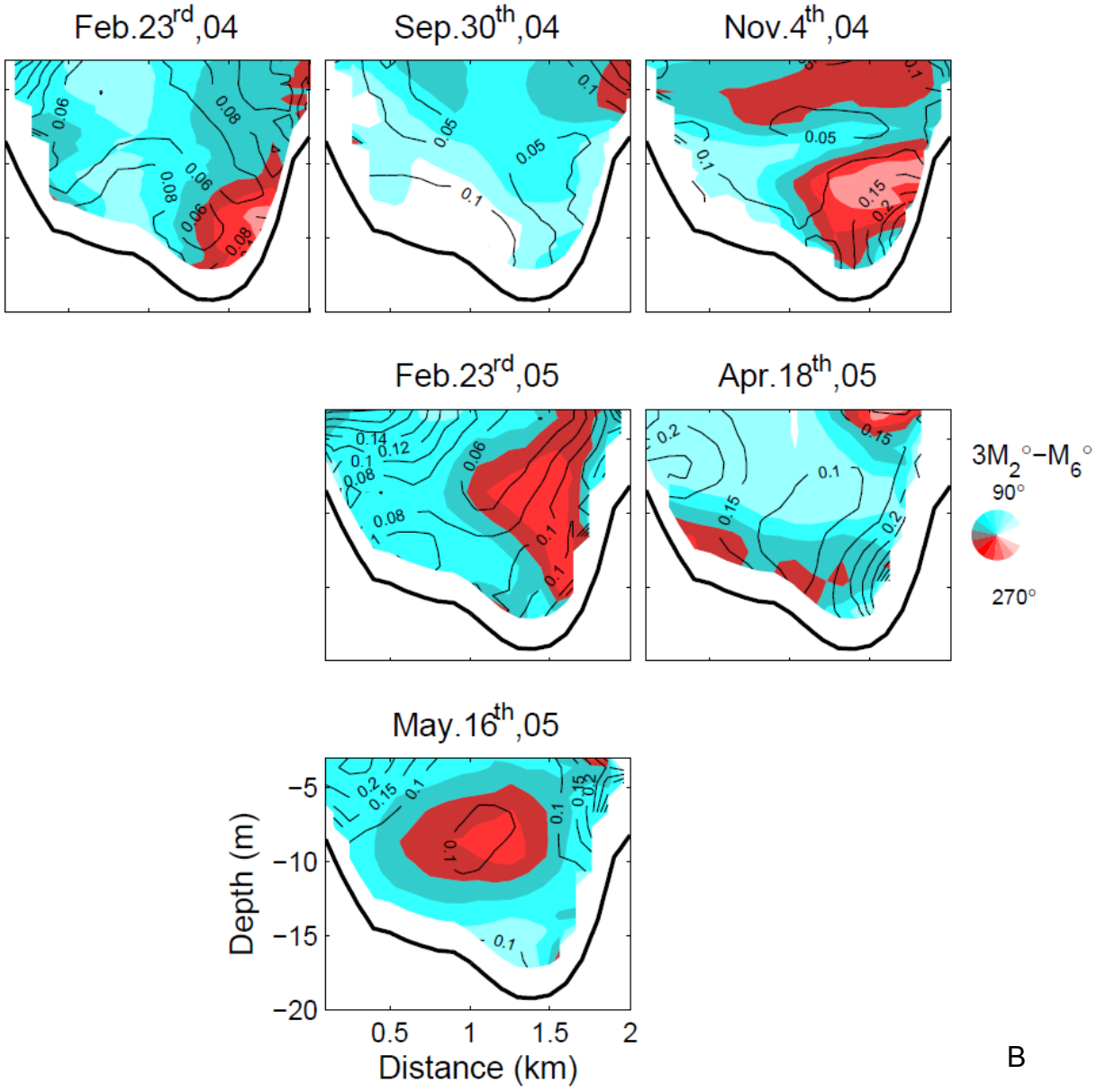

B

Figure 4-20. Continued

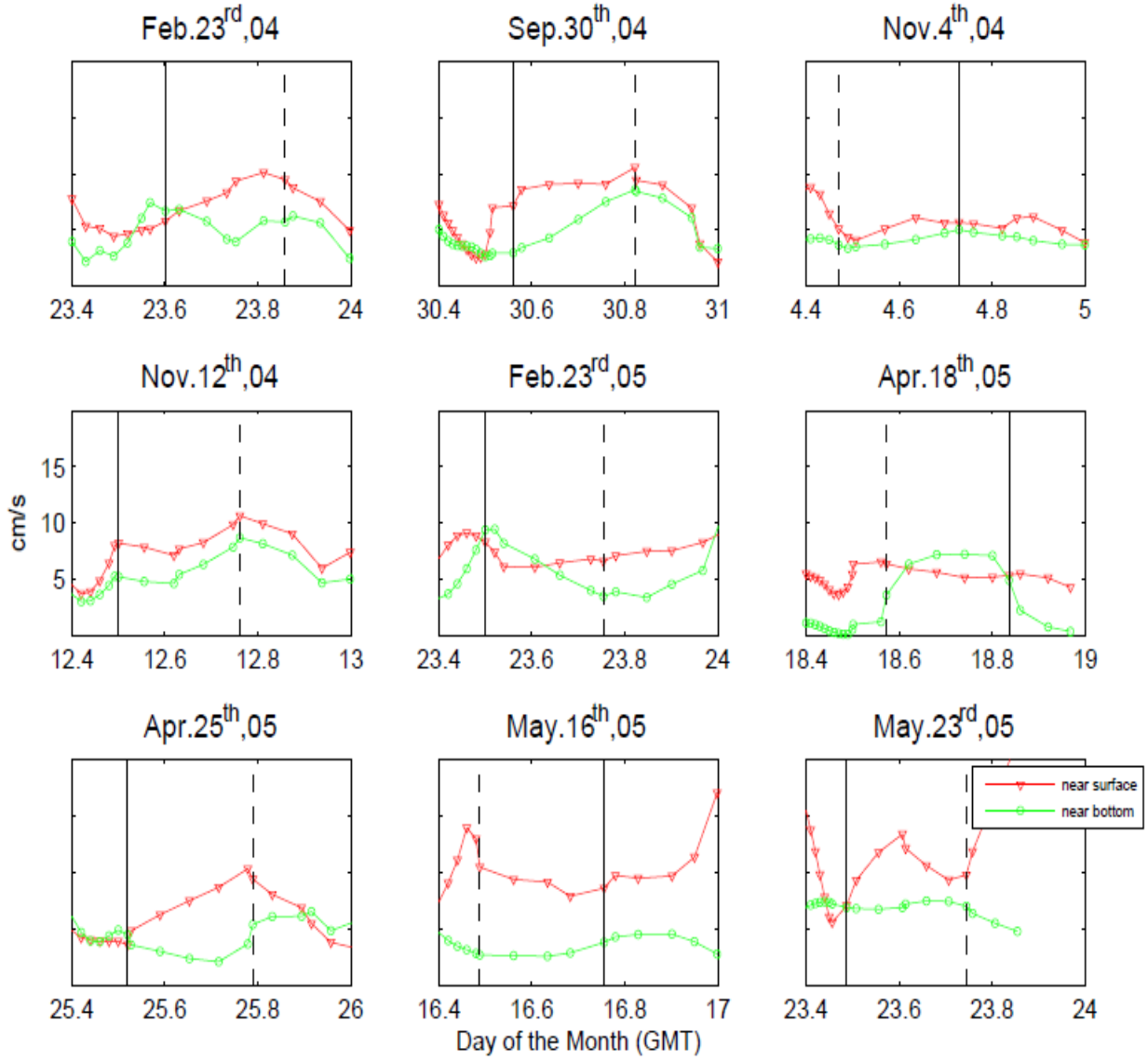

Figure 4-21. Tidal variation of the strength of secondary current near surface and bottom. Maximum flood and maximum ebb tides are denoted by black straight and dashed lines, respectively.

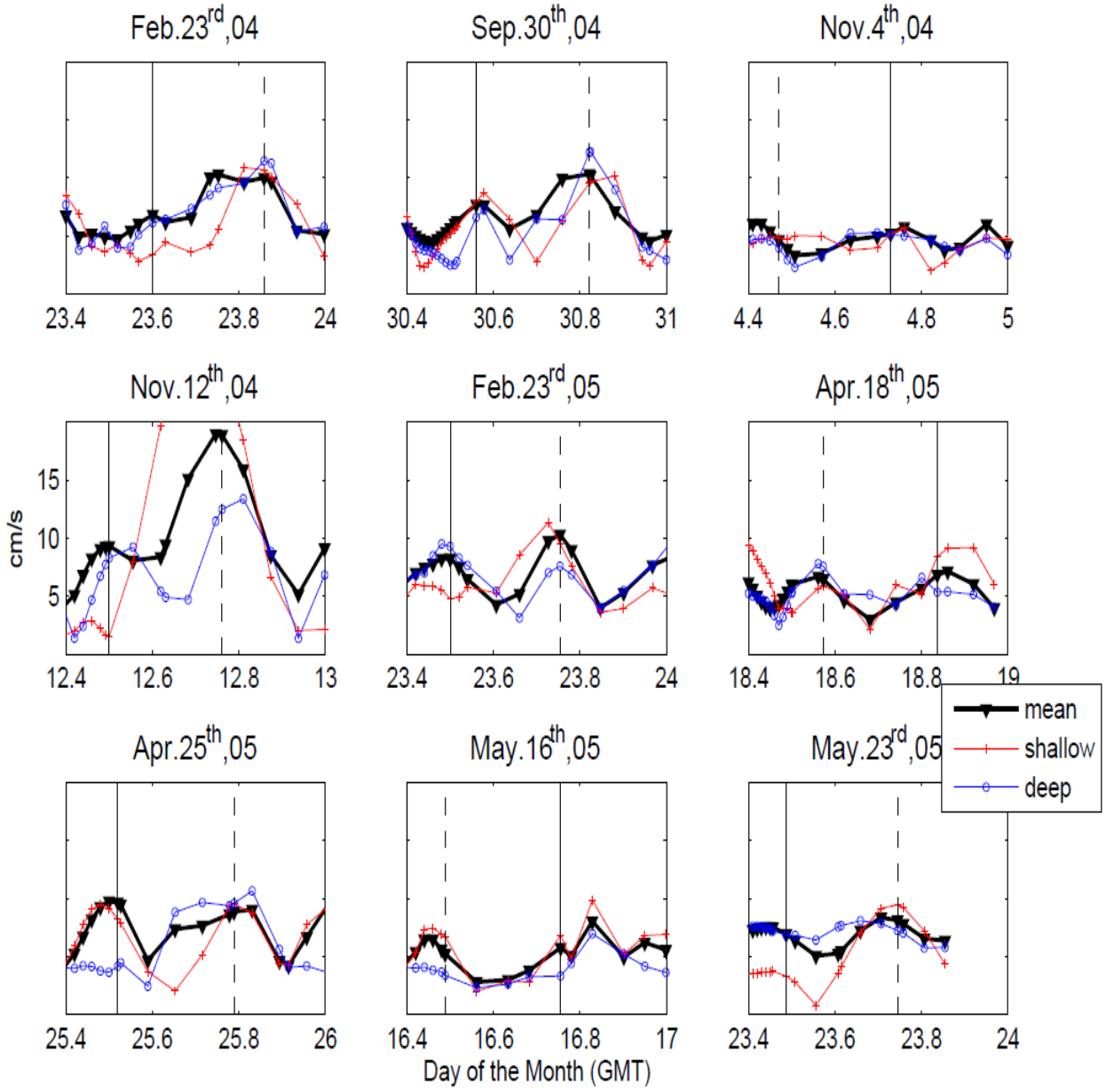

Figure 4-22. Lateral variation of the strength of mean secondary currents over a tidal cycle. Maximum flood and maximum ebb tides are denoted by black straight and dashed lines.

4.3.2 Asymmetry in Vertical Mixing

In order to determine the asymmetry of turbulent mixing over a tidal cycle, eddy viscosity coefficient, A_z was calculated. Both temporal and spatial variation of vertical exchange coefficient was determined by using a Richardson number-dependent turbulent closure proposed by Pacanowski and Philander (1981).

The vertical eddy viscosity coefficients were in the range of 10^{-4} to 10^{-2} m^2/s (Figure 4-23). In the channel highest values were observed throughout the whole cycle near the bed, and near surface (i.e., due to bed friction and wind forcing, respectively) during the 2004 surveys. This implied instabilities decreased near isopycnals which mostly appeared at mid-depths. Nov 4^{th} survey showed a clear evidence of such behavior when stratification persisted throughout the tidal cycle. In contrast to 2004 surveys, 2005 surveys showed more temporal asymmetry with higher eddy coefficients appearing near bottom. Mostly maximum ebb tides had tendency to have higher mixing coefficient near bed. Maximum flood tides appeared to have smaller mixing coefficient because of higher stratification.

4.3.2.1 Lateral variation of vertical mixing

To show the lateral variability of mixing coefficients, data from the shallower regions (i.e., first and third stations) were utilized (Figure 4-23). The flood-ebb asymmetry was more evident over shoals than in channel. Higher mixing rates were observed at or just before maximum ebb. In addition to that, the northern side of the channel showed higher instabilities with respect to the southern side. These asymmetries in vertical mixing are also linked to asymmetries in stratification as determined from the potential energy anomaly as described next.

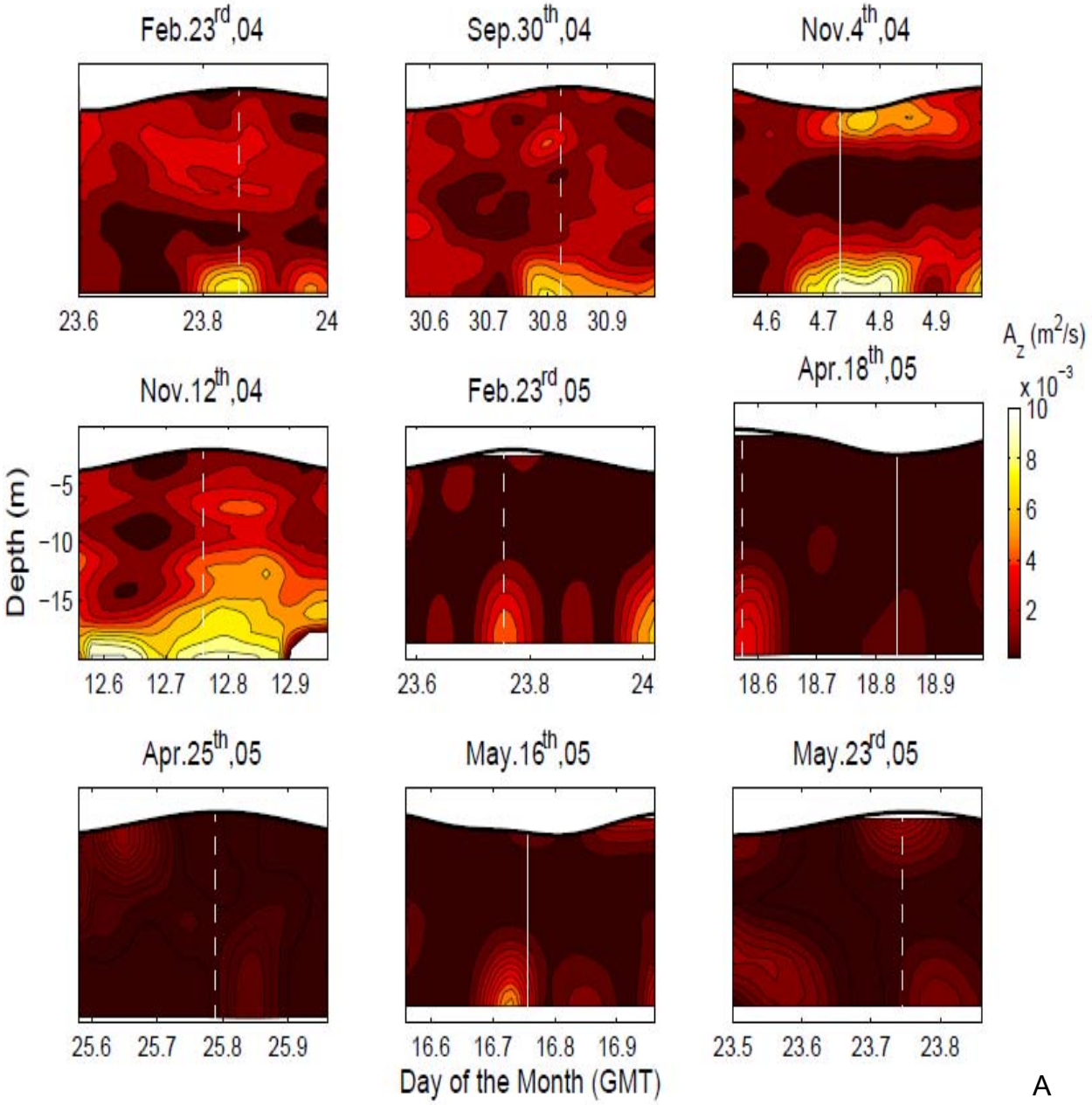

Figure 4-23. Tidal variation of vertical mixing coefficient. A) At Station 2. B) At Station 1. C) At Station 3.

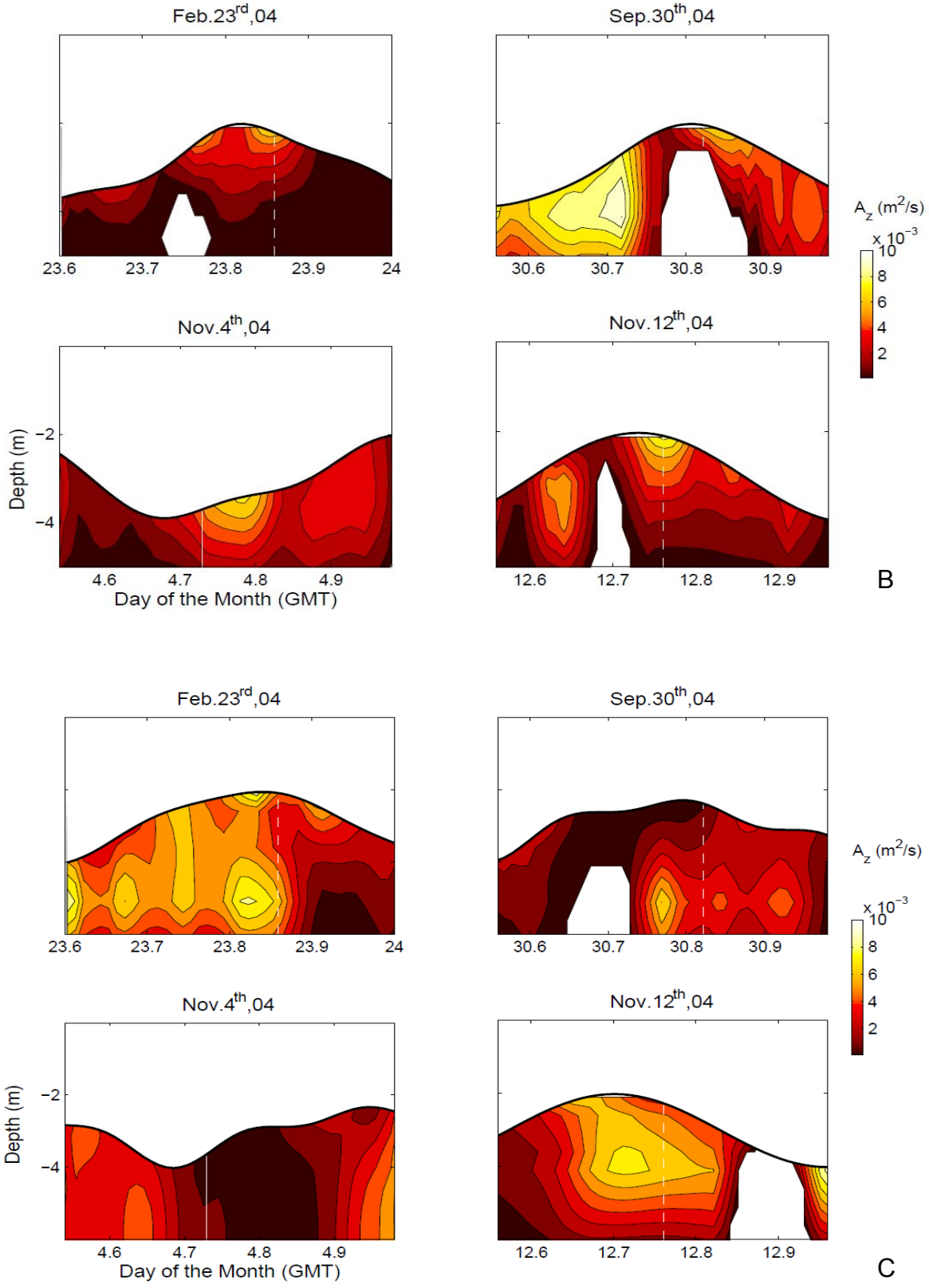

Figure 4-23. Continued

4.3.2.2 Potential energy anomaly

In order to quantify the water column stratification, the potential energy anomaly, ϕ (J/m^3), was calculated (Figure 4-24). For a given density profile, ϕ represents the amount of work required to mix the water column (Simpson et al., 1977; Simpson and Bowers, 1982):

$$\phi = \frac{g}{D}\int_{-H}^{\eta} z(\overline{\rho} - \rho)dz \tag{4-12}$$

$$\overline{\rho} = \frac{1}{D}\int_{-H}^{\eta} \rho.dz \tag{4-13}$$

where H is the mean water depth, η is the surface elevation, D = η+H.

The time rate of change of potential energy anomaly can also be utilized in order to observe which terms are influencing the stratification most. Burchard and Hofmeister (2008) provided a time-dependent dynamic equation for potential energy anomaly. The temporal evolution of stratification can be represented by:

$$\frac{\partial \phi}{\partial t} = \underbrace{\frac{g}{D}\frac{\partial \overline{\rho}}{\partial x}\int_{-H}^{\eta} u'zdz}_{(1)} + \underbrace{\frac{g}{D}\overline{u}\int_{-H}^{\eta}\frac{\partial \rho'}{\partial x}zdz}_{(2)} + \underbrace{\frac{g}{D}\frac{\partial \overline{\rho}}{\partial y}\int_{-H}^{\eta} v'zdz}_{(3)} + \underbrace{\frac{g}{D}\overline{v}\int_{-H}^{\eta}\frac{\partial \rho'}{\partial y}zdz}_{(4)} + \underbrace{\frac{g}{D}\int_{-H}^{\eta} A_z\frac{\partial \rho}{\partial z}dz}_{(5)} + \cdots \tag{4-14}$$

The overbar represents depth average and the tilde denotes fluctuations from depth averaged values. The first two term on the right-hand side of the equation represents along-channel non-mean and depth-mean straining, respectively. The third and fourth terms stand for lateral non-mean and depth-mean straining, respectively, and the fifth term is vertical mixing. Other terms are omitted since the main focus of this study is on straining and mixing. Figure 4-25 shows the relative contribution of these processes with positive ϕ_t indicating increasing stratification.

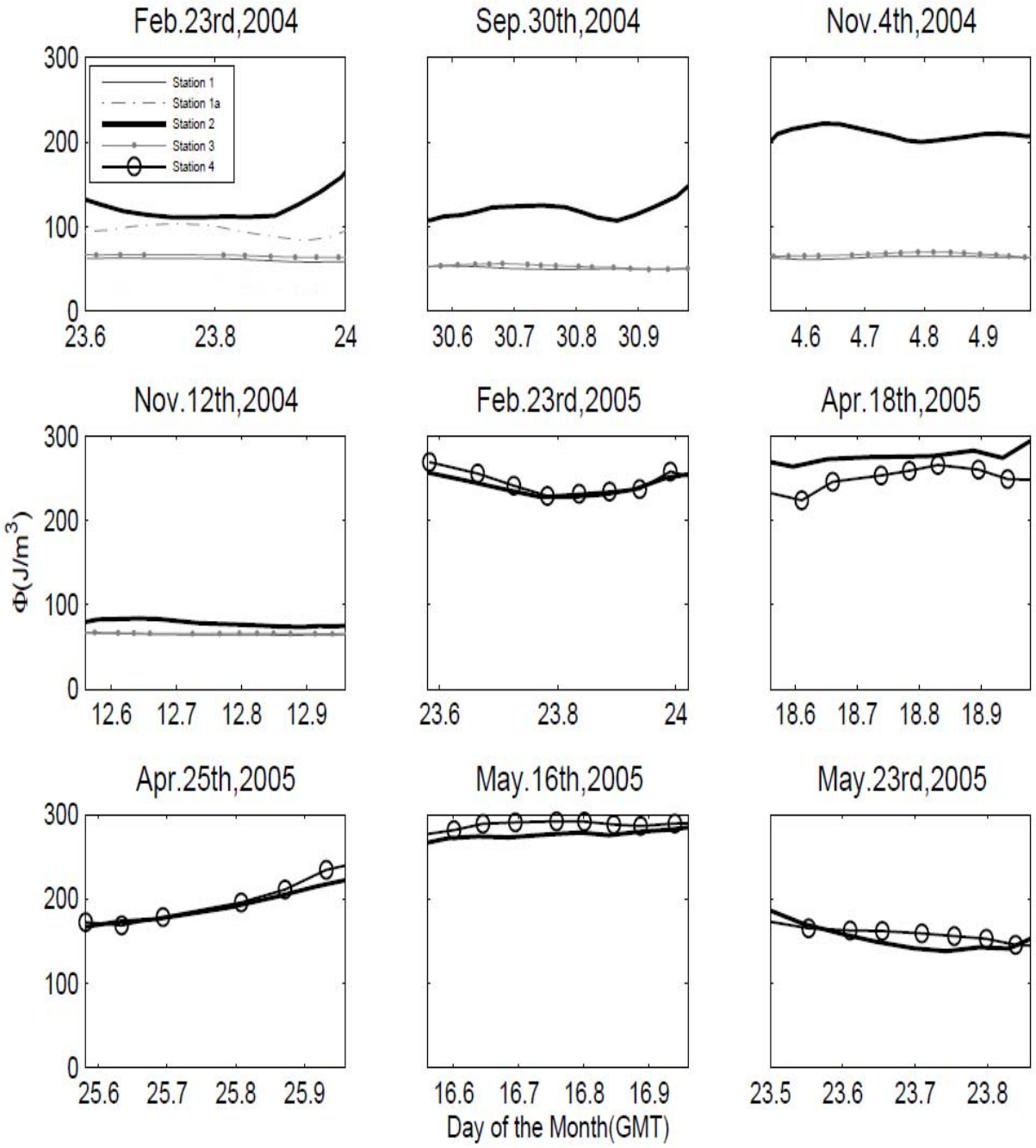

Figure 4-24. Potential energy anomaly for each CTD cast.

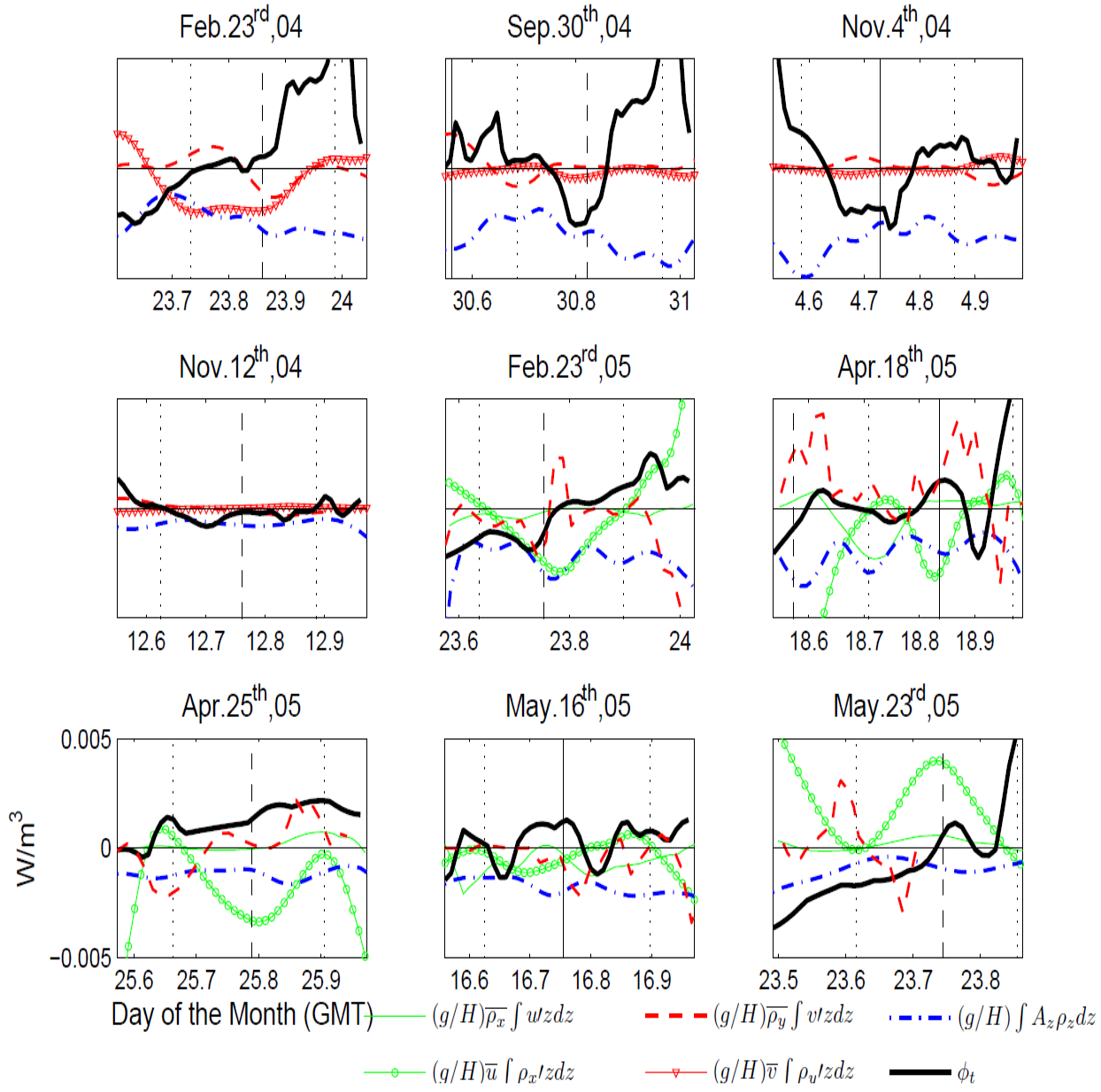

Figure 4-25. Temporal change in potential energy anomaly and the included terms.

CHAPTER 5
DISCUSSION

5.1 Observations vs. Numerical Model Results

Along channel net flow exhibited responsed to various forcing conditions. Most Spring tide surveys showed a laterally sheared structure with landward flow over the deeper bathymetry (i.e., northern side of the transect), and seaward flow over the southern side of the transect. Vertically sheared exchange persisted at neap tide surveys.

Cheng and Valle-Levinson (2009) categorized the variation in exchange patterns according to Rossby (i.e., the ratio of nonlinear advective terms to Coriolis forcing) and Ekman (i.e., the ratio of friction to Coriolis forcing) numbers by using a nonlinear numerical model. They concluded that the influence of advective accelerations on along channel flow is highest under high Rossby number and low Ekman number, driving a vertically sheared flow. With increased mixing high Rossby numbers exhibited both laterally and vertically sheared exchange. Their results showed that under weak mixing as nonlinear advection decreases the flow approaches geostrophy, and as mixing increases, lateral shear increases letting inflow concentrate in the channel and outflow over shoals (Figure 4-26).

Their numerical results were compared to our observations. Since the transect did not cover the whole mouth breadth, the shoals on both sides of the channel were missing to a certain extent. Keeping this in mind the same framework applied, by calculating Rossby and Ekman numbers for each survey and comparing the observed exchange patterns to the numerical results (Figure 4-27). The observations yielded Rossby numbers ranging from 0.30 to 0.76, and Ekman numbers ranging from 0.03 to

0.18, which corresponds to low to intermediate Ekman and Rossby numbers. The 1st and 4th surveys with higher Ekman numbers and lower Rossby numbers were consistent with the numerical results presenting a landward flow over depth and seaward over shoals. The 2nd and 3rd surveys with higher Rossby numbers and lower Ekman numbers exhibited more of a vertically sheared exchange with respect to the first two surveys. The 6th and 7th surveys mostly resembled the defined patterns; the 6th survey showed a tilted, vertically sheared flow, and the 7th survey, showed a bigger Rossby number (i.e., advective accelerations overcoming the Coriolis forcing). The rest of the surveys did not match the expected patterns because tides were not included in the numerical model. Since the surveys carried out in 2005 were more influenced by barotropic forcing, the tidal influence on exchange was greater. The numerical model's classification cannot be used to pre-define the exact pattern either, when the local or remote wind forcing are important.

The effect of local and remote forcing on exchange flow can be used to explain the shift from the numerical results. As stated previously local forcing altered the exchange flow during the 3rd, 5th, 7th, and 8th surveys when the winds were strongest. Southwesterly winds during the 3rd survey increased the inflow near bed as the stratification caused vertically sheared wind-driven exchange. The 5th survey, which was carried out in spring tides reflected the influence of up-estuary southeasterly winds, increasing the laterally sheared flow structure near the surface. The southwesterly down-estuary winds on the 7th survey (i.e., moderate Ek and high Ro) increased the lateral shear by augmenting landward flow in the channel. The northeasterly up-estuary winds on the 8th survey (i.e., low Ek and Ro) pushed the landward flow into the channel,

driving down-wind flows near surface and reducing the landward flow near bed causing vertical shears over a stratified water column. The unidirectional remote forcing caused increment in seaward flow due to set down at the adjacent shelf at 5th and 8th surveys leading to further departure of exchange flows from the expected Coriolis-influenced patterns. Increase in landward flows due to set up in the 6th and 7th surveys weakened the outflows and lifted them near surface while strengthening the inflows.

5.2 Observations vs. Analytical Model Results

Huijts et al. (2009) demonstrated the flow patterns emerging from lateral and vertical advection terms (vu_y and wu_z) in their analytical results. By considering along-channel tidal flow as strongest near the surface, and weaker near bed due to friction (i.e., tidal baroclinic pressure gradient ignored), and circulation due to Coriolis deflection (i.e., clockwise during flood and counter-clockwise during ebb when looking up-estuary in the northern hemisphere), relative tidal momentum transfers were analyzed across the cross-section. Relative excess and shortages of tidal momentum correspond to landward and seaward fluxes, respectively.

The tidal rectification process caused by vu_y was expressed by a relative excess of tidal momentum appearing near surface over the right side, and near bed over the left side. A relative shortage of tidal momentum appeared near the surface on left side and near the bed on the right side of the channel over a tidal cycle. This yields a residual four-celled structure (i.e., both vertically and laterally sheared). The tidal rectification process caused by wu_z can be expressed by relative excess and shortage of tidal momentum appearing on the right and left side of the channel respectively (i.e., laterally sheared two-celled structure). Total residual forces created by two mechanisms

(vu_y+wu_z) resembles more to the one created by wu_z with reduced lateral variability (Figure 4-28).

The tidal variation of lateral advection showed similarities with the four-celled pattern. However the subtidal lateral advection term yielded different structures depending on the relative importance of various forces. At spring tides, near-bed exchange described by the analytical model dominated, at neaps near-surface exchange dominated over the cross-section. The discrepancies between the analytical model and observations can be attributed to (1) lateral density gradients as the model assumes constant density gradient over the cross-section; (2) variable eddy viscosity as most of the observations showed relatively strong stratification; (3) tidal asymmetries; (4) lateral variability of the bathymetry.

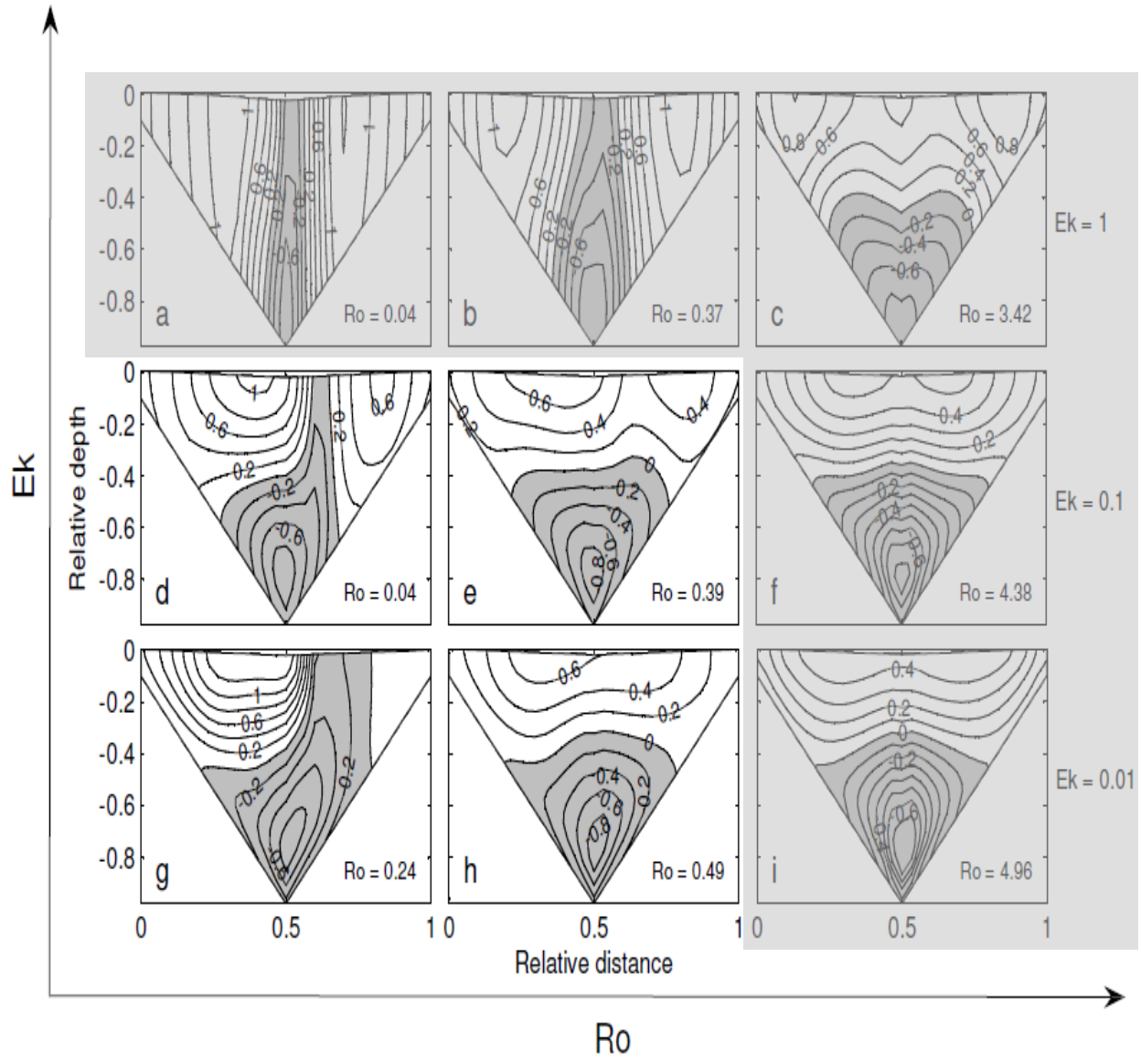

Figure 4-26. Nonlinear numerical results for subtidal along-channel flow changing with Ek and Ro numbers. (Source: Peng and Valle-Levinson, 2009).

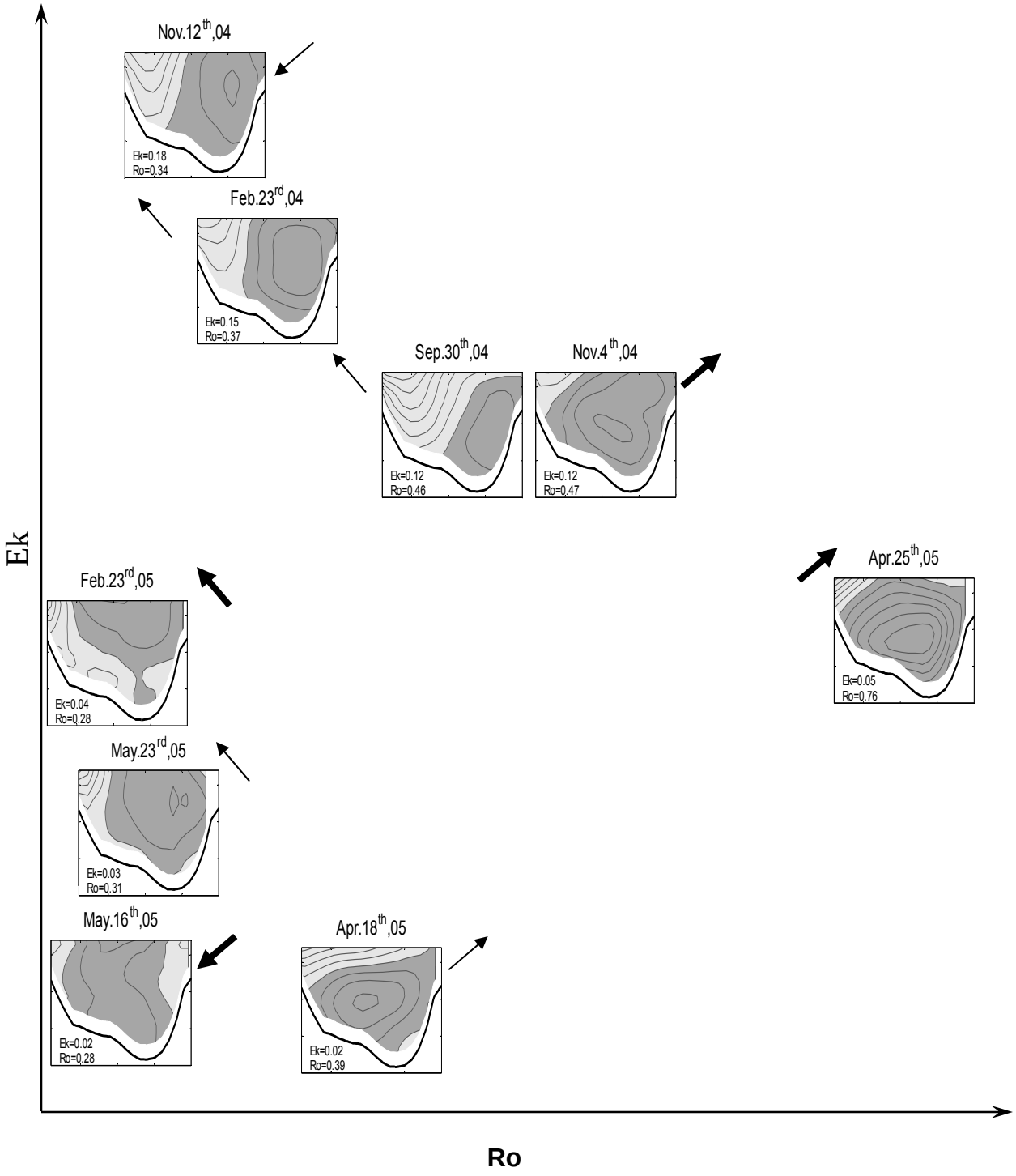

Figure 4-27. Classification of observed along-channel flow patterns with respect to Ek and Ro numbers.

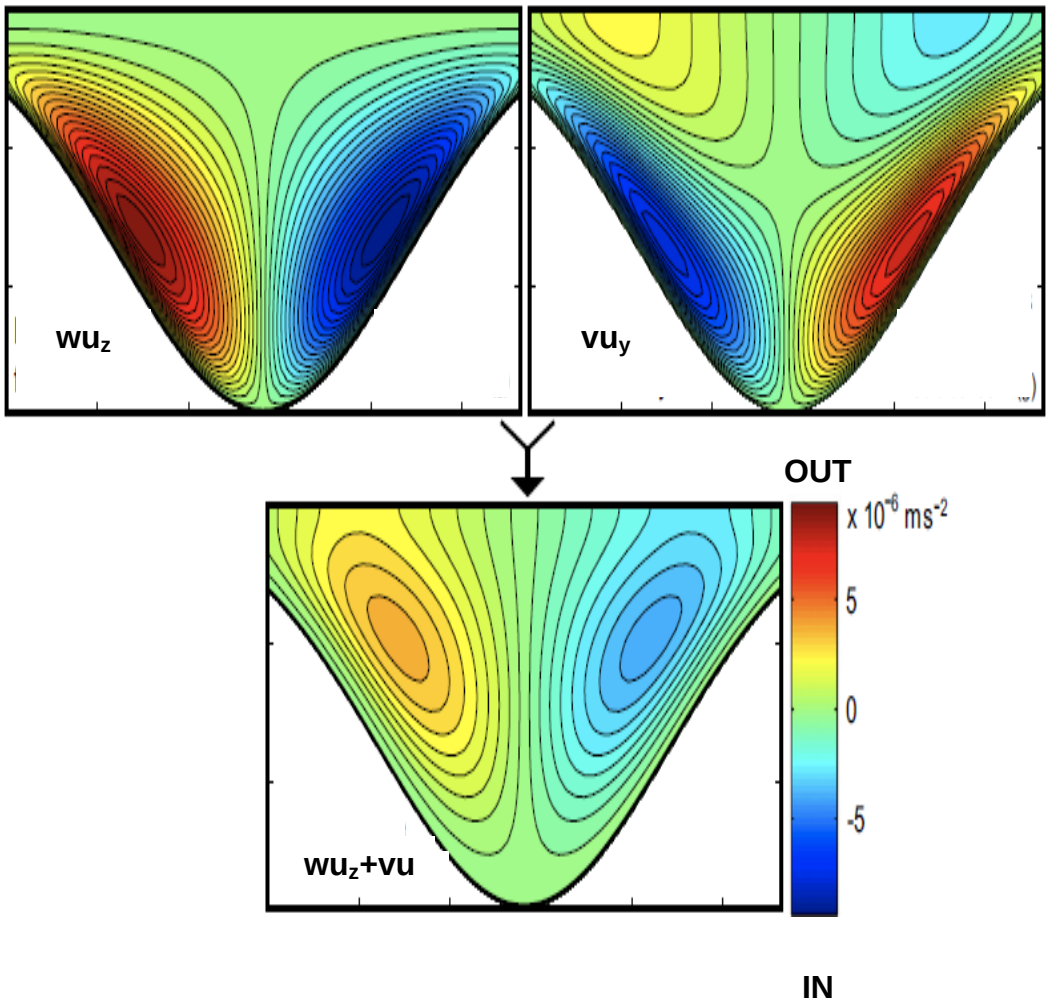

Figure 4-28. Analytical results for subtidal advective terms. (Source: Huijts et al., 2009).

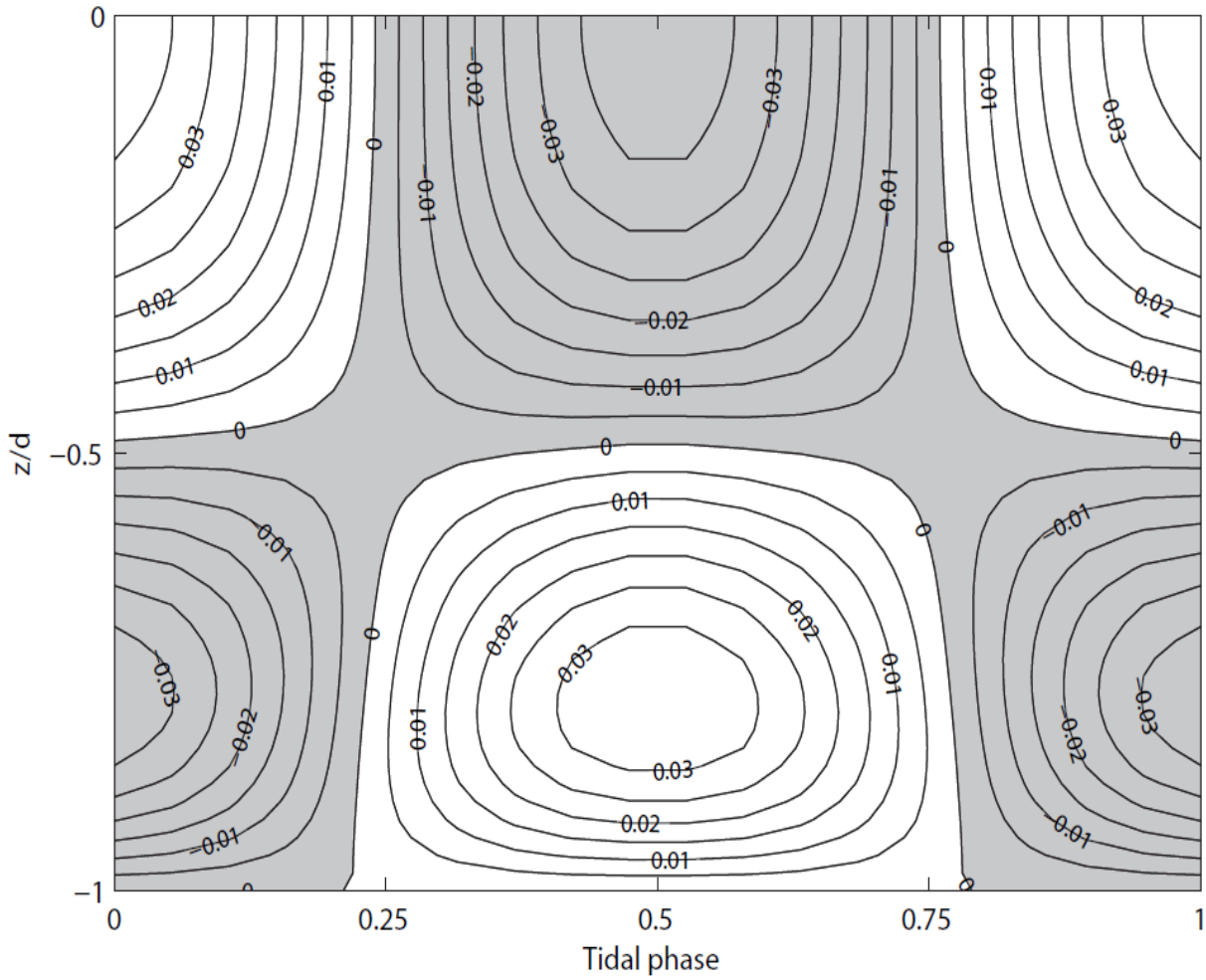

Figure 4-29. Tidal asymmetry induced residual currents. Horizontal axis is the timing of the onset of stratification (fraction of the tidal cycle). 0 represents the beginning of the flood, 0.5 represents the beginning of the ebb. Half of the tidal cycle is stratified. Vertical axis is dimensionless depth. Contours show dimensionless magnitude of the residual currents. Darker shades denote seaward flow. (Source: Cheng and Valle-Levinson, 2010).

CHAPTER 6
CONCLUSION

This study shows that nonlinear advective terms contribute to the along-channel momentum balance at leading order. Cross-sectional averages of nonlinear advection (uu_x+vu_y) demonstrated higher values at spring tides than neap tides due to increased tidal forcing.

Laterally sheared exchange flow patterns were observed for high Ekman numbers and low Rossby numbers. As the Rossby number got higher the exchange patterns became more vertically sheared, which is consistent with numerical results. Discrepancies were observed between numerical solutions and measurements for low Ekman numbers when local and remote forcing took over. Near-surface landward flows were observed for low Ek, and Ro when the wind forcing became dominant (i.e., local: up-estuary winds, remote: set-down). Under these circumstances lower Ek acted in favor of laterally-sheared exchange.

Lateral advection caused both vertically and laterally sheared patterns depending mostly on tidal forcing. At spring, lateral advection against Coriolis forcing by hindering lateral shear in u. At neap lateral advection reinforced the vertically sheared u. At spring, landward flows developed on the southern side of transect but at neap landward flows appeared on the northern side. This structure is a reminiscent of analytical model results.

Along-channel advection uu_x increased the lateral shears in along channel flow (i.e., seaward over shoals and landward in the channel). The discrepancy with numerical model for 5^{th} and 8^{th} surveys can be partly attributed to the influence of uu_x. Although Ro numbers for these observations were low (i.e., influence of nonlinear

advective terms on u is low), increased remote effects might be contributing to such results. Residuals induced by tidal asymmetries also affect along channel exchange flow. Asymmetries in lateral and along-channel flow cause variations in lateral and vertical shears leading to asymmetries in nonlinear advective terms, changing their contribution to the exchange flow. Asymmetries in along channel flow which is also correlated to the asymmetries in vertical mixing might be the reason for the near-surface landward flows observed in some of the surveys.

Tidal rectification mechanism described by Huijts et al. was observed roughly in most surveys showing a four-roomed structure over a tidal cycle. However lateral variations in bathymetry, lateral and vertical variations of along channel density gradients caused great distortions to such patterns. Asymmetries in lateral flow caused by the interaction between density gradients and curvatures during different phases yielded to asymmetries in lateral advective accelerations. Decoupling of lateral variations in bathymetry and friction caused asymmetric lateral shears in along channel flow during flood and ebb which affected lateral advection.

The observations showed that at spring tides the lateral advective terms become stronger than at neap tides in terms of the range of magnitude. In most cases the flood tides favored the down-estuary accelerations either at southern side near surface or northern side near bed, whereas ebb tides favored the up-estuary accelerations in the rest of the channel.

REFERENCES

Chatwin, P. C., 1976: Some remarks on the maintenance of the salinity distribution in estuaries. Estuaries and Coasts Marine Science, **4**, 555-566.

Cheng, P., and A. Valle-Levinson, 2009: Influence of lateral advection on residual currents in microtidal estuaries. J. Phys. Oceanogr., **39**, 3177-3190.

Hansen, D. V., and M. Rattray, 1965: Gravitational circulation in straits and estuaries. Journal of Marine Research, **23**, 104-122.

Hetland, R. D., and W. R. Geyer, 2004: An idealized study of the structure of long, partially mixed estuaries. J. Phys. Oceanogr., **34**, 2677-2691.

Huijts, K. M. H., H. M. Schuttelaars, H. E. de Swart, and C. T.Friedrichs, 2009: Analytical study of the transverse distribution of along-channel and transverse residual flows in tidal estuaries. Cont. Shelf Res., **29**, 89–100.

Huijts K.M.H, H. M. Schuttelaars, H. E. de Swart, and Valle-Levinson A., 2006: Lateral entrapment of sediment in tidal estuaries: An idealized model study. J. Geophys. Res, 111(C12016), doiI:10.1029/2006JC003615.

Jian S., and Jing L., 2006: Modeling study of the influences of tide and stratification on age of water in the tidal James River Estuarine. Coastal and Shelf Science, **68**, 101-112.

Kasai, A., A. E. Hill, T. Fujiwara, and J. H. Simpson, 2000: Effects of the Earth's rotation on the circulation in regions of freshwater influence. J. Geophys. Res, **105** (C7), 16,961-16,969.

Lacy, J.R., and Monismith, S.G., 2001: Secondary currents in a curved, stratified, estuarine channel. J. Geophys. Res, **106**(C12), 31283-31302.

Lerczak, J. A. and W. R. Geyer, 2004: Modeling the lateral circulation in straight, stratified estuaries. J. Phys. Oceanogr., **34**, 1410-1428.

Nidzieko, N.J.,Hench, J.L., and Monismith S.G., 2009: Lateral circulation in well mixed and stratified estuarine flows with curvature. J. Phys. Oceanogr., **39**, 831-851.

Nunez, R.A., and Simpson J.H., 1994: Turbulence closure modeling of estuarine stratification. J. Geoph. Res., **99**(C8), 16143-16160.

Officer, C. B., 1976: Physical Oceanography of Estuaries (and associated coastal waters). John Wiley, New York, 465 pp.

Cheng, P., and A. Valle-Levinson, 2009: Influence of lateral advection on residual currents in microtidal estuaries. J. Phys. Oceanogr., **39**, 3177-3190.

Cheng, P., and R.E. Wilson, 2009: Modeling influence of stratification on lateral circulation in a stratified estuary. J. Phys. Oceanogr., **39**, 2324-2337.

Pacanowski, R.C., and S.G.H. Philander, 1981: Parameterization of vertical mixing in numerical models of the tropical oceans. J. Phys. Oceanogr., **11,** 1443–1451.

Pritchard, D. W., 1956: The dynamic structure of a coastal plain estuary. Journal of Marine Research, **15**(1), 33-42.

Simpson J.H., Brown J., Matthews J., and Allen,G., 1990: Tidal straining, density currents and stirring in the control of estuarine stratification. Estuaries, **13**, 125-132.

Scully, M.E., and C.T. Friedrichs, 2007: The importance of tidal and lateral asymmetries in stratification to residual circulation in partially mixed estuaries. J. Phys. Oceanogr., **37**, 1496-1511.

Scully, M.E., W.R. Geyer, J.A. Lerczak, 2009: The influence of lateral advection on the residual estuarine circulation: A numerical modeling study of the Hudson River Estuary. J. Phys. Oceanogr., doi: 10.1175/2008JPO3952.1.

Stacey, M. T., J. R. Burau, and S. G. Monismith 2001: Creation of residual flows in a partially stratified estuary. J. Geophys. Res., **106**(8), 17,013-17,037.

Stacey, M. T., J. P. Fram, and F. K. Chow 2008: Role of tidally periodic density stratification in the creation of estuarine subtidal circulation. J. Geophys. Res., **113**, C08016, doi:10.1029/2007JC004581.

Valle-Levinson, A., K.C. Wong, and K.M.M. Lwiza 2000: Fortnightly variability in the transverse dynamics of a coastal plain estuary. J. Geophys. Res., **105**(C2), 3413-3424.

Valle-Levinson, A. 2008: Density-driven exchange flow in terms of the Kelvin and Ekman numbers. J. Geophys. Res., **113**, C04001, doi:10.1029/2007JC004144.

Valle-Levinson A., and Li C., 2000: Convergence of lateral flow along a coastal plain estuary. J. Geophys. Res, **105**(C7), 17045-17061.

Valle-Levinson A., Boicourt W.C., and Roman M.R., 2003: On the linkages among density, flow, and bathymetry gradients at the entrance of Chesapeake Bay. Estuaries, **26** (6), 1437-1449.

Wong, K.-C. 1994: On the nature of transverse variability in a coastal plain estuary, J. Geophys. Res., **99**(C7), 14,209-14,222.

BIOGRAPHICAL SKETCH

Nuvit Berkay Basdurak was born in Ankara, Turkey. He obtained his undergraduate degree in civil engineering. In 2004, he obtained his master's degree in hydromechanics at the Middle East Technical University, working with Dr. Halil Onder, on analyzing the prevention techniques of saltwater intrusion in coastal aquifers. He has been working, with Dr. Arnoldo Valle-Levinson, doing field studies on estuarine circulation. He received his Ph.D. from the University of Florida in the summer of 2010.